An Integrated 3D Safety-based Approach for the Design of Horizontal Curves using Reliability Analysis and LiDAR Data

by

Amr Ali Shalkamy Mohamed

A thesis submitted in partial fulfillment of the requirements for the degree of

Doctor of Philosophy

in

Transportation Engineering

Department of Civil and Environmental Engineering
University of Alberta

ABSTRACT

Safety-based design can be described as an approach in which safety is considered a core design input and the safety performance of proposed designs that follow this approach can be expected. Although current-day highway design guidelines are constantly updated to incorporate recent advances in research, there are still several limitations associated with the current design approach. Perhaps the biggest drawback is that the safety levels built into existing guidelines are largely unknown and safety is not explicitly considered as a design input. There is little to no knowledge about the safety implications of deviating from standard requirements. Moreover, current guides do not account for the stochastic nature of design inputs. Design inputs are therefore represented by deterministic values assuming near worst-case scenarios to determine design values leading to uneconomic designs in many cases. There is no information in design guidelines on whether a road designed to meet the minimum requirements of guidelines is capable of accommodating or exceeding driver demand, resulting in uneconomic design in many cases. To address these limitations, many design experts have promoted using reliability analysis as a robust methodology to quantify the risk (known as the probability of non-compliance, P_{nc}) that a certain design would fail to meet the requirements of the road user demand.

The majority of previous studies on reliability-based highway design focused on assessing the risk associated with horizontal curves considering only one criterion of non-compliance which is insufficient sight distance using 2D sight distance calculations. In fact, this does not represent the nature of the driving environment as non-compliance on curves could result from multiple non-compliance modes such as restricted sight distance and vehicle skidding. Also, sight distance can be restricted by 3D obstructions or the combination of horizontal and vertical alignments

which makes using a multimode, also known as a system, reliability analysis and 3D sight distance evaluation more realistic. More so, only a handful of studies established a link between P_{nc} and collisions. Therefore, establishing a link between the P_{nc} and safety utilizing 3D sight distance and multi-mode reliability analysis remains unexplored.

To address these limitations, this thesis adopts a safety-based design approach whereby relationships between driver capabilities, curve geometric attributes, and collisions are established. The thesis calibrates safety-based design charts for horizontal curves considering a system reliability analysis where the non-compliance could result from limited sight distance and vehicle skidding. To enable a robust and large-scale reliability analysis, the first phase of the thesis develops novel algorithms that facilitate curve detection and automatic extraction of curve geometric attributes on highways using mobile Light Detection and Ranging (LiDAR) data. Using this approach, curve attributes were collected, and the Available Sight Distance (*ASD*) was assessed in a 3D environment on 244 horizontal curves in Alberta, Canada. Monte Carlo Simulation was then used to calculate the associated risk levels, and full-Bayes multivariate Poisson lognormal regression was utilized to develop statistically significant safety performance functions that link P_{nc} to collisions. Safety-based design charts were then calibrated to relate curve attributes to risk levels and expected collision frequency. Structural Equation Modelling (SEM) was also used to study the interaction between curve attributes, P_{nc}, and collision frequency. The results of SEM presented curve features that directly affect P_{nc}, safety, and those who have an indirect influence on collisions, which was mediated through P_{nc}.

The results showed that there is a statistically significant relationship between P_{nc} and safety, indicating that higher P_{nc} rates are associated with higher expected crashes. The calibrated

charts showed the importance of using multi-mode reliability analysis, especially on curves with sharp radii where the difference between P_{nc} of a single-mode and P_{nc} of a multimode is considerable. An example of using the calibrated charts in estimating the expected safety benefits of geometric improvements was introduced. Guidance to practitioners on using the proposed charts was also provided. The developed charts are ready to use by designers and can offer practitioners a tool to estimate the safety consequences of design alternatives and aid the decision-making process of rehabilitation projects. In summary, the research presented in this dissertation is a step forward towards adopting a safety-based design of highways and is of crucial importance from both theory and practical perspectives.

PREFACE

All the work presented in this thesis has been published in peer-reviewed journals in the areas of transportation engineering and remote sensing.

1. **Shalkamy, A.**, & El-Basyouny, K. (2020). Multivariate models to investigate the relationship between collision risk and reliability outcomes on horizontal curves. *Accident Analysis & Prevention*, *147*, 105745.
2. **Shalkamy, A.**, Gargoum, S., & El-Basyouny, K. (2021). Towards a more inclusive and safe design of horizontal curves: Exploring the association between curve features, reliability measures, and safety. *Accident Analysis & Prevention*, *153*, 106009.
3. **Shalkamy, A.**, & El-Basyouny, K. (2021). Calibrating Safety-based Design Charts for Horizontal Curves using System Reliability Analysis and Multivariate Models. *Journal of Transportation Safety & Security*. DOI: 10.1080/19439962.2021.1992552.
4. **Shalkamy, A.**, El-Basyouny, K., & Xu, H. Y. (2020). Voxel-based methodology for automated 3D sight distance assessment on highways using mobile light detection and ranging data. *Transportation Research Record*, *2674*(5), 587-599.
5. **Shalkamy, A.**, Karsten, L., Gargoum, S., & El-Basyouny, K. (2020). A framework to detect horizontal curves and assess their geometric properties from remotely sensed point clouds. *International Journal of Remote Sensing*, *41*(21), 8328-8351.

Dedicated To My Parents, Mona Ismaiel & Ali Shalkamy

M beloved wife, Samaa Agina

My sweet daughter, Salma

ACKNOWLEDGEMENTS

Above all, praises are first to Allah, by whose grace enabled me to finish this work successfully. I would like to extend my sincere gratitude and appreciation to my supervisor, Dr. Karim El-Basyouny, for giving me the opportunity to pursue this degree and for his valuable support and guidance throughout the completion of this research. His time, support, and confidence in my capabilities helped me recognize my true potential and grow in several areas.

I would like to express my deepest gratitude to Alberta Innovates, Transportation Association of Canada, Transport Canada, Canadian Transportation Research Forum, and the University of Alberta Faculty of Graduate Studies and Research for the financial support throughout my degree. I would also like to thank the Natural Sciences and Engineering Research Council of Canada (NSERC) for offering me the financial support to extend this work further upon graduation. My thanks are also extended to Alberta Transportation for providing the LiDAR data used in this research.

I also would like to extend my sincere thanks and appreciation to the examination committee members Dr. Qipei Mei (Chair), Prof. Yasser Hassan, Dr. Wei Victor Liu, Dr. Yong Li, Dr. Tony Qiu, and Dr. Karim El-Basyouny for their time, assistance, and insightful feedback and comments. I also would like to extend my sincere thanks to Dr. Stephen Wong for his feedback and insightful comments.

I owe sincere thanks to my M.Sc. supervisor Dr. Dalia Galal Said at Cairo University for all of her support, guidance, and help throughout my Master's degree and after. Her belief in my abilities and motivation have had great positive impacts on my abilities. Special thanks are also

due to my Master's supervisor Dr. Laila Radwan for her support during my degree and years of undergraduate study at Cairo University.

I would also like to express my appreciation to my fellow Transportation Engineering colleagues at the U of A, Dr. Suliman Gargoum and Dr. Mostafa H. Tawfeek. Special thanks to Suliman for his help, encouragement, and insightful discussions.

I would like to extend my sincere gratitude and thanks to my parents for their prayers, help, love and presence in my life. I am forever grateful to my beloved mother for her unlimited support, love, and care. She has always helped me become a better person and make greater achievements throughout the years. With all my love, I would also like to very much thank my wife, Samaa Agina, for the endless support and infinite effort she has made to assist me to focus on completing this work. My love and gratefulness to her are impossible to measure. Also, I extend my thanks to my dear sisters Samar, Omnia, and Dina, and my brother Mostafa for their love and being in my life.

Lastly but very importantly, I would also like to thank my mate and dear friend Ahmed Mohamed for his continuous support, great help, and love throughout our many years together.

TABLE OF CONTENTS

LIST OF FIGURES

LIST OF TABLES

LIST OF ABBREVIATIONS

2D: two-dimensional

3D: three-dimensional

AADT: Average Annual Daily Traffic

AASHTO: American Association of State Highway and Transportation

AIC: Akaike Information Criterion

ASD: Available Sight Distance

BGR: Brooks-Gelman-Rubin

BIC: Bayesian Information Criterion

CL: Chord Length

DOTs: Departments of Transport

DSMs: Digital Surface Models

DTM: Digital Terrain Models

DV: Dependent Variable

EB: Empirical Bayes

FB: Full Bayes

FORM: First Order Reliability Method

GIS: Geographic Information System

GPS: Global Positioning System

HDS: Highway Design Software

HSM: Highway Safety Manual

I + F: Injuries plus Fatalities

KML: Keyhole Markup Language

LAS: Laser

LiDAR: Light Detection And Ranging

LSF: Limit State Functions

MCMC: Markov chain Monte Carlo

MCS: Monte Carlo Sampling

MVPLN: Multivariate Poisson Log-normal

NHTSA: National Highway Traffic Safety Administration

PBD: Performance-Based Design

PC: Point of Curvature

PDF: Probability Density Function

PDO: Property Damage Only

PI: Point of Intersection

P_{nc}: the probability of non-compliance

PT: Point of Tangency

R: Radius

SEM: Structural Equation Modelling

SPF: Safety Performance Functions

TAC: Transportation Association of Canada

Z: Azimuth

1 INTRODUCTION

1.1 Background & Motivation

It is globally accepted that road collisions are a major cause of death and exert a substantial economic burden on both individuals and governments. Several studies showed that driver behaviour, roadway geometric features, pavement conditions, and vehicle characteristics are major contributing factors to collision occurrence [1, 2]. As an example of highway geometric attributes that affect safety, the radius of a curved segment has generally been found to have an inverse relationship with collisions [3, 4]. These studies also reported that road geometry has a significant impact on driving behaviour and affects both the path and speed of vehicles on horizontal curves. Accordingly, improving the geometric design of roadways including horizontal curves would improve driving behaviour, decrease the potential of driver errors, and therefore improve safety. While vehicle manufacturers work to improve the safety of vehicles, roads should be designed to provide a safe driving environment for both users and vehicles.

Although roads are designed following design guidelines, several researchers have consistently shown that geometric characteristics of curved segments have significant relationships with crash occurrence [4-7]. The design of horizontal curves has been considered to entail significant safety concerns for several years [8]. Collisions that occur on curves are more severe and often cause major injuries and fatalities [9]. For example, in the United States, about 25 percent of fatal road collisions on highways occur on curved sections. More so, 87 percent of these fatal collisions are caused by run-off-the-road and head-on crashes that are likely to occur on horizontal

curves [10, 11]. These statistics highlight the significant social and potential economic consequences of roadway collisions. It also emphasizes the importance of improving road design practices to better safety.

The current practice of road safety initiatives is categorized into two main approaches, reactive approach and proactive approaches [12]. The reactive approach to safety involves targeting locations that have a high number of collisions to identify concerns and propose potential remedial action. This approach is based on the analysis of road collisions that have already occurred and therefore, any proposed countermeasure is considered reactive in nature. A major limitation with this approach is the reliance on a high number of fatal and injury collisions to occur before any safety improvements are implemented. The reactive approach is studied to a satisfactory degree and several case studies and statistical models that follow this approach are available [13-15].

Such a reactive approach to road safety is not appropriate during the planning and design stages of road facilities. A more pertinent approach should be 'proactive' (i.e., preventing unsafe roadway conditions from occurring in the first place) by addressing them either at the planning or design phases of a road's development life cycle. The proactive approach involves the development of Safety Performance Functions, SPF (i.e., statistical models) that serve as safety indicators aiming to assess road safety of a proposed design at early stages. A significant advantage of adopting such an approach is that it does not require road collisions to occur before safety measures are taken. In addition, making modifications during the planning and design stages is less costly than implementing changes to an already existing roadway facility. Thus, the proactive

approach to safety is of great importance to assess current designs of road facilities, and it also can be used to provide the necessary tools and statistical models to assess the potential safety risk associated with proposed designs. Unfortunately, current design guidelines do not provide a direct link between a proposed design and the associated safety level. When designing roads following today's guidelines, the level of safety in the suggested design is uncertain, and safety is considered a by-product measure. Indeed, it has been established that there is a need to explicitly address road safety considerations in current design guides [5, 16].

1.1.1 Safety in Current Design Guidelines

Road facilities are currently designed following design guidelines that were developed by various transportation agencies. In the US, the American Association of State Highway and Transportation Officials, AASHTO [17], produces and updates a policy on the geometric design of highways and streets. In Canada, the Transportation Association of Canada (TAC) publishes books and guidelines that govern the design of highways in the country [18]. The highway geometric design process involves dimensioning the roadway elements to provide safe, comfortable, and aesthetic road conditions for road users. The output of this process is a set of deterministic dimensions to ensure a satisfactory driving environment.

Although design guidelines are developed with some safety considerations, they do not provide enough information on the expected safety performance of roadways designed following the recommended requirements. Therefore, it is unclear how safe a road that meets the minimum criteria of current guidelines [19].

Even though highway design guidelines are continuously evolving, there are still several outstanding concerns. How safe is a proposed design? How do roadway elements affect the safety level of a proposed design or its alternatives? What are the safety consequences of deviation from design guidelines? Is road rehabilitation an economically feasible alternative to improve the safety of an existing highway? Answering questions related to the safety of a proposed design is not an easy task since the existing design guidelines are not capable of providing a measure of the safety or the reliability of an existing road or proposed design [4, 19, 20].

The recent editions of design guides refer designers to the Highway Safety Manual (HSM) for information on the substantive safety impacts of design [21]. The HSM provides a predictive methodology to quantify the expected number of collisions of a road facility under existing road conditions and conditions that have not yet been implemented. This predictive procedure is used to estimate the anticipated number of crashes at an individual site after a highway is divided into homogenous sites with similar characteristics such as road segments or intersections. The evaluation procedure could vary by the type of road element being analyzed. The HSM prediction models estimate the expected number of collisions at an individual site relying on regression models (i.e., SPFs) developed using data of a large number of similar sites. These safety performance functions are usually a function of a few variables such as Average Annual Daily Traffic (AADT) volumes and roadway segment length.

Although this procedure can be useful in many design-related situations, it relies on historical collision records at similar sites and on SPFs to be developed. Thus, this approach has limited utility when used as a prediction tool when designing road facilities where data about

similar sites are not available or inaccurate. More importantly, using this approach, a road facility will still have to be designed according to the current deterministic approach suggested by design guidelines, and it can then be evaluated when regression models (i.e., SPFs) about similar locations are available, knowing that these similar sites were designed and constructed following that deterministic approach that does not account for uncertainties in design inputs. Therefore, there is a need for a framework that can be used to assess the risk directly connected to the suggested design by highway guidelines without the reliance on data about sites similar to the road facility being designed. The ultimate goal of a more reliable approach is to have similar sites constructed based on a safety-based design approach with the availability of SPFs about these sites in later stages. In this case, these SPFs can be used to assess the safety risk associated with proposed design alternatives following a safety-based design approach.

The main concern with the current design guidelines is that the provided level of safety is largely unknown, and safety is not explicitly considered as a design input [22, 23]. As a result, when a road is designed following the requirements of design guides, it is implicitly assumed to be a safe design and intended to provide a good, but unknown, level of safety [24, 25]. Moreover, when design values are selected, they are often considered to be on the conservative side resulting in an uneconomic design [16, 26]. Using these cautious values would increase the construction costs, becoming a hurdle towards the overall cost-effectiveness of road projects. There is little to no investigation into the consequences of deviating from the values provided by the current practices of roadway design [5, 27, 28]. Although safety levels can be maximized by applying a higher limit, road designers are often constrained by a limited right-of-way. The design output in

such a case is usually applying the minimum design requirements. When a designer has to make critical choices, the existing design guidelines do not provide information about the safety consequences for making such decisions [29, 30]. To address this concern, safety should be explicitly considered as a design input and safety-based design charts should be developed and utilized. Adopting a performance-based design approach could help road designers in quantifying the safety levels of different design alternatives and investigating the cost-effectiveness of various dimensioning scenarios.

1.1.2 Accounting for Uncertainties in Design Guidelines

Another big concern regarding current guidelines is that there are various sources of uncertainty that affect the design process. First, even though several design inputs such as vehicle operating speed and perception and reaction time are stochastic variables, they are currently assumed to be deterministic and derived from probability distributions to conservatively represent the population of road users [31]. The selection of such values is typically not based on quantitative safety measurement with known safety margins. This approach ignores the stochastic nature of design inputs assuming near worst-case scenarios for design inputs which could result in uneconomic designs [5, 32]. Researchers emphasized the presence of major issues due to the inescapable randomness in design variables and recommended adopting an integrated probabilistic analysis and reliability theory into the highway design process [5, 28, 30, 33, 34].

More so, highway design guides, such as AASHTO and TAC, were produced based on a combination of empirical research, experience, and engineering judgment [5]. For example, the selection of model forms, parameters, and inputs to design a certain element is based on

engineering theories and research [35]. These uncertainties have led to unquantifiable levels of safety that are currently subject to criticism by researchers [22, 23]. A common approach to account for this uncertainty is to use conservative values and apply the upper limits proposed by design guides, however, the selection of these limits is not based on a defensible framework and the safety margin remains unknown [35]. Moreover, applying the upper limits of design values could lead to higher costs of highway construction projects.

The above discussion underlines the need to address and account for uncertainties in design in order to lead to a more realistic design procedure. Although it is impossible to avoid uncertainties when designing roadways, it can be estimated and accounted for using the reliability theory which aims to quantify the level of uncertainty involved in highway design. Reliability theory is a part of the probability theory that offers a framework to road safety professionals to address the safety implications of deviation from a particular design. In structural engineering, the reliability theory is used to estimate the probability of failure or collapse corresponding to having applied loads (demand) greater than the structure resistance (supply). Navin adopted a terminology for this probability in highway engineering as the probability of non-compliance (P_{nc}) [24]. This probability is a measure of non-performance (i.e., non-compliance) and can be defined as the probability that a particular element fails to perform as intended.

Utilizing reliability analysis in road geometric design allows design engineers to investigate the influence of each individual element on the overall design. This was emphasized by Haukass [36] who indicated that using reliability analysis can help rank design inputs of a design problem according to their relative importance and influence in the design output, allowing targeting the

most important inputs to improve the overall model. He also emphasized that using the output of the reliability analysis, which is the P_{nc}, can be used in the decision-making process when comparing different design alternatives and can also be used in calibrating reliability-based design charts.

1.2 Problem Statement

As discussed, current highway design guidelines adopt a deterministic design approach which ignores the importance of the probabilistic nature of design inputs [16, 37]. The deterministic approach adopts near worst-case scenarios to determine a specific conservative value for each factor involved in the design model which leads to uneconomic design solutions. Even when using conservative values, this approach lacks the explicit consideration of safety and does not account for the variability in driver behaviour [7]. Generally, road designers assume that designs that fulfill the minimum requirements of the guidelines are inherently safe. However, the safety performance of the design output proposed by this deterministic approach is unknown. Also, there is little knowledge about the safety implications of deviating from standard requirements (e.g., providing sight distance or curve radius lower than standard values) [27, 28, 31, 38]. More so, current guidelines of highway geometric design do not account for uncertainty in design parameters. Design guides treat design inputs such as operating speed, perception and reaction time (PRT), and friction coefficient as deterministic parameters ignoring their stochastic characteristics [32, 35, 39].

The shortcomings of the deterministic design approach demonstrate the need for a performance-based design methodology or a supplementary framework that accounts for uncertainty in design inputs and explicitly considers the safety in the design stage. Reliability analysis has been considered as a firm approach to account for uncertainties in design parameters by treating them as random variables. In this approach, the reliability theory is used to quantify the risk associated with deviation from specific design values. This risk is generally referred to as the probability of non-compliance (P_{nc}), which is generally the probability that the supply provided by a design is exceeded by the demand. To a highway designer, the P_{nc} can be defined as the probability that a proposed design element (e.g. provided sight distance) would not be sufficient to meet the needs (i.e., required sight distance) of the driver population [25, 27]. For example, a P_{nc} of 0.30 associated with sight distance compliance mode indicates that 30% of the time, drivers would have insufficient sight distance. Using a probabilistic design approach enables estimating the expected risk levels associated with proposed designs, which can not be provided by current deterministic design guidelines. More so, risk values (i.e., P_{nc}) associated with different road elements such as horizontal curves can be linked to related historical collisions providing designers with a scientific-based tool to assess the influence of proposed designs on safety. Risk levels can also be used as targeted safety levels enabling the calibration of probabilistic design guidelines.

The majority of previous work on reliability-based highway design focused on evaluating the risk associated with horizontal curves. Several studies utilized reliability analysis to quantify the risk corresponding to insufficient sight distance on curved segments considering the non-compliance resulting from one failure mode, in which the non-compliance occurs when the

Available Sight Distance (*ASD*) is less than the required sight distance [16, 26, 27, 39-42]. Previous studies emphasized the need for future work that considers three main shortcomings related to the assessment of the *ASD*, non-compliance modes on curved segments, and relating the P_{nc} to safety.

First, the importance of assessing the *ASD* in a three-dimensional (3D) world has been demonstrated in previous research [26, 43, 44]. However, except for a handful of studies, the majority of previous work on the reliability-based design of horizontal curves have used a two-dimensional (2D) sight distance assessment in which the *ASD* is calculated using a 2D projection approach based on the radius and lateral clearance of the curve. Assessing drivers' visibility based on 2D sight lines does not simulate the real driving environment. It could also be inaccurate since sight distance can be restricted by horizontal curves combined with vertical curvature or by any other 3D obstacles such as roadside barriers.

Second, the majority of previous studies focused on assessing the risk for only one mode of non-compliance (i.e., limited *ASD* using 2D projection). For example, Ibrahim and Sayed quantified the risk associated with insufficient 2D sight distance on horizontal curve segments [5]. Many other studies also estimated the risk associated with sight distance limitations [16, 27, 35, 41]. However, non-compliance on curved sections can occur due to more than one noncompliance mode such as insufficient sight distance and vehicle skidding [30, 31]. In this case, utilizing a multi-mode, also known as system reliability-based approach, that considers multi-mode of non-compliance and 3D *ASD* assessment is required.

Third, the relationship between the reliability measure (i.e., P_{nc}) and the collision frequency is not well established. There have been a handful of studies that explored the relationship between

risk levels and collision frequency based on 2D *ASD* calculations [6, 7, 34]. However, the link between the risk measure (P_{nc}) and collision frequency utilizing real-world 3D sight distance assessment and using system reliability (i.e., insufficient sight distance combined with vehicle skidding) remains unexplored [45, 46]. Understanding this relationship will provide significant insights into the reliability of a proposed road design and its influence on road safety in terms of collision impacts.

More so, although previous work has quantified the risk (P_{nc}) associated with horizontal curves with some recent studies developed relationships between P_{nc} and safety, the P_{nc} remains a statistical measure that is not informative enough to roadway designers. It does not provide them with enough information on the geometric attributes of road elements and their interactions with safety. The relationship established between reliability measures and safety focused entirely on developing a direct link between the P_{nc} and collisions without addressing either the potential direct influence of roadway geometric attributes on crashes or the indirect effect geometric features could have on collisions through their effect on the P_{nc}.

In other words, although some previous studies on horizontal curves showed that there is a statistically significant relationship between P_{nc} associated with limited sight distance and collisions, it is unknown whether or not curve attributes confound this relationship by directly affecting safety or influencing safety through their effect on $P_{nc.}$ Thus, there is a need to explore the underlying relationships between geometric attributes of roadway design elements, uncertainty, and safety. The impacts of geometric design attributes on the P_{nc} as well as the direct and indirect (through the impacts on P_{nc}) impacts of those attributes on safety need to be modelled

and understood. Understanding the impacts of geometric characteristics on P_{nc} and safety is crucial for design professionals. Investigating such relationships could significantly improve the understanding of the impacts of various curve attributes on non-compliance and safety.

Finally, the majority of previous studies have relied on conventional techniques to extract curve features (i.e., radius, deflection angle, etc.) such as using as-built documents or AutoCAD drawings. Generally, there is a lack of as-built plans for large highway networks as well as a lack of information on roadside features (e.g., vegetation) that can obstruct sight distance and are not normally documented on as-built drawings. In many cases, when these sources of curve attributes are available, they could be outdated or some information about curves might be missing or need to be calculated using other curve attributes [47]. Using outdated and limited information could affect the resulting P_{nc} and provide biased results about the associated safety levels. Also, implementing a large-scale reliability analysis using conventional data sources is challenging due to the large amount of manual work needed to extract the required information on all the study curves, assuming that data availability was not an issue. It is believed that the lack of accurate and/or large-scale data sets has led many previous studies to use either simulated curves or limited datasets with short road segments [25, 27, 30, 39]. Therefore, having an accurate and preferably large-scale dataset is necessary to ensure proper consideration of risk levels associated with roadway elements.

1.3 Research Objectives & Significance

While addressing the previously discussed research gaps, the ultimate goal of this thesis is to demonstrate one significant application of using reliability analysis in highway engineering: the

calibration of safety-based design charts for horizontal curves. Meeting such a goal requires achieving multiple objectives as detailed in the next few paragraphs:

- The main objective of this thesis is to apply a multi-mode (system) reliability analysis to first calculate the probability of non-compliance (P_{nc}) of limited 3D *ASD* on horizontal curves combined with the probability of vehicle skidding, considering the effect of longitudinal grades (i.e., vertical alignment). Considering multiple modes of noncompliance is a better representation of the actual demand on the road. Also, using 3D sight lines assessment provides a better representation of the driving environment. It takes into account the potential effect of various obstacles that exist in the real environment such as roadside barriers, cut slopes, trees, etc. and which can obstruct the driver's sight line and cannot be captured using a 2D assessment approach.
- The second objective is to develop SPFs to link the system P_{nc} to historical collision frequency using Full Bayes Multivariate Poisson Log-normal (MVPLN) regression. Using the MVPLN help account for any potential correlation between different severity levels (i.e., property damage only, *PDO*, and injuries plus fatalities, *I*+*F*) [48]. Establishing a link between the system P_{nc} and safety is a major contribution of this work. Developing such a relationship would help accelerate the adoption of probabilistic design guidelines. It would help quantify the safety implications corresponding to proposed designs and facilitate the ability to evaluate the risk associated with deviation from current design guides. Moreover, developing SPFs that incorporate the probability of noncompliance corresponding to more than one mode of noncompliance can explain the influence of all possible modes of failures

on the collision occurrence and can improve the ability of the model to predict road collisions while providing a better understanding of the sources of variations in the model output.

- The third objective is the calibration of safety-based design charts for horizontal curves. The calibrated performance-based design charts relate geometric and traffic characteristics of horizontal curves such as the operating speed and the *ASD* to the multi-mode P_{nc} and road collisions. The charts are calibrated using a system reliability approach and utilizing 3D *ASD* assessment. An example is discussed to demonstrate the feasibility of using the developed charts to estimate the expected safety benefits, in terms of collision reductions, associated with potential geometric improvements of a curved segment with design limitations.
- To help understand the direct and/or indirect influence of different curve attributes on safety, one of the objectives is to study the relationship between P_{nc} and collisions while accounting for curve attributes that could mediate and confound this relationship. In other words, the objective is to model the relationship between P_{nc} and collisions while also modelling the relationship between curve attributes and collisions to determine whether or not curve attributes affect collisions directly or indirectly (through their effect on P_{nc}). This is achieved through using a path analysis approach, a form of Structural Equation Modelling (SEM), to simultaneously model the relationship between P_{nc} and safety, curve attributes and safety, and the effect of curve features on P_{nc} and whether or not this entails an indirect influence on collision frequency. More specifically, the aim here is to explore

the indirect influence curve attributes can have on collision frequency through their impacts on P_{nc}, which is a practical motivation behind this objective.

- To provide an accurate and rich database for the reliability analysis, this research utilizes a set of novel algorithms to extract horizontal and vertical curve features and assess the available sight distance (i.e., 3D *ASD*) on curved sections using Light Detection And Ranging (LiDAR) data. The developed algorithms facilitate the automated detection of the presence of curved segments on highways and the extraction of their attributes using 3D LiDAR point clouds. Using this approach, horizontal curves were detected, and road geometry information was extracted from 5,802 kilometers on 76 highways in Alberta, Canada. This enables access to a large amount of data and facilitates large-scale and reliable use of the reliability theory on horizontal curves. In fact, the benefits of the automated and efficient manner in which this data is extracted extend far beyond using the dataset in reliability analysis. The developed novel algorithms provide both transportation agencies and researchers with tools that enable access to an abundant amount of information about geometric characteristics of highway infrastructure. The developed algorithms can be used to build a reliable inventory of information on horizontal and vertical alignments that could be of great value in geometric and safety assessments of existing highways along with its readiness for use in several transportation studies.

In summary, this research contributes to the body of literature by developing a link between theoretical noncompliance and historical collision data using 3D sight distances and system reliability analysis. The calibration of performance-based design charts demonstrates the value of

utilizing reliability analysis in highway design. The ability to evaluate the trade-offs between the cost of rehabilitation projects and expected safety levels requires the availability of a quantitative method to assess the safety of proposed modifications. As an example of geometric design code calibration, the calibrated charts can offer road designers the ability to estimate the safety benefits of proposed geometric improvements. The proposed charts can help transportation agencies to study the economic feasibility of rehabilitation projects of horizontal curves, especially those with high collision frequency associated with the studied non-compliance modes. The calibrated charts provide the opportunity of quantifying the safety consequences of deviation from geometric design guidelines.

The developed reliability-based design framework incorporates both reactive and proactive approaches to road safety by developing SPFs incorporating reliability indices and by providing a tool that can be used in the design stage to assess the risk associated with different design alternatives. From a practical perspective, the thesis provides predictive tools that can be used by road designers to assess the risk associated with different design alternatives and allow them to have a better understanding of the safety margin corresponding to each design option. It also can help in quantifying the safety implications of modifying the geometric conditions of existing roads. Overall, this research is a step forward towards developing performance-based design guidelines.

1.4 Research Methodology & Organization

To accomplish the research objectives, the workflow presented in Figure 1 was followed. The first stage involved detecting horizontal curves and extracting their geometric attributes using LiDAR data. To achieve this, a set of novel algorithms were developed, tested, and used to obtain

information on horizontal and vertical alignments along with assessing the *ASD* on highway curved sections. Collision data of the studied segments were then combined with their geometric and traffic data to establish the dataset needed for reliability calculations.

The second stage included utilizing the reliability theory to assess the risk associated with the studied non-compliance modes. The risk was estimated for each horizontal curve while considering the probabilistic nature of design inputs. This was followed by establishing a link between risk levels and safety (i.e., historical collisions). Design charts were then calibrated to relate curve geometric and traffic characteristics, to risk levels and safety using the developed SPFs. Finally, SEM was used to simultaneously model the relationship between P_{nc} and safety while accounting for curve attributes that could mediate and confound this relationship to determine whether or not curve attributes affect collisions directly or indirectly (through their effect on P_{nc}).

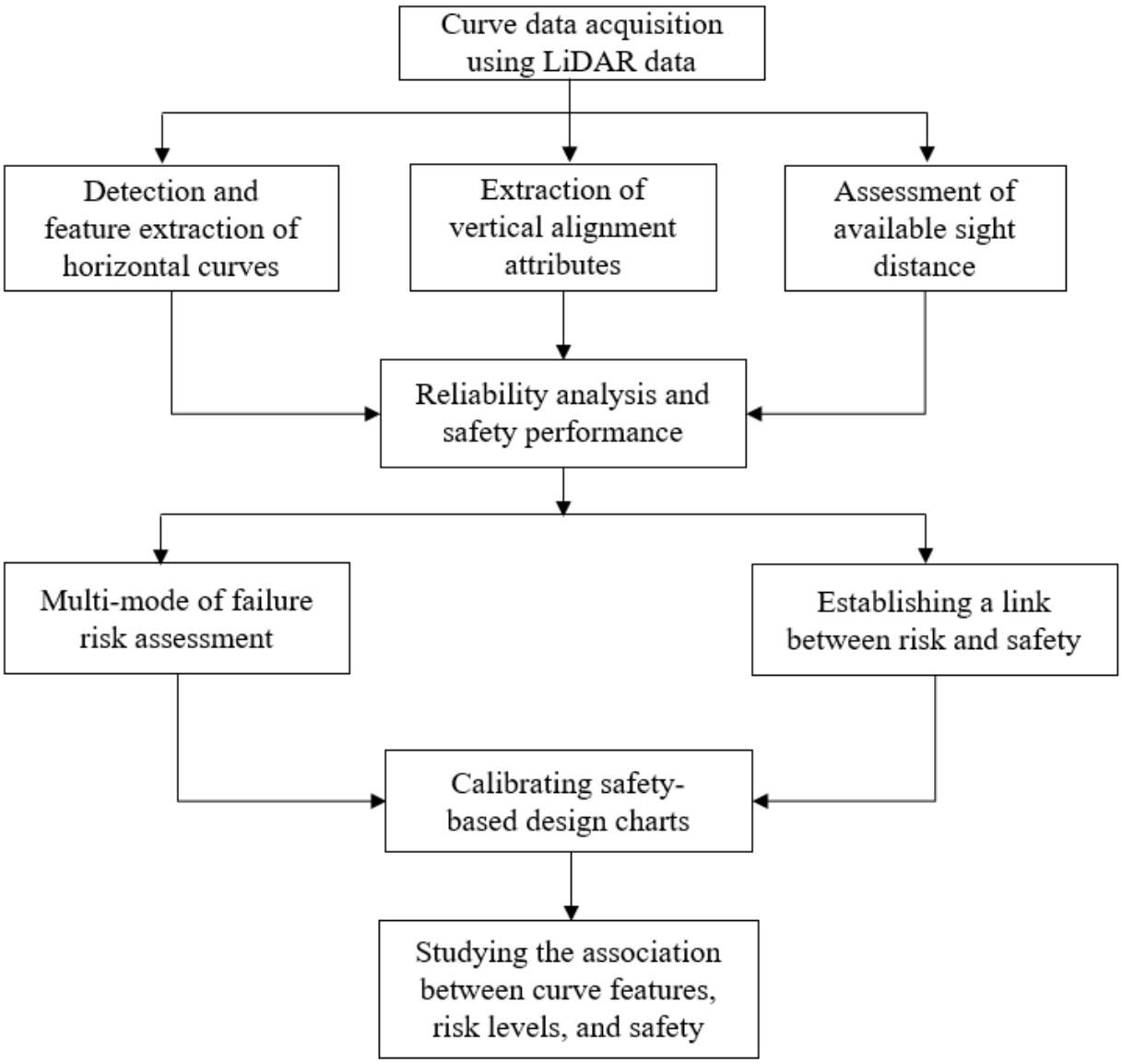

Figure 1: A summary of the research framework

1.5 Thesis Structure

The remainder of the thesis is divided into seven chapters that are organized in the following manner.

Chapter 2 presents a literature review of the reliability theory and previous studies on the reliability-based design of horizontal curves. It also provides background information on LiDAR data and summarizes the efforts of previous work on automated detection and extraction of curve features including sight distance assessment.

Chapter 3 is dedicated to utilizing LiDAR technology in data acquisition and establishing an inventory of curve information for reliability calculations. It provides details on different algorithms that were developed to detect horizontal curves on highways and extracts their attributes including horizontal alignment features and vertical grades. Moreover, the chapter includes information on current practices of sight distance assessment, highlights that using 2D visibility assessment could lead to misleading conclusions and presents an automated method for assessing sight lines in a 3D environment. The chapter contains a detailed description of the extraction procedure of the developed algorithms, the results of algorithm testing and validation as well as applying the developed procedure on a large scale. This Chapter is a combination of research that has been published in *Transportation Research Record, the Journal of Transportation Research Board* and the *International Journal of Remote Sensing*:

- **Shalkamy,** A., El-Basyouny, K., & Xu, H. Y. (2020). Voxel-based methodology for automated 3D sight distance assessment on highways using mobile light detection and ranging data. *Transportation Research Record*, *2674*(5), 587-599.

- **Shalkamy,** A., Karsten, L., Gargoum, S., & El-Basyouny, K. (2020). A framework to detect horizontal curves and assess their geometric properties from remotely sensed point clouds. *International Journal of Remote Sensing*, *41*(21), 8328-8351.

Chapter 4 is devoted to using reliability analysis to quantify the risk associated with insufficient sight distance and vehicle skidding on highway curved segments. The chapter presents detailed information on Limit State Functions (LSF) as well as random and deterministic variables associated with each LSF. Also, it includes details on using Monte Carlo simulation to estimate the system P_{nc}. The closing section of the chapter presents the results of risk assessment and their implications.

Chapter 5 is dedicated to the safety-based design of highway horizontal curves. It presents developing safety performance functions that relate curve attributes to the system reliability outcome. It then provides detailed information on calibrating design charts for horizontal curves where curve geometric and traffic characteristics are linked to expected collision frequency. Moreover, the chapter presents examples of using the developed design charts to predict the expected collision frequency associated with a proposed design and using the charts in quantifying the potential safety improvements of modifying curve geometry. Also, the chapter discusses the difference between the calibrated charts and the current design guidelines and discusses the feasibility of developing similar charts by other jurisdictions.

- The work presented in Chapters 4 and 5 was divided into two papers, one of which has been published in *the Journal of Accident Analysis and Prevention* while the other one has been published in the *Journal of Transportation Safety and Security*:

- **Shalkamy**, A., & El-Basyouny, K. (2020). Multivariate models to investigate the relationship between collision risk and reliability outcomes on horizontal curves. *Accident Analysis & Prevention*, *147*, 105745.
- **Shalkamy, A.**, & El-Basyouny, K. (2021). Calibrating Safety-based Design Charts for Horizontal Curves using System Reliability Analysis and Multivariate Models. *Journal of Transportation Safety & Security*. DOI: 10.1080/19439962.2021.1992552.

Chapter 6 explores the association between P_{nc}, curve features, and safety. It presents using SEM to model the relationship between P_{nc} and safety while assessing the indirect effects of curve features on collisions that could be mediated through P_{nc}. A version of this chapter has been published in *the Journal of Accident Analysis and Prevention:*

- **Shalkamy**, A., Gargoum, S., & El-Basyouny, K. (2021). Towards a more inclusive and safe design of horizontal curves: Exploring the association between curve features, reliability measures, and safety. *Accident Analysis & Prevention*, *153*, 106009.

Chapter 7 presents a summary of the research conducted in this thesis and includes a discussion of the contributions of this work as well as highlighting research limitations and potential areas for future research.

2 LITERATURE REVIEW

This chapter provides an overview of the reliability theory and previous studies on the reliability-based design of horizontal curves. It also presents background information on LiDAR data, horizontal curves and sight distance assessment, and summarizes previous work on curve detection and feature extraction including sight distance assessment.

2.1 Reliability Analysis

2.1.1 Reliability Theory

The term reliability usually refers to the complement of the P_{nc} as shown in Equation 1. In the context of highway design, researchers define the P_{nc} as the probability that a particular design does not meet the standard requirements.

$$Reliability = 1 - P_{nc} \quad (1)$$

Reliability can generally be defined as the ability of a system to accommodate the demand of a particular design element against the capacity of this element [49]. The basic elements of a reliability problem are two elements namely supply (S) and demand (D). The performance function (G) of a system is conventionally expressed as the difference between S and D and noncompliance occurs (i.e., G yields negative values) when the demand exceeds the supply. The performance function (also referred to as the limit state function; LSF) of a reliability problem can be written as follows:

$$G\ (x_1, x_2, \ldots, x_n) = S(x_1, x_2, \ldots, x_n) - D(x_1, x_2, \ldots, x_n) \quad (2)$$

where G is the performance function or LSF; S stands for Supply; D stands for Demand; $X_1, X_2, \ldots, X_n$ are variables (usually random variables) of supply and demand.

The outcome of the analysis of a reliability problem is usually the probability of noncompliance (P_{nc}) as expressed by the following equation:

$$P_{nc} = P\ (G\ < 0\ ) = \int_{\ldots..} \int_{G \leq 0} f(x)dx \quad (3)$$

where P_{nc} is the probability of noncompliance; f_x is the joint probability density function (PDF) for the random variables; and the integration is performed over the unacceptable domain (i.e., where D exceeds S)

Another way of describing the reliability of a system or a product is the reliability index (β) as shown by Equation 4. The reliability index is defined as the ratio between the margin of safety and the combined variance where the margin of safety is the difference between the expected value of the supply and that of demand [4].

$$\beta = \frac{E(S)-E(D)}{\sqrt{VAR\ (S)+VAR\ (D)}} \quad (4)$$

Where β = the reliability index; E(S) = expected value of supply, E(D) = expected value of demand; VAR(S) = variance of supply; and VAR(D) = variance of demand

The probability of noncompliance (P_{nc}) can also be calculated as follows:

$$P_{nc} = \phi\ (-\beta) \quad (5)$$

where $\phi(.)$ is the standard normal cumulative probability distribution function.

If the problem has only one LSF (e.g., sight distance), it is usually referred to as a component reliability problem or a single mode of non-compliance. When there are two or more

LSFs (e.g., G_1 for sight distance and G_2 for vehicle skidding), this is considered a system (multi-mode) reliability problem.

2.1.2 System Reliability Analysis

System reliability is concerned with design situations where two or more LSFs are defined. For example, if it is assumed the non-compliance on horizontal curves could result from sight distance deficiency and vehicle skidding, there would be two LSFs, one for each design criteria. In general, there are two types of system reliability commonly considered in engineering practice: (i) series system reliability problem in which the system failure occurs if any of the multiple LSFs yield negative outcomes and (ii) parallel system reliability problem where the system fails only if there is a failure in all the modes (i.e., all LSFs are negative) concurrently. The P_{nc} of the series and parallel systems can be calculated, as indicated in Equation 6 and Equation 7, respectively [50].

$$P_{nc} = P\left[\bigcup_{k=1}^{k} g_k(x) \leq 0)\right] \quad (6)$$

$$P_{nc} = P\left[\bigcap_{k=1}^{k} g_k(x) \leq 0)\right] \quad (7)$$

where k represents the number of limit state functions; and $g_k(x)$ is k$^{\text{th}}$ limit state function.

In the case of horizontal curves, the non-compliance of the system is assumed to occur if there is either insufficient sight distance or potential for vehicle skidding on the curve (i.e., two LSFs). Thus, the system reliability presented in this thesis is based on a series system reliability problem. It is worth noting that the system probability of non-compliance here is related to the design deficiencies, not individual drivers. In other words, combining the two design criteria (i.e., limited sight distance and vehicle skidding) is based on the assumption that sight distance can be

limited a long a section where vehicle skidding could happen (i.e., side friction demand is greater than the side friction supply).

In a series system reliability problem with two modes of non-compliance, the probability of non-compliance can be calculated as follows:

$$P_{nc\ system} = P_{nc1} + P_{nc2} - P_{nc1,nc2} \quad (8)$$

where $P_{nc\ system}$ is the probability of non-compliance of the system; P_{nc1} is the probability of non-compliance of the first mode (i.e., insufficient sight distance); P_{nc2} is the probability of non-compliance of the second mode (i.e., vehicle skidding); and $P_{nc1,nc2}$ is the joint probability of failure (i.e., the intersection of the two failure events).

The joint probability of failure is the likelihood that the two LSFs are violated at the same time. Assuming the failure in the first mode is event A and the failure in the second mode is event B, there could be two scenarios. If A and B are assumed to be statistically independent, the joint probability can be calculated using Equation 9. Otherwise, the joint probability can be calculated using the conditional probability principle, as shown in Equation 10. Although some previous studies assumed that failure modes on horizontal curves were independent [32], recent studies considered that the modes of non-compliance could fail at the same time and accounted for the correlation between LSFs [30, 31]. Thus, this thesis assumes that the two LSFs are correlated; hence, the conditional probability is used to calculate the joint probability according to Equation 10.

$$P_{nc1,nc2} = P(A \cap B) = P(A) * P(B) \quad (9)$$

$$P_{nc1,nc2} = P(A \cap B) = P(A|B) * P(B) \quad (10)$$

where $P(A)$ is the probability that the first mode fails; $P(B)$ is the probability that the second mode fails; $P(A \mid B)$ is the probability that the first mode (i.e., event A) will fail given the knowledge that the second mode (i.e., event B) has already failed.

2.1.3 Previous Studies on Reliability-based Design

Reliability analysis is a commonly used approach in risk analysis in structural engineering and has been recently advocated as a powerful tool in transportation engineering with an emphasis on roadway design [49]. Navin cited many concerns regarding the implicit level of safety included in highway design guides [33, 51]. The study provided meaningful arguments in favor of using reliability analysis in road design. The author investigated the possibility of quantifying the level of safety built into various roadway components. The method used the basic equations of highway design and assumed that all variables are independent and have a normal distribution. It was indicated that the safety index, represented by the reliability index, may be estimated using the proposed method, and introduced a generic equation to be used in uncertainty-based studies in roadway design.

Faghri and Demetsky [52] showed the potential of using reliability theory to assess the risk associated with sight distance limitations at railroad grade crossings. Easa [53] proved that using reliability analysis is a valuable tool that could be used to design a specific feature when he used a probabilistic approach to successfully design the intergreen (yellow plus all-red) time interval at signalized intersections. The goal was to redesign the intergreen time to eliminate the issue of having the driver not be able to stop or safely clear the intersection. In order to solve this research

problem, the author used the concept of equating the stopping sight distance with the distance required to clear the intersection. As a result, the author developed a closed-form model to estimate the intergreen times. In a different study, Easa [54] proposed a probabilistic method for sight distance design at railroad crossings. The method accounted for the randomness in the design inputs and provided information about the probability of noncompliance of the design. The author indicated that the results of this method were generally conservative.

As discussed in previous sections, a poor design of horizontal curves may lead to significant safety problems. Several efforts advocated the use of reliability theory to assess the risk associated with the design of horizontal curves. Echaveguren, Bustos [55] introduced a method using reliability theory to calculate the safety margin of an existing horizontal curve. The margin of safety is represented by the reliability index. The results showed that horizontal curve radius and skid resistance had the highest impact on the probability of noncompliance while the superelevation rate had little influence. Dhahir and Hassan [56] used reliability analysis to estimate the probability of non-compliance based on the difference between available and demanded lateral friction on horizontal curves. The results of the study can be used to estimate the probability of non-compliance on a specific horizontal curve to determine the minimum radius required for a certain risk value. The findings indicated that the minimum radii values recommended by AASHTO would result in inconsistent values of probability of non-compliance for different design speeds.

De Solminihac, Echaveguren [57] noted that design guides provide deterministic values considering the behaviour of drivers is uniform. In order to address this, the authors proposed a

methodology to estimate the risk associated with design components. They calculated the skid resistance reliability index for low volume roads. You, Sun [58] conducted a comparative study using two performance functions (skidding and rollover) on horizontal curves. Each mode of failure was analyzed separately as a single-mode reliability problem and the results showed different values of probability of failure for each one. Himes and Donnell [49] used reliability analysis to assess vehicle skidding (resulting from the demand side friction exceeding design side friction) on horizontal curves. The results showed that the values provided by current design guides are sufficient considering no effects of vertical grades. It was also concluded that using a reliability index of 3.0 is appropriate in the probabilistic approach of horizontal curve design. Dhahir and Hassan [28] proposed a reliability-based framework for the design of horizontal curves considering vehicle dynamic stability and driver comfort. The authors recommended future work to enhance the proposed design framework through developing safety performance functions to relate safety to reliability measures.

There are multiple studies focused on using the reliability theory to estimate the risk associated with limited sight distance on highways using 2D sight distance assessments. Khoury, Hobeika [59] used Monte Carlo simulation techniques and risk analysis to develop a procedure to estimate the risk associated with limited passing sight distance on straight road segments. The study indicated that AASHTO's model for passing sight distance (PSD) overestimated the PSD requirements. Richl and Sayed [25] applied reliability theory to assess the risk associated with varying sight distance restrictions on a set of horizontal curves. The authors used horizontal curves with narrow medians as when the median is narrow, a driver may not be able to stop within the

available sight distance which is restricted by the median barrier. The probability of not being able to stop was estimated for different sigh distance limitation scenarios. The study concluded that the available sight distance is insufficient when there is a narrow median combined with a sharp horizontal curve. The authors recommended future research to develop a link between P_{nc} and safety.

Wood and Donnell [41] used 2D *ASD* calculations to compute the probability that a driver would not stop within the *ASD* in case of approaching a curved segment and within a curve. The results showed that the probability that drivers would not have adequate stopping sight distance was greater when approaching the curve than along the curve. The study encouraged future work to explore whether there is a relationship between reliability measures and collisions. Sarhan and Hassan [26] used reliability analysis to calculate the horizontal sight offset on horizontal curves considering the effect of the vertical alignment. Demonstrating the feasibility of developing probabilistic design charts, the authors calibrated a design chart for a 400 m horizontal curve combined with vertical curves where the chart covers a range of design speeds from 90 to 130 km/h. The study emphasized that using 2D-based sight distance calculations can lead to inaccurate results since sight distance could be limited as a result of both vertical and/or horizontal obstructions. The authors recommended further research on exploring the relationship between risk levels and safety and using real road segments.

Sarhan and Hassan [16] used a reliability-based approach utilizing Monte Carlo Simulation to estimate the probability of hazard (POH) resulting from insufficient sight distance. The method was applied on an assumed 1-km road segment using 2D and 3D sight distance projections where

the sight distance was assumed to be restricted by the side slope. The results showed that the current deterministic approach is conservative resulting in low POH values indicating that the current design practice may be uneconomic. The study however showed the importance of considering the effects of the vertical alignment on horizontal curves. The authors recommended further research on the safety implications of different risk levels.

Based on a 2D projection of sight lines and with no relation to safety, a few studies proposed a framework for calibration of design s guidelines as well as modifying existing conditions. Ismail and Sayed [35] proposed a framework for calibrating design guidelines for vertical crest curves to yield consistent risk (probability of non-compliance) values. Hussein and Sayed [27] presented a method to calibrate design charts for the middle ordinate of horizontal curves considering one mode of non-compliance (i.e., insufficient two-dimensional sight distance). The results of the study showed that the calibrated values are lower than the values proposed by AASHTO [17] and the difference between the two increases with the decrease of horizontal curve radius. The authors concluded that design guidelines are conservative at high design speeds and have inconsistent risk levels for different design speeds. As an example of applying reliability theory to redesign roadway elements, Ismail and Sayed [38] used multi-objective optimization to investigate the possibility of reducing the risk associated with limited sight distance on nine horizontal curves by re-dimensioning of cross-section elements. Using reliability analysis, an average risk reduction of 25% was achieved providing efficient use of the available right of way and suggesting re-dimensioned cross-sections with lower and more consistent risk levels.

Ibrahim and Sayed [42] also used reliability analysis to re-dimension cross-section elements of cross-sections where available sight distance is restricted, in order to minimize the overall risk associated with limited sight distance. The results showed that incorporating reliability risk measures (P_{ncs}) in optimizing cross-section elements resulted in a reduced expected number of collisions and consistent risk levels for both directions of travel. Ismail and Sayed [39] used different case studies to study the effect of sight distance limitations on horizontal curves, quantify the risk caused by deviation from design guidelines, and investigate the variation in the associated risk among different curved segments. For the case studies used by the authors, it was concluded that the proposed design was associated with high-risk levels due to sight distance restrictions and the risk values found to vary significantly among different road segments. The authors recommended more research on creating a link between collision frequency and risk measures (P_{nc}).

In response, a link between reliability measures and collisions was established in less than a handful of studies based on a single mode of non-compliance (i.e., insufficient sight distance) and 2D sight distance assessment. Ibrahim and Sayed [6] were the first to develop statistical models that relate safety to the P_{nc} associated with insufficient sight distance using a 2D projection where the *ASD* is calculated based on the available lateral clearance and curve radius. First Order Reliability Method was used to estimate the risk associated with each horizontal curve. Two groups of Negative Binomial SPFs were developed with and without the risk measures (P_{nc}). The developed models were statistically significant, and the results showed that the developed collision prediction models included P_{nc} significantly outperformed the traditional group of models that

excluded the risk measures. It was also found that the predicted number of collisions increases with the increase in the probability of non-compliance. Jesna and Anjaneyulu [34] used two-dimensional sight distance as a single mode of noncompliance on horizontal curves and estimated the corresponding risk measures. The analysis was also repeated separately to assess the risk associated with the superelevation and extra widening provided on horizontal curves. The authors developed safety performance functions (SPFs) incorporating reliability indices represented in the reliability index. Safety evaluation criterion was developed and EPDO was used as a safety measure. The results indicate that the value of EPDO decreases with the increase of the reliability index In a recent study, Dhahir and Hassan [60] used reliability analysis utilizing naturalistic driving data to develop SPFs that relate historical collisions to risk levels associated with horizontal curves. The use of naturalistic driving data helped overcome limitations associated with the current practice of data collection and enabled considering the effect of weather and pavement conditions. The sight distance assessment in this study was based on 2D projection estimating the available sight distance based on lateral clearance (i.e., lateral obstructions) and curve radius. This group of studies generally emphasized the importance of using 3D sight distance assessment and considering multiple modes of non-compliance when developing a link between reliability measures and safety.

With most of the studies focusing on 2D sight distance evaluation, a limited number of studies quantified the risk associated with a single non-compliance mode (sight distance deficiencies) in a 3D world. used a Geographic Information System (GIS)-based software to calculate the *ASD* along a 12-km road segment. The authors then quantified the risk at locations

with sight distance deficiencies. They recommended future work to relate the P_{nc} to historical collision data on road segments and compare crash occurrences and severities. In another study, de Santos-Berbel, Essa [45] compared using 2D and 3D methodologies of sight distance estimation and then used reliability analysis to estimate the risk level (probability of noncompliance) associated with each sight distance modelling method and investigate the safety influence of using each estimation technique. The results indicated that there were significant differences between different sight distance modelling techniques in most cases. It was also found that the sight distance modelling approach could have a significant effect on the estimation of the probability of noncompliance. The authors emphasized the importance of using 3D modelling of sight distance when evaluating the risk associated with road design. Hassan and Easa [61] also developed a model to investigate the influence on sight distance design requirements in case of considering 3D sight distance instead of 2D projections. The results of this study indicated that the design requirements of 3D-based design may be significantly different from the values corresponding to using 2D-based design. The study concluded the need to use 3D-based design guidelines for sight distance modelling.

With most previous studies focusing on studying the risk associated with only one design limitation, Essa and Sayed [30] used a 2D-based reliability analysis approach to estimate the risk corresponding to two modes of non-compliance on highway curved sections. The authors used a case study of five horizontal curves to evaluate the risk resulting from considering two modes of noncompliance and compared the results with the results of a previous study of Hussein and Sayed [27] that considered only one mode of noncompliance. The results showed significant differences

in the probability of noncompliance in the case of using two modes of failure (i.e., noncompliance) instead of using only one mode of failure, especially for sharp horizontal curves. The study also evaluated the standard design of the five horizontal curves, and it was found that there are inconsistencies and significant variability in the risk associated with the standard design where the probability of noncompliance ranged from less than 1 to 80%. Since the study used two-dimensional sight distance in the analysis, the authors recommended using three-dimensional sight lines assessment in multi-mode reliability analysis and emphasized the significance of future research that investigates the relationship between the system reliability measures and collision frequency. The study also neglected the effect of vertical alignment (longitudinal grades) which needs further investigation.

In a different study by You and Sun [32], the authors developed a dynamic simulation model to investigate the reliability of vehicle stability on horizontal curves. The study focused on addressing the effect of vehicle skidding and vehicle rollover. It was indicated that the probability of rollover is minimal, and passenger cars are likely not prone to rollover. The results also showed that the probability of non-compliance decreases with the increase in superelevation rate, and it increases with the increase in longitudinal slope.

In a recent study, Alsaleh and Sayed [31] used a 2D projection to quantify the P_{nc} associated with three modes of non-compliance (insufficient sight distance, vehicle skidding, and vehicle rollover). The authors emphasized the importance of considering multiple modes of non-compliance on horizontal curves. However, the study showed that the vehicle rollover effect is negligible for passenger cars indicating that the P_{nc} values for a system of three non-compliance

modes are almost the same as the P_{nc} values associated with two modes of non-compliance. The authors recommended using 3D-based sight distance evaluation and system reliability along with developing SPFs to relate collision frequency to reliability outcomes

2.1.4 Discussion & Research Gaps

As evident from the review, there have been numerous studies that utilized the reliability theory to quantify the risk associated with current practices of horizontal curve design. However, there are fundamental shortcomings and research gaps that have been identified, emphasizing the need for further research. First, the majority of previous studies focused on assessing the risk for only one mode of non-compliance with a handful of studies adopting a multi-mode reliability-based design of horizontal curves using 2D sight distance assessment. As discussed, the failure to meet the driver's demand on horizontal curves may occur due to more than one mode of noncompliance. Moreover, using 2D sight distance calculations is unrealistic and does not represent the real conditions in the driving environment, where in many situations, the sight distance could be limited by the road vertical profile or by combined horizontal and vertical curves emphasising the importance of using 3D sight distance calculations in reliability analysis. Both using a 2D projection and a single mode of non-compliance were considered limitations in previous work that recommended further research on reliability-based design of horizontal curves using 3D sight distance considering multi-mode reliability analysis.

Second, the relationship between reliability measures and the collision frequency is not well established. The few studies that explored the relationship between P_{nc} and safety were based on 2D sight lines evaluation and a single non-compliance mode. Indeed, the link between the risk

measure (P_{nc}) and collision frequency utilizing real-world 3D sight distance assessment whether using system reliability or a single mode of non-compliance remains unexplored. To the best of the author's knowledge, no study, to date, has attempted the development of highway design charts while creating a link between proposed design guidelines and expected collision frequency. More so, no study, explored the interaction between curve geometric attributes, P_{nc}, and safety and whether or not curve attributes confound the relationship between P_{nc} and safety by directly affecting collision frequency or influencing safety through their effect on P_{nc}. This causes the P_{nc} to remain as a statistical number that does not provide enough information to roadway designers on the geometric attributes of road elements and their interactions with safety

Third, due to the unavailability of accurate as-built drawings of roadways, the majority of previous studies used either a limited number of horizontal curves or used computer programs to generate data sets to be used in the analysis. This could lead to using insufficient or outdated information of curve characteristics which could affect the resulting P_{nc} and safety leading to biased outcomes. It also makes implementing a large-scale reliability assessment challenging due to the large amount of manual work needed to extract the required information on a large number of sites, assuming that as-built drawings are available.

This clearly highlights the need for more research to help accelerate the move towards adopting a probabilistic approach for highway design. As discussed in the first chapter of this thesis, this research adopts a 3D safety-based multimode reliability analysis to demonstrate a considerable application of using reliability theory in highway engineering: the calibration of safety-based design charts for horizontal curves. The thesis also studies the interaction between

curve attributes, risk levels, and safety. This provides a framework on how risk levels could be translated into relationships that provide more information to highway designers on the influence of design elements on the expected safety level of the overall design.

In summary, despite the presence of several efforts on reliability-based design of horizontal curves, the review shows that more work is still required in this area. Developing a design framework with safety on its core provides a needed understanding of the relationship and interaction between proposed designs and their safety performance. The results of this work could be directly applicable to assess the risk associated with a proposed design in which the minimum requirements of design guides are not met, which is a situation, current design guides cannot provide a safety margin for. Finally, this research could be of great value to the field of highway design and road safety from both a practical and academic perspective.

2.2 Background on LiDAR Data

Light Detection and Ranging (LiDAR) is a remote sensing technology that utilizes light rays omitted from a laser scanning system to collect positional information about surrounding objects. The laser scanners constantly emit light rays at surrounding objects where the information about the scanned targets is collected based on the properties of the reflected light beams. Information collected about objects includes georeferenced spatial information, the intensity of returns, scanning angle, and time. The continuous scanning of objects around the scanners creates a 3D highly dense point cloud such as that seen in Figure 2.

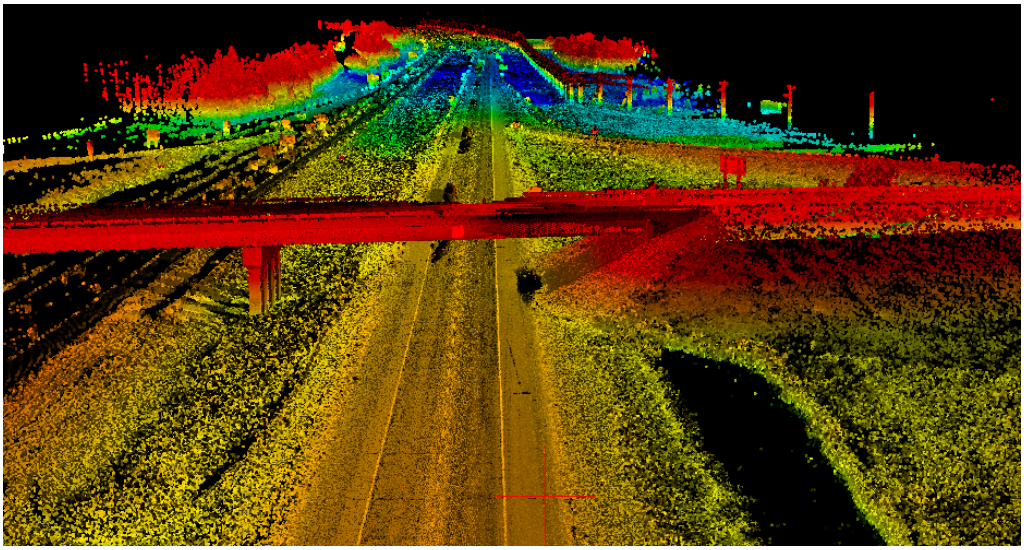

Figure 2: LiDAR point cloud sample

There are different types of LiDAR data. Generally, LiDAR data can be airborne or Terrestrial. The latter can be either static when the scanning system is mounted on a tripod or mobile when the scanning equipment is mounted onto a moving object such as a vehicle, an aeroplane, or a boat. Mobile LiDAR and Airborne LiDAR are the common data sources used in a variety of applications in Transportation Engineering with Mobile LiDAR being the most prevalent. Mobile LiDAR systems provide a collection of data with higher point density, a good view of road pavement, and a better view of vertical surfaces such as building sides and faces of roadside features but cannot capture the top of buildings. Airborne LiDAR systems collect data with lower point density, a better view of pavement and building surfaces, but have a poor view of vertical faces [62]. Airborne LiDAR systems also have the advantage of providing a more synoptic view of scanned areas and have a wider field of view, however, such a wider range comes at the expense of lowered density of collected point cloud [63].

Various data collection methods and scanning equipment have different advantages and disadvantages. Vendors of laser scanning systems also recommend typical applications for their products. For example, more detailed information about roadside features can be obtained using mobile LiDAR scanning, while a wider range of areas can be covered using Airborne LiDAR. Airborne LiDAR can be better used in a variety of applications including mapping, road alignment selection, feasibility studies, vegetation planning and environmental assessment while Mobile LiDAR is used when more dense and accurate scanning is needed [64].

In Mobile LiDAR scanning, the system is mounted on a data collection truck that travels along the highway of interest while constantly scanning the highway and surrounding environment. This results in a 3D point cloud image consisting of closely spaced points that provide a robust representation of the road environment (Figure 2). The high point density of such datasets allows the extraction and assessment of several roadway geometric characteristics, such as horizontal curve feature extraction and sight distance assessment, in a highly accurate and efficient manner. The advantages of using Mobile LiDAR make it a very common approach to transportation applications since road features can be captured with a high level of detail using this technique [62]. More so, one of the merits that give Mobile LiDAR the edge over other remote sensing techniques is its ability to capture a highly detailed representation of entire roadway segments and surrounding environment in a single survey pass through driving along a highway at posted speed limits.

2.3 Horizontal Curve Detection & Feature Extraction

This section provides background information on horizontal curves and presents a review of literature on previous work conducted on curve detection and feature extraction.

2.3.1 Background

Horizontal curves are essential to creating a smooth transition between tangential road segments; however, they have been considered a significant safety concern for several years [65]. Research relating collisions to geometric road characteristics has consistently shown horizontal curves to be a major contributing factor to different types of severe collisions. For instance, evidence from the literature shows that severe run-off-road and head-on collisions are more likely to occur on curves [66]. In the United States, about 25 % of fatal road collisions occur on curved sections. More so, the National Highway Traffic Safety Administration (NHTSA) has indicated that the horizontal alignment of the roadway contributes to about 76 % of single-vehicle collisions in the United States [67]. Previous research has also shown that run-off-road crashes on horizontal curves are 1.5 to 4 times higher than collisions on straight segments [68]. In fact, previous research has shown that different curve attributes including curve radius, curve length, and tangent length all influence the frequency of collisions on horizontal curves [69-71]. These statistics signify the importance of properly designing horizontal curves to improve road safety, which is the key objective of this thesis.

Information about horizontal curves is of great importance to help ensure the safe operation of highways. For instance, evaluating the potential of vehicle skidding or rollover on curves requires information about the geometric characteristics of curved elements [72]. Similarly, certain

geometric features of curves such as curve radius, deflection angle, and curve length are essential to predicting operating speeds on a roadway [69]. Horizontal curves and their attributes also impact the amount of sight distance available on a highway [70].

In lieu of the above, transportation agencies are often required to maintain an accurate and updated inventory of geometric attributes of horizontal alignment in order to make well-informed decisions on potential safety improvements required on curved road segments. Unfortunately, using traditional methods (i.e., chord offset and compass methods) to constantly maintain a record of horizontal curves and their attributes is an extremely challenging task, which is time-consuming, laborious, and sometimes inaccurate. This is particularly true when considering the size of highway networks in North America and the number of curves that could potentially exist on such networks.

To overcome the challenges associated with conventional techniques, several methods have been used to extract information about the horizontal alignments in the past using satellite and aerial images [73, 74]. One common issue with such techniques is that they often utilize commercial software packages, such as ArcGIS and AutoCAD for the extractions. This requires manual digitization of the start and endpoints of each horizontal curve to obtain relatively accurate measurements. Such an undertaking results in a large amount of manual work, which makes using these techniques slightly impractical and uneconomical, especially for large-scale network-level analysis.

A more efficient approach to estimating horizontal curve attributes is through using the Global Positioning System (GPS) points to recreate a road's alignment. Although this helps collect data more efficiently, data points are typically collected along a single path, which makes

estimating the geometric characteristics in different lanes a challenge. Moreover, the low density of GPS data, its scattered nature, and low accuracy could sometimes lead to inaccurate estimation of curve attributes [47].

With the limitations associated with previously discussed methods, LiDAR has recently been utilized to extract geometric attributes of roads. As discussed, scanning a highway using mobile LiDAR create a highly dense and accurate representation of the surrounding environment in a single survey pass and at highway speeds. This helps agencies scan large road networks in a short time period with minimal disruption to traffic. Previous research has shown that Mobile LiDAR data can be utilized to extract highway geometric features, including attributes of horizontal alignment in a robust and efficient manner [47, 75-77]. Moreover, unlike GPS data, the high density of a LiDAR point cloud means that alignment attributes extracted from the dataset for one lane of analysis can be replicated across all lanes on a highway.

Although interest in using LiDAR data for transportation applications has grown significantly in recent years [62, 78], not much research has been done on the feasibility of utilizing these rich datasets to extract horizontal curve attributes on a large scale. The majority of work that does exist has been limited to performing extractions on a limited number of short highway segments [47, 79]. To address this gap and help prepare the dataset needed for reliability analysis, this research develops a novel algorithm utilizing LiDAR data for the automated network-level detection of highway horizontal curves and the extraction of their attributes. More details on the developed method are discussed in the next chapter. As part of the thorough literature review

conducted in this dissertation, the next section summarizes previous work on detecting curved segments and extracting their geometric characteristics.

2.3.2 Previous Studies

Different approaches for detecting horizontal curves and estimating their attributes have been proposed in the literature. Some studies attempted developing computational methods to measure horizontal curve features using a ball bank indicator and digital compass to record lateral acceleration and change in heading of a vehicle driving along a curve [80-82]. The curve radius is then calculated using the point-mass equation. Although such techniques are effective in estimating the curve radius and other attributes, they require that a test vehicle is driven at a constant speed along the curve while identifying the Point of Curvature (PC) and the Point of Tangency (PT) of each curve in advance. This makes such techniques infeasible when the detection of curves is required on a network level.

Many researchers have proposed using GPS data to extract horizontal curve attributes. Li, Chitturi [68] proposed a methodology to extract data about horizontal curves using Geographic Information System (GIS) roadway maps. An algorithm was developed that uses the change in bearing angle between two successive segments to identify curved elements. And a curve is detected when the change in heading angle exceeds an adjustable threshold. The algorithm had a curve detection rate of 96.7 % and was validated using horizontal curve data obtained from Bing aerial maps.

Imran and Hassan [83] developed a GPS-based procedure to determine features of horizontal alignment on two-lane rural highways. The algorithm used the change in angle between

successive points to separate data points of both straight and curved elements. To detect tangent elements, only 75 % of the straight data points were used to avoid portions that might have transitional curves. The first, the middle, and the last sets of points of the mid 50 % of the curved element points were used to locate the center and the radius of the curve. After a number of iterations, the algorithm extracts curve information including curve radius and curve length. The authors tested the methodology on a roadway segment with nine horizontal curves with the results showing an average difference of 1.55 % and 16.7 % between the extracted and actual values for curve radii and curve lengths, respectively.

Ai and Tsai [84] proposed a GPS-based technique where they used the Kasa Circle Fitting method to identify curved elements that fit several of the neighbouring points onto a circle. This method uses an iterative process by gradually increasing the number of points included until a certain error value is reached. The proposed algorithm was tested on both real and simulated data and was able to identify horizontal curves with a detection rate of 90.1 %. Other studies compared using different GIS methods and tools, such as Curve Finder, Curve Estimator, and Curve Calculator, to extract information about curved elements from GPS data [85, 86]. These studies emphasized the importance of collecting highly dense points in order to achieve higher accuracies.

Holgado-Barco and González-Aguilera [79] proposed a semi-automatic method to extract horizontal alignment attributes from LiDAR. Extracted attributes included curve length and radius. The proposed method was tested on both real and simulated data reporting an average error of 2 % for the real data. Gargoum and El-Basyouny [47] also proposed a method to extract geometric attributes of horizontal curves from LiDAR data. The proposed method extracts horizontal curve

features including curve radius, length, curve center coordinates, and deflection angle. The proposed procedure was tested on two, two-lane highway segments (four km each) with the authors reporting an average error of less than 3%.

Although several studies have proposed different approaches to extract information on highway horizontal curves with a high level of accuracy, most of these attempts used GPS data to estimate curve information which requires manual work to convert or process the data. In addition, some studies utilized commercial software packages, such as ArcGIS, to extract horizontal curve attributes. This makes the application at the network level a laborious task due to the manual nature of processing the GPS data and the interventions required for processing. Moreover, little attention has been dedicated to using LiDAR data to extract attributes of curved elements on a network-level scale. As part of the data acquisition process, this thesis develops a fully automated algorithm to identify locations of horizontal curves and extract their attributes on a network level using LiDAR Data. The performance of the proposed algorithm for accurately estimating curve attributes was validated using as-built drawings. The validation process showed that the algorithm was able to estimate the attributes of curved segments with a high level of accuracy in an efficient and fully automated manner.

To illustrate the feasibility of using the method on a large scale, the algorithm was employed to detect curves and extract their attributes on a total of 242 km of LiDAR data collected along different rural highways in Alberta, Canada. The algorithm was successful in the detection and feature extraction on all horizontal curves on the test highways at a data extraction rate of 2.32 seconds/km. Providing a fully automated algorithm to extract curve attributes with such accuracy

and efficiency is a powerful tool that could be used by transportation agencies to establish a reliable inventory database for their road networks. This would help them make informed decisions regarding the safety assessment and development of roadways.

2.4 Available Sight Distance Assessment

This section provides background information on sight distance and sight distance evaluation; and presents a review of previous research performed on assessing sight lines on roadways.

2.4.1 Background

A key element in highway geometric design is providing sufficient sight distance to road users. Stopping sight distance is commonly defined as the minimum visible distance needed by a driver to come to a safe and complete stop before striking an obstruction on the roadway [17]. The *ASD* can be defined as the length of the visible roadway segment ahead of the driver which is required by road design guides to be greater than the minimum requirements. However, the sight distance can often be restricted by many features along the roadway horizontal and vertical alignments or by the pavement surface of the road [87]. On horizontal curves, the driver's line of sight can be obstructed by lateral objects, such as buildings, trees, and hills. The visibility on crest vertical curves can be limited by the road surface along the vertical curve itself. In fact, providing adequate sight distance on highways is crucial for both road operation and safety.

It is necessary for a driver to be given enough visible distance to react, in case a hazardous situation is encountered, in order to avoid being involved in a collision. In fact, researchers found that limited sight distance has a large effect on the occurrence of road collisions [6, 34]. Although

designing highways that meet the sight distance requirements of design guides, in theory, ensure that sufficient sight distance will be available along the highway, the presence of some constraints (e.g., practical or financial) during the design and construction stages may lead to insufficient sight distance at some locations [88]. In addition, highway rehabilitation and pavement maintenance work during the road's service life could result in changes to the original road design, altering the *ASD* at certain locations. Therefore, assessing the *ASD* on in-service highways is critical to ensure that minimum requirements are met throughout the planned service life.

Current practices of *ASD* estimation are time-consuming, labor-intensive, and sometimes inaccurate due to the non-consideration of the presence of roadside features that are not documented on 2D as-built plans. Assessment of *ASD* is often conducted separately for horizontal and vertical alignment [89]. In many situations, the sight distance obstruction can result from the combination of a horizontal and vertical curve at the same location. *ASD* is often evaluated through long site visits, conducting a manual graphical assessment or most commonly using Highway Design Software (*HDS*). *HDS* use Digital Terrain Models (*DTM*) including information on road cross-sections and horizontal and vertical alignment to perform the *ASD* calculations. Such an approach is inaccurate since common sight distance obstacles, such as trees, buildings, and vegetation, cannot be modelled and contained in *DTMs* [90]. In real conditions, the *ASD* is highly influenced by several 3D sight obstructions, such as road surface on vertical crest curves, traffic signposts, road barriers, fences and vehicles parked on the roadside. Thus, assessing the *ASD* considering the presence of such objects is critical to better represent the actual driving

environment. An accurate representation of road conditions is fundamental in order to acquire a reliable assessment of sight distance.

In recent years, attention has shifted to the use of the GIS to facilitate a 3D estimation of *ASD* on roadways. GIS-based applications use Digital Surface Models (DSMs) that consider vegetation, buildings, and other obstacles that could reduce the driver's visibility [91]. The data sources used in these applications can be aerial images, LiDAR images or DTMs, including vector cartography (i.e., information on 3D obstacles) [92]. The majority of GIS-based applications focus on the evaluation of 3D *ASD* using ArcGIS tools [93]. Although this has been very useful, the manual input required during different stages of the assessment process hinders the large-scale implementation and, to some extent, requires a considerable amount of manual work.

With the recent technological advances, the use of remotely sensed data in obtaining information on roadway elements has been increasing. LiDAR data sets can be used to assess ASD on highways in a fully automated and accurate manner. There have been some attempts to evaluate ASD on highways using LiDAR point clouds. However, a fully automated method for the computation of available 3D sight distance has yet to be developed. The next section summarizes previous studies on assessing sight lines along roadways before discussing the developed algorithms in the next Chapter.

2.4.2 Previous Studies

There have been a number of efforts to assess the sight distance on roadways. One of the earliest studies was conducted by Hassan and Easa [87]. They proposed a method to calculate the sight distance along the road’s horizontal alignment. Although the method was efficient and accurate, it

was solely based on road horizontal geometry. A part of their study was developing computer software to assess the no-passing zones on two-lane two-way roadways. Another study by Lovell [94] also focused on determining *ASD* when it is only limited by road horizontal alignment. The proposed procedure was recommended for use in flat areas or in the planning and preliminary stages of designing highway facilities.

Although researchers have been considering determining the *ASD* on highways, the number of studies that provide an automated computation of 3D sight distance is limited. Nehate [89] used GIS data to compute the *ASD* along roadways. Piecewise parametric equations were used to represent the road surface and obstructing objects. The sight distance was then assessed by looking for the intersection between sight lines and any obstructions. Due to the smoothness of the second-order curves, the bumpy pavement surface on vertical curves was not accurately considered in the assessment. Thus, the authors attributed the model to be of moderate accuracy. In a more recent GIS-based study, Castro and Iglesias [92] used ArcGIS to obtain *ASD* on highways. The extraction results of *ASD* were compared to values estimated by road design software. There were no statistically significant differences between the two methods, but in many cases, the design software estimated shorter distances because of its ability to better detect vertical curves.

Researchers' interest had shifted towards utilizing LiDAR data to evaluate the *ASD* after Khattak and Shamayleh [95] tested the feasibility of using Aerial LiDAR data to obtain stopping and passing sight distance on a highway in Iowa state, United States. ArcGIS tools were used to assess the sight distance at selected locations. Some sections were found to have sight distance insufficiencies. Site visits to these locations were then conducted and confirmed the presence of

obstructing objects. In a more recent study, Castro, Anta [96] used aerial LiDAR data for sight distance evaluation using ArcGIS tools. The authors indicated that the processing time in this study is lower compared to that in Castro and Iglesias [92]. Khattak and Hallmark [44] utilized LiDAR data to identify potential sight distance obstructions at intersections. Using videotapes, the authors indicated that 90% of the actual obstructions were identified by the proposed method.

In 2015, Bassani, Grasso [90] used mobile mapping systems to perform sight distance analysis. Photogrammetric images of a road segment were collected and then converted into point clouds. A DSM was then generated, and ArcGIS tools were used to calculate the ASD. The results showed successful detection of previously known obstructing features along the studied segment. However, the authors recommended further studies to automate the sight distance estimation process considering 3D models. A year later, Castro, Lopez-Cuervo [91] used both aerial and mobile LiDAR data in a sight distance analysis. The authors showed that DSMs created by mobile LiDAR provide a more accurate representation of the real road conditions due to their greater density.

In a more recent study, Gargoum, El-Basyouny [88] introduced a semi-automated method utilizing ArcGIS tools to compute the sight distance on highway segments using mobile LiDAR data. A Microsoft Visual Basic code was then written to calculate the sight distance from the ArcGIS outputs. A location with limited sight distance was detected. The authors also indicated that the processing time was one of the main challenges when dealing with a high number of observes and targets.

As demonstrated throughout the literature review, the importance of considering a *3D* assessment of *ASD* is well recognized. However, the progress has been limited due to the unavailability of 3D road models and the complexity of the computations needed for 3D analysis. Even when evaluating *ASD* in the 2D space using as-built drawings, this source of information sometimes could be outdated due to the regular maintenance and pavement operations that affect the accuracy of original as-built documents or inaccurate due to the lack of 2D as-built drawings for the 3D roadside features and vegetation that could represent sight obstructions. In fact, most previous studies that introduced 3D-based methods to evaluate the *ASD* on roads used GIS data and/or LiDAR images and utilized software tools such as ArcGIS to perform the visibility assessment. This requires considerable manual work which hinders the large-scale implementation. Therefore, a fully automated approach utilizing accurate and updated information that represents the current 3D road environment (i.e., LiDAR) has yet to be developed.

While establishing an inventory for reliability-based horizontal curve design, this thesis adds to the existing body of literature by developing a fully automated methodology through which the *ASD* on highways can be assessed using mobile LiDAR data. The 3D nature of LiDAR point cloud models enables accounting for various sight obstructions that could cause visibility problems such as vegetation, buildings, road furniture, and the combination of both horizontal and vertical alignments. Not only this, the 3D models of driving environment that are made available through LiDAR technology represent easy-to-access highway corridors that can be visited an unlimited number of times, without causing any traffic disruptions, to further investigate the presence of sight distance deficiencies or any other safety issues. The automation of sight distance evaluation

could save transportation agencies large amounts of time and money if a large-scale safety audit is desired, assuming that sight lines can be assessed manually which is largely an invalid assumption. The sight distance assessment procedure presented in this thesis was tested and validated following recommendations of design guidelines to ensure the accuracy of the obtained results. The results showed that the algorithm is accurate in evaluating the *ASD* on highways and identifying locations with sight distance deficiencies. Even though this algorithm is one step towards the data preparation for reliability analysis, on its own, represents an appealing solution to departments of transportation for safety and visibility assessments on highways.

3 DATA EXTRACTION FROM LIDAR DATA

This Chapter provides details about utilizing LiDAR data in developing a set of novel algorithms to automatically detect highway curved segments and extract their geometric attributes including the 3D ASD on highways to establish the dataset required for reliability analysis. The chapter is concluded by presenting a summary of geometric and collision data prepared for reliability analysis.

3.1 Introduction

As discussed, road geometry data used in previous reliability-based studies were manually obtained from Departments of Transportation (DOTs), extracted from aerial photographs, satellite images, or by using commercial software (i.e., AutoCAD). Information acquired using conventional surveying methods could be outdated due to road resurfacing operations and the installation of roadside features that are not normally captured as 3D objects by traditional surveying methods. The recent surge in computing power and the high density of LiDAR point cloud has led several agencies to consider using such technology to obtain information about various roadway elements [19, 97]. Compared to traditional methods, using LiDAR data increases the efficiency and robustness of the information extraction process. It also helps alleviate the burden associated with the conventional estimation of road geometry attributes, such as excessive labour work, long site visits, and traffic disruption caused during the data collection.

According to many researchers, the ability to adopt utilizing LiDAR as an alternative to conventional methods relies on the development of alternative applications that enable obtaining

the information from LiDAR data datasets in a more efficient manner [19, 98, 99]. Jalayer, Gong [99] compared the efficiency of different methods such as data obtained from field visits, aerial maps, and remotely sensed data in developing safety performance functions. The authors concluded that mobile LiDAR has the potential to replace other alternatives subject to developing more efficient data extraction methods.

In recent years, road feature extraction from LiDAR has gained some momentum with a focus on extracting road features such a lane marking, traffic signs, and light poles [100-103]. However, not much work has focused on obtaining information on roadway geometric characteristics [19]. For example, Kumar [104] dedicated a PhD thesis to the extraction of road edges, lane markings, and road roughness from LiDAR data. Haiyan [105] also focused on extracting road edges, pavement cracks, and lane markings. More so, Ai [106] devoted a PhD thesis on extracting traffic signs from LiDAR data. Even studies that exist on extracting geometric attributes of roadways suffer from various limitations with the main shortcoming being the manual input required when applying these proposed methods. The significant number of manual interventions hinders the ability to assess microscopic design elements such as ASD, especially when a large-scale assessment is required. Some researchers believe that the lack of full utilization of LiDAR data in transportation applications is attributed mainly to the lack of expertise [19, 107].

Based on the above and the review of literature presented in the previous chapter, it is demonstrated that a handful of studies utilized LiDAR data to extract horizontal curve features and assess the available sight distance along roadways [79, 88, 92, 96]. Work conducted on extracting characteristics of horizontal curve suffers from the manual input needed and infeasibility and

applying the proposed procedure on a large scale, while sight distance assessment methodologies do not account for overhanging objects as well as the manual input required. Therefore, a part of this dissertation is dedicated to developing a set of algorithms to detect highway horizontal curves, extract their geometric features, and assess the ASD in a fully automated and efficient manner while enabling large scale implementation.

Although the main aim of developing these algorithms is to establish a reliable data set for use in reliability analysis, the feature extraction procedure developed as part of this dissertation overcomes the aforementioned limitations and could be of great value for transportation agencies when aiming to assess highway networks. In fact, it is worth mentioning that in addition to using LiDAR data in extracting information on horizontal curves and computing ASD, the large number of applications for which the same LiDAR data set can be used makes this data a greatly appealing option for transportation agencies that can result in significant cost and time savings [44]. Langston and Walker [108] collected LIDAR data for a DTM of a 42-mi highway corridor and reported savings of $1.5 million and at least 9 months, compared with traditional methods of acquiring DTM data. In a different study, the Savannah-Area Geographic Information System agency collected countywide LIDAR data to generate contour maps for a project intended to improve drainage of the Hardin Canal in Georgia, USA [109]. The agency reported estimated construction savings of $7 million. In fact, the associated costs with LiDAR data collection can be offset through utilizing the same LiDAR sets in a variety of other applications including the extraction of information on various geometric attributes related to cross-sections, road signage and markings, horizontal and vertical alignments, and road safety audits applications [44, 75, 101]. Adopting

LiDAR data in managing highways and road networks could be a new epoch of asset management, design review, and safety audits techniques.

3.2 LiDAR Data Used in this Research

The data used in this research was collected on several two-lane two-way highways in the Province of Alberta, Canada. Data was collected by Alberta Transportation using a laser scanning system equipped with two REIGL VQ 450 scanners mounted on a data collection truck. The system has a scan rate of up to 1.1 million points/sec. The data collection vehicle drove along scanned highways at posted speed limits of up to 100 km/h, creating 3D models of scanned segments without causing any disruptions in traffic movement. Although point cloud density varies across the point cloud, densities can range from 150 to 1000 points/m^2 on the pavement surface, with an average point density of 300 points/m^2 [63].

Data collected along a highway is saved in several Laser (LAS) files. Each LAS file contains up to 30 million points representing point cloud data for a four km segment of the highway. Due to the high density of points collected, the size of a LAS file containing points of a four km section could reach 700 MB. The data was collected and stored by Alberta Transportation, and it was transferred to the author as zipped (compressed) files on five TB portable hard drives. In order to protect data privacy, these drives were kept in a secure place and were shared for processing under confidentiality agreements.

3.3 Horizontal Curve Detection & Feature Extraction

This section provides a thorough description of the developed algorithm for detecting highway curved segments and extracting their geometric characteristics. It provides information on the methodology, algorithm testing and validation, application on a large scale, and discusses the performance of the algorithm.

3.3.1 Background

Although several approaches to extract horizontal alignment have been proposed in previous research, none of those studies demonstrated the feasibility of extracting such information on a large scale. The procedure developed in this thesis enables the automated detection of horizontal curves and extraction of their attributes on a network level. More so, the developed algorithm obtains additional information on horizontal alignment characteristics such as length of road straight segments (i.e., between curves, and curve superelevation rate while also identifying the curve direction (i.e., to the right or to the left). To the best of the authors' knowledge, a fully automated estimation of horizontal curve attributes from LiDAR data on a network level has not been accomplished in previous research. Providing a fully automated procedure to extract such information could help transportation agencies to establish a reliable database of horizontal alignments, which, in turn, would facilitate making well-informed decisions regarding the safety assessment and development of roadways.

The developed method focuses on automatically detecting highway horizontal curves on a large scale and estimating all their attributes including the length of straight sections between curves, curve direction (to the left or the right), defection angle, curve radius, superelevation rate,

chord length, and curve length. The method was first validated using data from both as-built drawings and 20 km of simulated data with predefined curve attributes. The algorithm was then applied on a large-scale using LiDAR data of five highways totalling 242 km.

3.3.2 Methodology

The method developed for detecting horizontal alignment and extracting curve attributes includes four main stages: i) road lane centerline definition in which points that represent the lane centerline are extracted, ii) horizontal curve detection utilizing changes in azimuth of vectors created from lane centerline points to detect locations of curved segments, iii) multiple feature extraction including the length of straight segments between curves, curve angle, chord length, curve radii, and superelevation rate of circular curves, and iv) detection and feature extraction of spiral curves between straight sections and circular curves. The method is explained in more detail as follows:

3.3.2.1 Lane centerline extraction and vector definition

The first step of the curve extraction process is to extract points that represent the centerline of the lane of analysis, also known as trajectory points. These are points that run along the lane of analysis (for which curve attributes are desired). The points typically run parallel to the road's axis and cover the entirety of the road segment's alignment. To obtain this set of points, the LiDAR dataset was filtered, whereby, only points that fall within the Nadir plane (i.e., a zero-degree angle) of the scanning system are retained. Since these points are impacted by the position of the scanning system and hence the vehicle on which it was mounted, occasional deviations in the orientation of the points due to a change in the vehicle's yaw angle might occur. To eliminate the impact of the

yaw angle, the moving average technique is applied to estimate an average position for every three consecutive points within the trajectory path.

To support a network-level analysis (i.e., analysis of entire highways), the code runs through a number of LAS files for successive road segments (i.e., 4 km each) and combines the extracted points to represent the lane centerline along the entire highway. The code also checks for continuity between the centerline points across different segments (i.e., points extracted from successive LAS files). This is done by sorting the points representing the centerline in ascending eastings and northings and then computing the distance between consecutive points. If the selected road segments are not continuous or if a significant gap is found within the data, this gap is flagged indicating that additional datasets for missing parts are needed. Figure 3 illustrates the process of combining successive LAS files before conducting the network-level analysis.

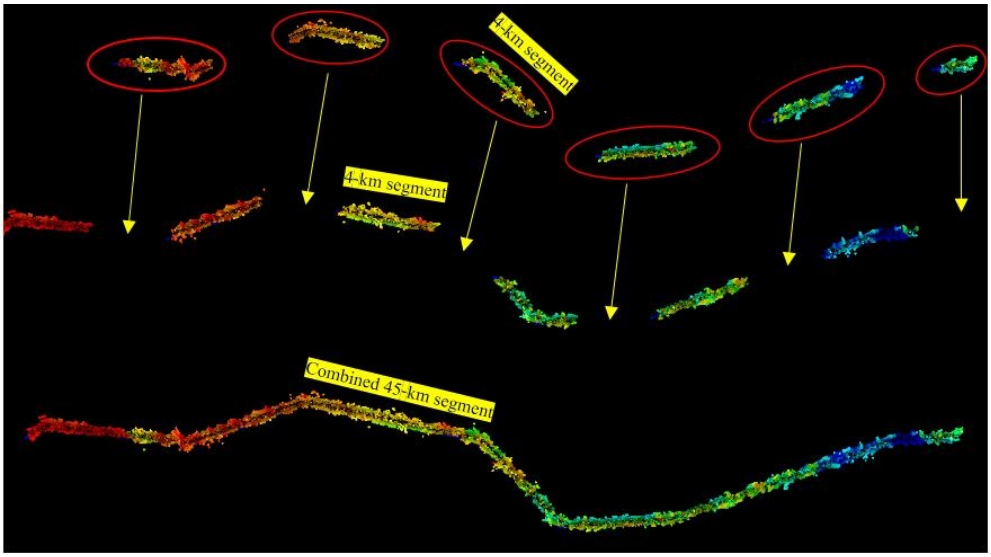

Figure 3: Combining successive LAS files for network-level analysis

(colour-coded by elevation ranges representing variations in vertical alignment)

After extracting the lane centerline points and accounting for possible deviations, multiple vectors along the centerline are defined between each two successive position vectors. Let $\boldsymbol{P}_i$ represents the start-point of a vector and $\boldsymbol{P}_{i+1}$ defines the endpoint of the same vector. In this case, this vector ($\boldsymbol{V}_j$) can be defined as follows:

$$\boldsymbol{V}_j = \boldsymbol{P}_{i+1} - \boldsymbol{P}_i = \begin{bmatrix} x_{i+1} - x_i \\ y_{i+1} - y_i \\ z_{i+1} - z_i \end{bmatrix} \tag{11}$$

where $\boldsymbol{P}_i = \begin{bmatrix} x_i \\ y_i \\ z_i \end{bmatrix}$; $\boldsymbol{P}_{i+1} = \begin{bmatrix} x_{i+1} \\ y_{i+1} \\ z_{i+1} \end{bmatrix}$; $x, y,$ and z are the coordinates of position vectors; i and j are counters starting at 1 with an increment of 1.

The number of vectors defined varies based on the length of the road segment and the vector length which can be altered by the user. In this research, the length of vectors is chosen to be 20 m (i.e., the distance between position vectors $\boldsymbol{P}_i$ and $\boldsymbol{P}_{i+1}$). Analysis of a large number of segments that contain curves with a wide range of radii showed that this length (i.e., 20 m) is appropriate to detect all curves. However, it can be altered by the user according to the foreseeable sharpness of curved sections (i.e., sharp curves may need a shorter distance to be detected). It is worth mentioning that the procedure explained in this section utilizes the points extracted along the lane centerline. This can be replicated (i.e., these points can be moved) across all lanes on a highway to estimate curve attributes for other lanes or along the road centerline if desired. Trajectory points can be offset into other lanes by estimating vectors that are normal to the trajectory of the first lane [75]. Trajectory points can then be moved into neighbouring lanes along those normal vectors. The offset distance depends on the new lane for which curve attributes are

desired. For example, if the analysis is to be repeated for the next lane, the offset distance would be equal to the width of one lane (i.e., two times the width of half a lane). Once the trajectory points have been moved into the new lane, the same detection and extraction procedure explained in the following sections can be used to estimate curve attributes. It is worth noting that this thesis measures the curve radius along the travel lane centerline while design guidelines normally use the road centerline. The difference between curve radius along lane centerline and road centerline equals to half the width of a travel lane for two-lane two-way highways which would not be big enough to make a difference in the results (e.g., 0.6% difference for a curve radius of 300 m and a lane width of 3.6 m).

3.3.2.2 Curve Detection

Horizontal alignment elements (i.e., straight sections, circular curves, and spiral transitional curves) can be detected and their attributes can be estimated using the centerline extracted in the previous section. The geometric parameters of horizontal alignment elements can be obtained using two alternative attributes, namely the azimuth and the curvature. The azimuth (z) of a vector along the centerline can be calculated as follows:

$$z = \text{arctg}\left(\frac{\Delta x_{i+1}^{i}}{\Delta y_{i+1}^{i}}\right) \times \frac{180}{\pi} \quad (12)$$

where Δx and Δy are the x and y coordinate differences between consecutive points along the centerline (i.e., start and endpoints of trajectory vectors); π is a constant = 3.14.

The curvature (z') can be estimated using the first derivative of the azimuth as follows:

$$z' = \frac{z_{i+1} - z_i}{L_{i \to i+1}} \quad (13)$$

where z_i is the azimuth value at the position i and $L_{i \to i+1}$ is the distance between the two points.

The segmentation of road horizontal alignment elements can be done based on azimuth or the curvature information. Figure 4 shows the theoretical azimuth and curvature diagrams (i.e., ideal case) of a horizontal curve with spiral transition curves between the tangent and curved sections. As shown by the azimuth diagram, straight sections correspond to horizontal lines (i.e., no change in azimuth), circular curves correspond to inclined lines (i.e., steady change in azimuth), and spiral transition curves correspond to second-degree curves (i.e., gradual change in azimuth). As for the curvature, straight sections have zero curvature represented by horizontal lines, circular curves have constant curvature (i.e., horizontal lines) and spiral transition curves have a gradual change in curvature (i.e., inclined lines) transitioning from straight to curved elements.

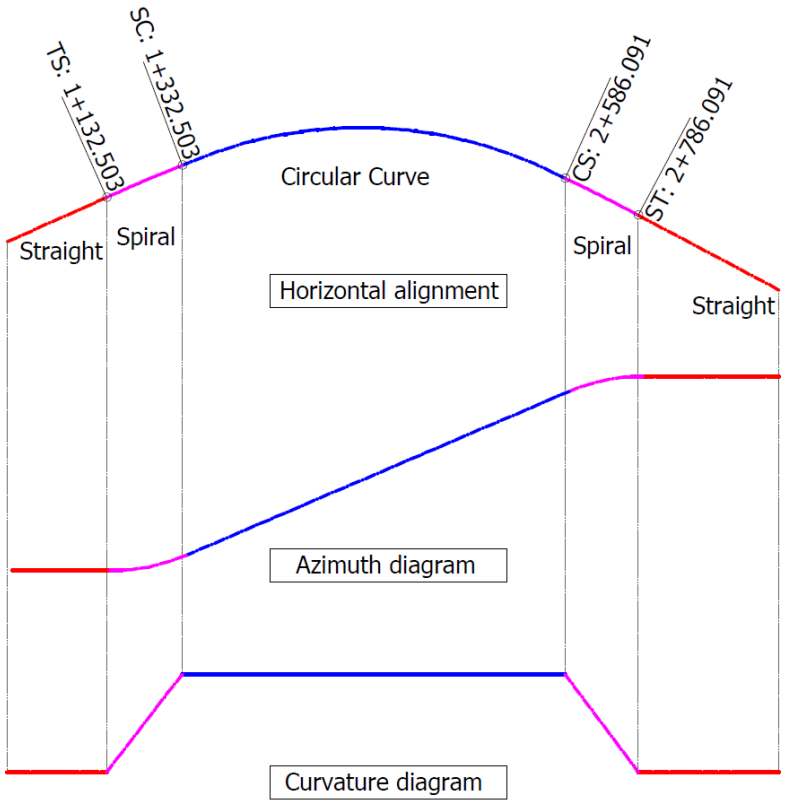

Figure 4: Azimuth and curvature diagrams a theoretical curve

Since the azimuth and curvature can be used alternatively, the change in azimuth is used to detect the presence of horizontal curves. Figure 5 illustrates using the change in azimuth (i.e., bearing angle) in curve detection. To identify tangent and curved elements, the azimuth of each vector is calculated and compared with the azimuth of the previous vector. When the change in the azimuth is greater than a predefined threshold, a new curve should begin, or the currently detected curve should continue. However, if the change between the current vector and the previous one is less than the threshold, this point is considered the end of the curve and the beginning of a tangent element. To avoid the influence of bearing angle fluctuations on curve detection (false positive curves), the code requires the change in bearing angle to be persistent (i.e.,

sustained for a particular length) to be considered a curve. Analysis of a large number of LiDAR data segments showed that the change in azimuth along horizontal curves with a wide range of radii is between 0.5° and 3.71°. A sensitivity analysis is conducted to test the influence of azimuth change threshold and vector length on detection accuracy. Table 1 shows detection rates resulted from performing a sensitivity analysis on LiDAR data of 40 km of Highway 661 using different values of azimuth change threshold and vector length. As shown, a detection rate of 100 % is obtained when using a vector length of 20 to 30 m and a change in azimuth of 0.3° to 0.5° as shown in the table below. However, a vector length of 20 m and an azimuth change threshold of 0.5° are used in this research to make sure that short curves are not missed by the algorithm when using a longer vector length (i.e., 30 m) and smooth curves are not missed when using a smaller change in azimuth (i.e., 0.3°).

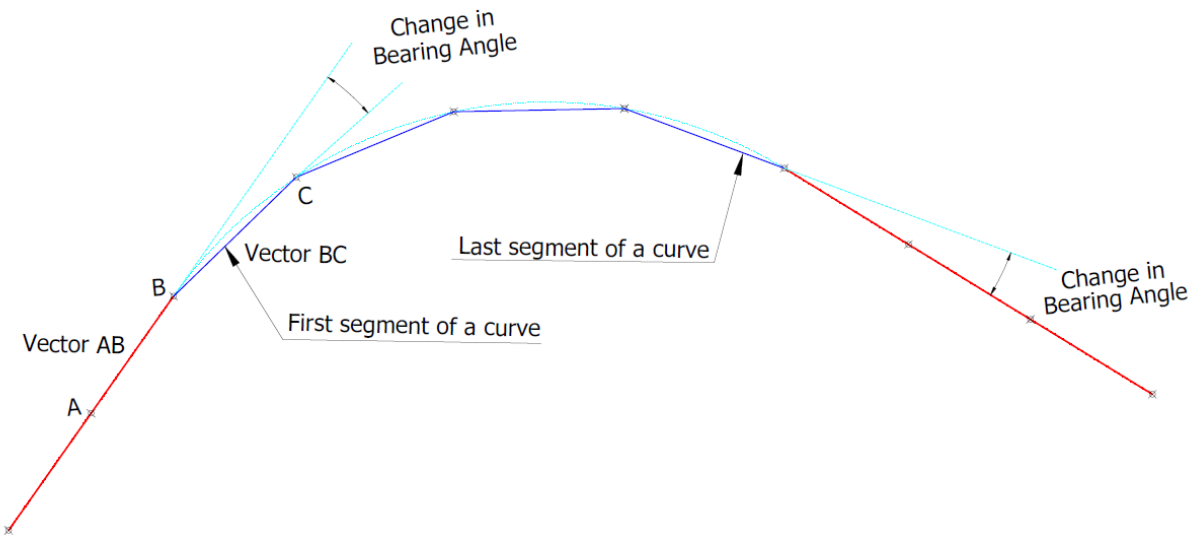

Figure 5: Curve detection using the change in Azimuth

Table 1: Curve detection rates at different detection parameters (%)

Vector length (m)	Change in azimuth (°)			
	0.3	0.5	0.7	0.9
10	83.3	83.3	83.3	66.7
20	100.0	100.0	100.0	66.7
30	100.0	100.0	83.3	66.7
40	83.3	83.3	83.3	66.7

3.3.2.3 Extraction of Curve Attributes

After classifying the segments into straight and curved segments and identifying curve start and endpoints (PC and PT points) based on the change in azimuth, the next step was to identify all other curve-specific attributes such as the point of intersection, length of straight segments between curves, curve deflection angle, chord length, curve radii, and superelevation rate. Figure 6 shows the extracted attributes of the horizontal alignment. The next few paragraphs summarize the method used to estimate each of those attributes.

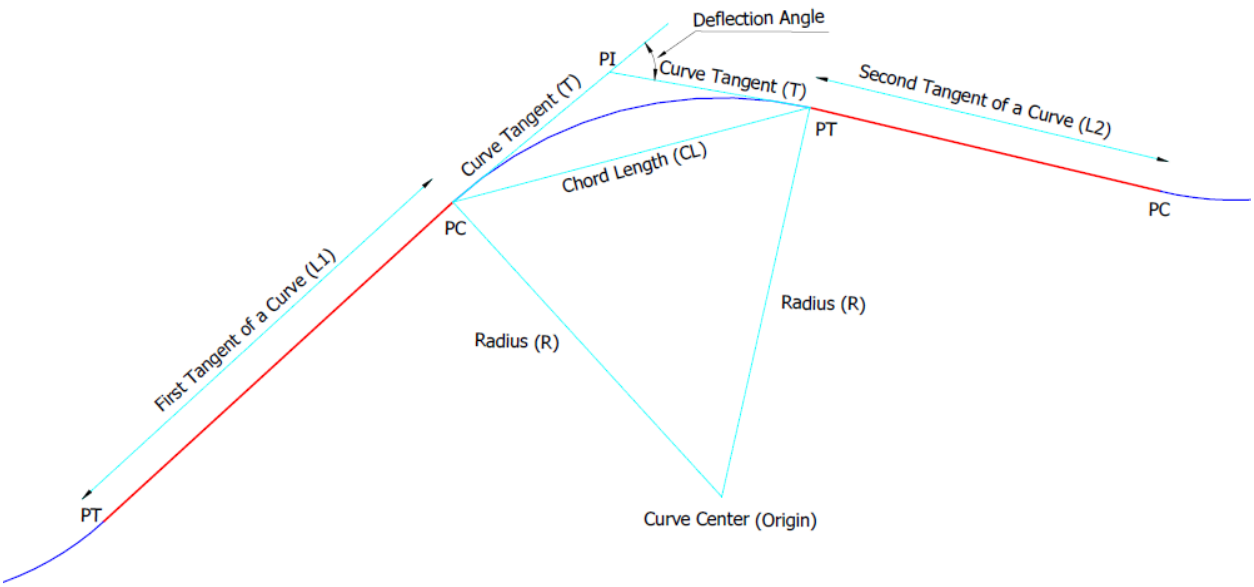

Figure 6: The extracted geometric attributes of horizontal alignment

To estimate the *Point of Intersection* (PI) the group of points located before the PC point and the after the PT of a horizontal curve are classified as tangent elements of the horizontal curve. Two linear regression models are then estimated for the two straight sections (i.e., tangents) and PI is located by identifying the intersection point of the two equations. Similarly, the difference in bearing between the two tangents is computed to estimate the *deflection angle.*

The *length of straight segments* (L_1, L_2) is estimated by calculating the Euclidean distance between the endpoint of the current curve (PT) and the start point of the succeeding curve (PC). *The chord length* (CL) is estimated by calculating the Euclidean distance between the curve start and endpoints (PC and PT) while the curve tangent (T) is computed by estimating the distance between the point of intersection (PI) and the curve start and endpoints.

For *curve radii* (*R*), lines normal to the tangents on either end of the curve were estimated at PC and PT. To identify the location of the curve's center, the intersection point of the two normal lines was estimated. The curve radius is then estimated by calculating the Euclidean distance between the PC and PT points and the curve's origin.

Estimating the superelevation rate of each curve was done using the methodology proposed by Gargoum, El-Basyouny [75] which involves extracting road cross-sections and estimating their slopes. The algorithm involves defining vectors perpendicular to the road axis. This is followed by extracting points from LiDAR point cloud within proximity of these vectors representing the highway cross-section. Multivariate Adaptive Regression Splines are then utilized to identify points at which the cross-slope changes on the extracted cross-section. Finally, the cross-slope on curves (i.e., superelevation rate) is estimated using linear regression. It is worth mentioning that the algorithm is modified to estimate the superelevation rate at the mid-point of the horizontal curve.

The methodology described above was coded in MATLAB [110]. The algorithm loops through multiple scan files collected along a highway and work on detecting curves and estimating their attributes in a fully automated manner.

3.3.2.4 Spiral transition detection

Spiral curves provide a gradual change in curvature from a straight to a curved road element. In order to determine whether the horizontal curve includes transition curves or not, the change in curvature was used. Spiral curves are usually defined using three elements: circular curve radius

(R), spiral length (L), and the spiral parameter (A). The spiral parameter can be obtained using the following equation:

$$A^2 = R \times L \quad (14)$$

To calculate the spiral parameter, the spiral length (L) needs to be estimated. Figure 7 shows the azimuth and curvature diagrams obtained by the algorithm from LiDAR data of a curve. The change in both azimuth and curvature obtained from LiDAR data (i.e., real data) follows the same trend of theoretical data (i.e., ideal data) as previously discussed when referring to Figure 4. As shown in Figure 7, the pattern of change in both the azimuth and the curvature display spiral transitions. As shown, the curvature equals to Zero along the tangent section; is constant along the circular section of the curve; and varies along the spiral element. The estimation of the length of spiral curves involves three steps: a) linear regression equations were developed for the points that represent tangent, spiral, and curved sections; b) these linear equations were then intersected defining the intersection knots shown in the figure; c) the spiral length was estimated as the distance between these points. Once the spiral length is estimated the spiral parameter can be calculated using equation 14.

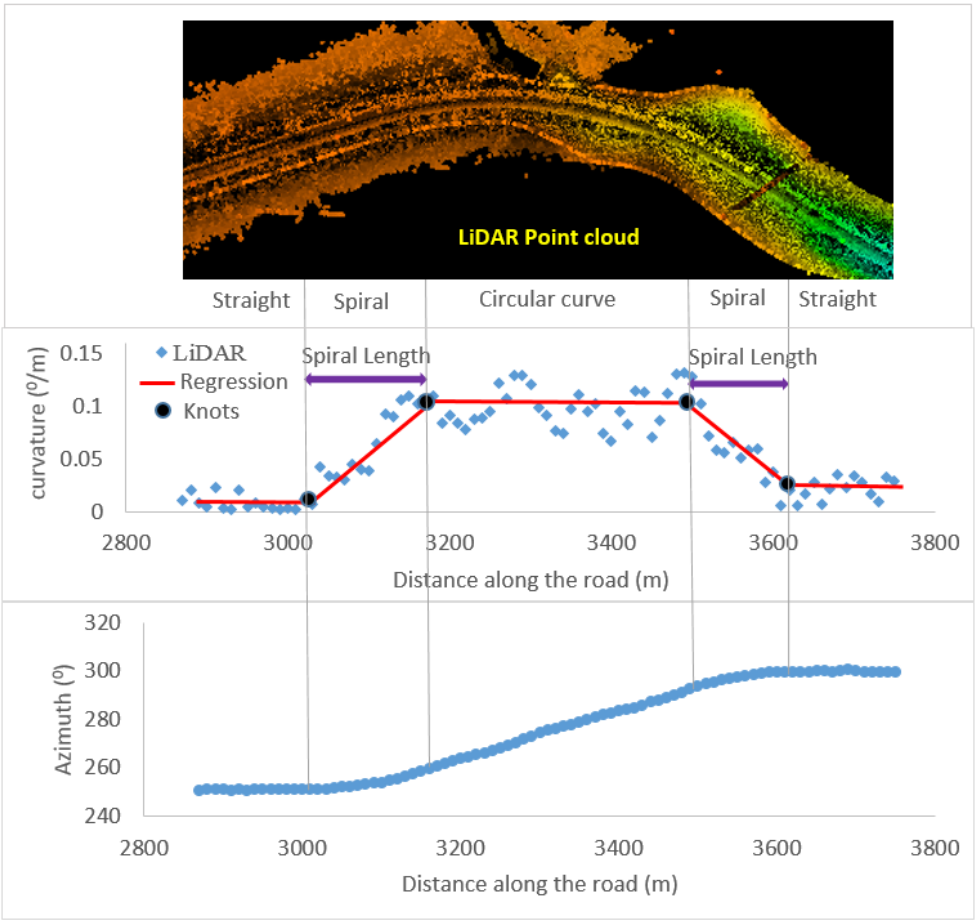

Figure 7: Azimuth and curvature diagrams from LiDAR data of a curve

3.3.3 Algorithm Testing and Validation

The algorithm was first validated using LiDAR data of highway segments for which as-built drawings (i.e., ground truth data) are available. More so, it was also validated using simulated experimental data. To ensure the feasibility of large-scale implementation, the algorithm was then applied on LiDAR data of 242 km of highways.

3.3.3.1 As-built Drawings and Simulated Data

As-built drawings were obtained from the Alberta Transportation database and were only available for an 8 km segment of Highway 36 containing two horizontal curves. One curve is circular while the second contains spiral transition curves. The developed methodology was tested on the LiDAR data collected along this section. The algorithm extracted the centerline, detected the curves and estimated their geometric characteristics. The obtained curve attributes were then compared to the information documented on the as-built drawings.

To this end, the algorithm was validated using ground truth data (i.e., as-builts) which contained two curves. Due to the limited availability of as-built drawings for numerous curves, and to ensure that the algorithm was tested on a large scale, another simulated experimental case was created. A roadway centerline with multiple horizontal curves was generated using AutoCAD Civil 3D software. This segment was developed based on a set of predefined curve attributes. This simulated data includes centerline points (i.e., simulating the trajectory points) that can be used by the proposed algorithm to define the centerline vectors and then execute the proposed procedure. The simulated segment was 20 km long and contained five horizontal curves with different degrees of curvature (i.e., sharp and mild curves). The algorithm was then used to detect the presence of horizontal curves and estimate their geometric attributes. The results obtained by the algorithm were compared to the predefined values that were initially used to generate the simulated centerline.

Figure 8 shows the analyzed simulated segment with its corresponding change in the azimuth diagram along the horizontal alignment. From the figure, straight and curved elements

can be seen intuitively as tangent elements have no change in azimuth; however, curves have a constant change (in an ideal case).

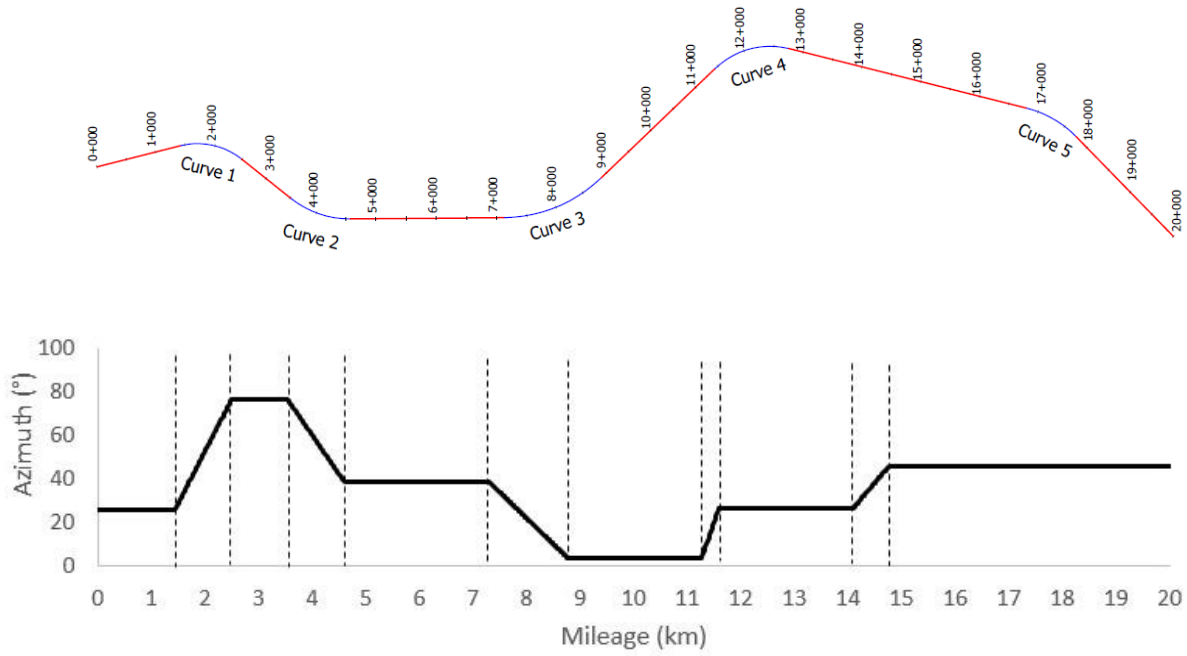

Figure 8: Azimuth change along the horizontal alignment of the simulated segment

3.3.3.2 Result Validation

Table 2 shows the results of running the code on LiDAR data of the Highway 36 subsection. It presents information on curve attributes obtained from as-built drawings and the corresponding information extracted from the LiDAR scan of the highway.

Table 2: Extraction results of as-built and LiDAR data for Highway 36

Element	Attribute	As-built (ground truth)	Detected (LiDAR)	Difference (%)
Tangent 1	Length (m)	N/A	2474.32	N/A
Curve 1	Turn Direction	Right	Right	N/A
	Delta (°)	24.00	23.99	0.058
	Radius (m)	1746.50	1809.00	3.580
	Curve length (m)	762.00	783.92	2.896
	Chord Length (m)	737.10	758.55	2.828
Tangent 2	Length (m)	652.88	642.36	1.638
Curve 2	Turn Direction	Right	Right	N/A
	Delta (°)	49.30	49.01	0.588
	Radius (m)	582.50	606.60	3.973
	Entry Spiral length (m)	106.68	105.61	1.000
	Exit Spiral length (m)	106.68	103.07	3.386
	Curve length (m)	N/A	534.80	N/A
	Chord Length (m)	N/A	512.87	N/A
Tangent 2	Length (m)	197.00	189.40	3.858

The table shows the percent difference between the actual estimates (i.e., as-builts) and those obtained using the proposed method. The percent difference between the estimates ranged from 0.058 % to 3.973 %, indicating that the code was able to extract the curve attributes successfully with an accuracy of 96.027 % to 99.942 %. It is also worth noting that the attributes of spiral transition curves were accurately extracted. The percent difference for estimating the spiral length was 1.000 % and 3.386 % for entry and exit spiral curves respectively.

It is worth noting that the highest percent difference was 3.580 % (62.50 m difference) for estimating the radius of curve 1 and 3.973 % (24.10 m difference) for curve 2. This difference could be attributed to the possibility that the code has been inexact by one or two vectors when locating the curve start and endpoints (PC and PT) which resulted in some differences between ground truth values and detected estimates. The algorithm might be inexact because the real PC and PT points might not be at an exact PC and/or PT point that is defined by the code. In other words, PC and PT points are identified based on exceeding the threshold of change in azimuth between vectors. When a PC or PT point is located, it would be at either a start or an end point of the vector at which the azimuth change threshold is exceeded. This does not necessarily mean that the defined PC and PT points are at the exact same locations of the real PC and PT points of the curve. The located curve start and end points can be shifted by one or two vectors. The impact of this imperfection on the estimated curve attributes is not significant as demonstrated by the extraction results. Based on applying the algorithm on the ground truth data, this resulted in a percent difference of up to 3.973 % between real values of curve attributes and those estimated by the proposed method. This translates to a minimum accuracy of 96.027 % in detecting curved sections and estimating their attributes.

Although the algorithm was found to be accurate when validated using ground truth data from as-built drawings, it was also tested on a simulated road centerline of a 20 km segment. The actual curve attributes that were used to construct the simulated road centerline in AutoCAD Civil 3D are shown in Table 3. Random noise was added to the planimetric coordinates (X, Y) of centerline points of the simulated trajectory to simulate the nature of lidar-based trajectory points.

Random noise was added with standard deviations of 0.02 and 0.04 m to test the influence of different noise levels on curve detection and feature extraction accuracy. The algorithm was tested on the smooth simulated data (i.e., zero noise) and data with both noise levels.

Table 3 summarizes horizontal alignment attributes extracted by the algorithm in all cases. The results show that when using random noise with a standard deviation of 0.02 m, the estimated curve attributes are nearly identical as those resulting from using smooth simulated trajectory points (i.e., with zero noise). The algorithm was able to detect all curves and extract their attributes with percent differences between the estimated and the actual values ranging between 0 to 1.874 % (accuracy of 98.126 % to 100 %). In the case of adding noise with a standard deviation of 0.04 m to the simulated data, the percent differences between the estimated and the actual values were almost the same as the percent differences resulted from using smooth data when estimating the majority of curve attributes. However, for some curve features, the percent difference slightly increased. It ranged from 0 to 3.304 % compared to a range of 0 to 1.874 % in the case of using smooth data (i.e., zero noise). This indicates the algorithm was able to detect curved sections and estimate their geometric characteristics with an accuracy of 96.696 to 100 % from simulated trajectory points with different noise levels. These results show that the proposed algorithm is of a high level of accuracy in curve detection and feature extraction when deviations in vehicle trajectory are up to 0.04 m.

Table 3: Extraction results of actual and detected data for the simulated segment

Element	Attribute	Actual (simulated)	Simulated data (Smooth & with 0.02 m Noise)		Simulated data (with 0.04 m Noise)	
			Detected (LiDAR)	Difference (%)	Detected (LiDAR)	Difference (%)
Tangent 1	Length (m)	1431.61	1430.00	0.113	1430.00	0.113
Curve 1	Turn Direction	Right	Right	NA	Right	-
	Delta (°)	50.69	50.69	0.000	50.69	-0.002
	Radius (m)	1200.00	1205.29	0.441	1205.25	-0.438
	Curve length (m)	1061.65	1079.97	1.726	1079.98	-1.727
	Chord Length (m)	1027.37	1034.93	0.736	1034.91	-0.734
Tangent 2	Length (m)	1025.92	1030.00	0.398	1040.00	-1.372
Curve 2	Turn Direction	Left	Left	NA	Left	-
	Delta (°)	37.66	-37.66	0.003	-37.66	-0.002
	Radius (m)	1600.00	1610.56	0.660	1597.64	0.148
	Curve length (m)	1051.64	1069.98	1.744	1060.00	-0.795
	Chord Length (m)	1032.81	1040.73	0.767	1031.29	0.147
Tangent 3	Length (m)	2557.27	2560.00	0.107	2570.00	-0.498
Curve 3	Turn Direction	Left	Left	NA	Left	-
	Delta (°)	41.94	-41.94	0.001	-41.94	0.002
	Radius (m)	2400.00	2401.69	0.070	2380.54	0.818
	Curve length (m)	1756.80	1769.99	0.751	1749.98	0.390
	Chord Length (m)	1717.84	1720.83	0.174	1702.16	0.921
Tangent 4	Length (m)	2554.36	2560.00	0.221	2559.99	-0.220
Curve 4	Turn Direction	Right	Right	NA	Right	-
	Delta (°)	55.82	55.82	0.007	55.82	-0.007
	Radius (m)	1350.00	1362.85	0.952	1369.64	-1.455

Element	Attribute	Actual (simulated)	Simulated data (Smooth & with 0.02 m Noise)		Simulated data (with 0.04 m Noise)	
			Detected (LiDAR)	Difference (%)	Detected (LiDAR)	Difference (%)
	Curve length (m)	1315.32	1339.97	1.874	1349.97	-2.635
	Chord Length (m)	1263.91	1276.88	1.026	1285.75	-1.728
Tangent 5	Length (m)	4049.67	4050.00	0.008	4050.00	-0.008
Curve 5	Turn Direction	Right	Right	NA	Right	-
	Delta (°)	30.90	30.90	0.000	30.90	0.000
	Radius (m)	1750.00	1760.93	0.625	1761.57	-0.661
	Curve length (m)	943.79	959.99	1.716	960.00	-1.717
	Chord Length (m)	932.39	938.38	0.642	938.39	-0.643
Tangent 6	Length (m)	2251.99	2230.00	0.986	2179.97	3.304

3.3.4 Network-level Assessment

3.3.4.1 Extraction Results

The primary aim of this step is to test the feasibility of utilizing the extraction algorithm on a large scale. To that end, the algorithm was used to detect curves and extract their attributes on 242 km of five highways where LiDAR data was collected. In order to test the robustness of the algorithm, the segments were selected in a manner that ensures variability in their geometric characteristics, including the sharpness of curves, number of lanes, roadside vegetation, and functional classification. The 242 km were broken down as follows: 60 km on Highway 1 (HWY 1), 45.2 km on Highway 2 (HWY 2), 44 km on Highway 17 (HWY 17), 68.47 km on Highway 58 (HWY 58),

and 23.96 km on Highway 661 (HWY 661). Figure 9 shows images of LiDAR data for road test segments.

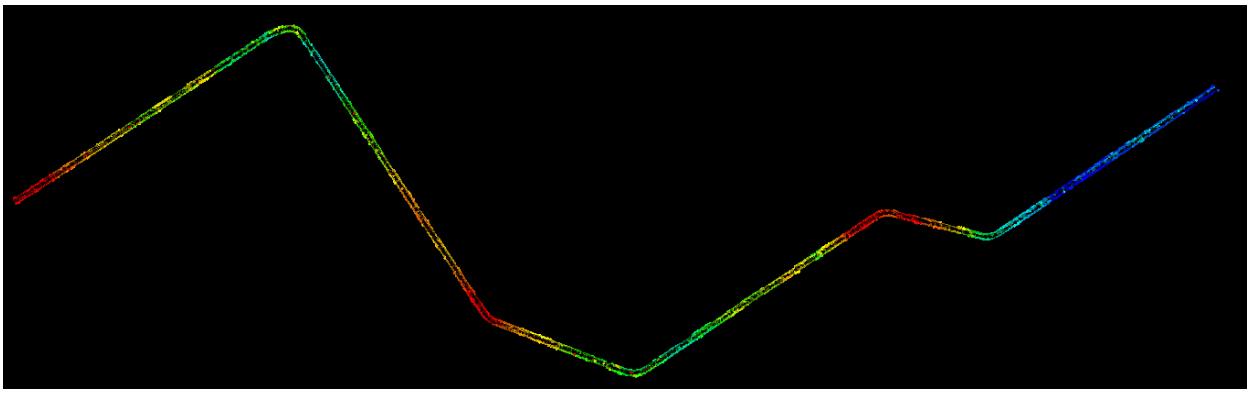

a. Highway 1 (Station 0+000 to Station 60+000)

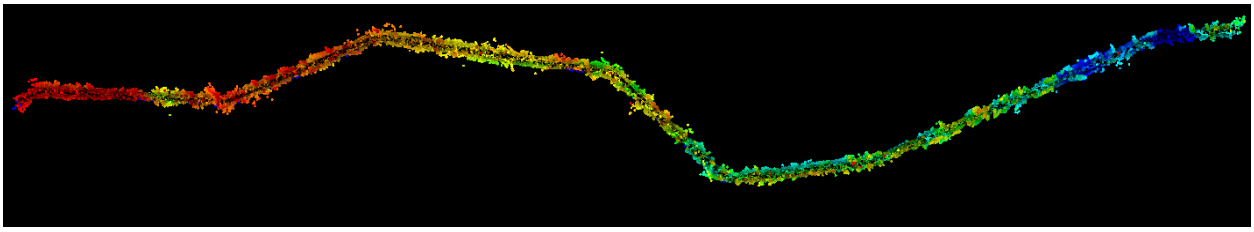

b. Highway 2 (Station 0+000 to Station 45+199)

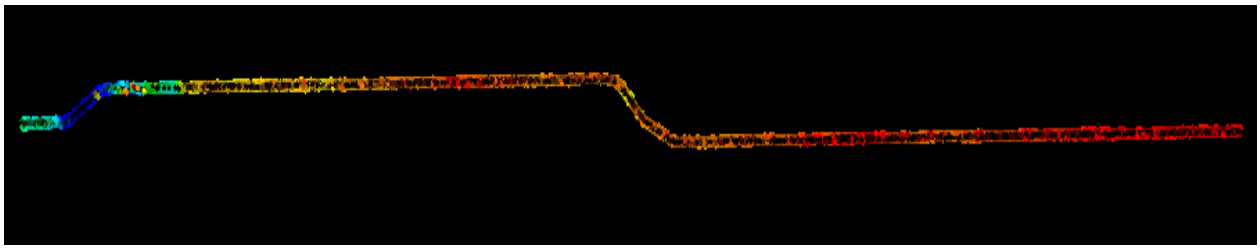

c. Highway 17 (Station 0+000 to Station 44+000)

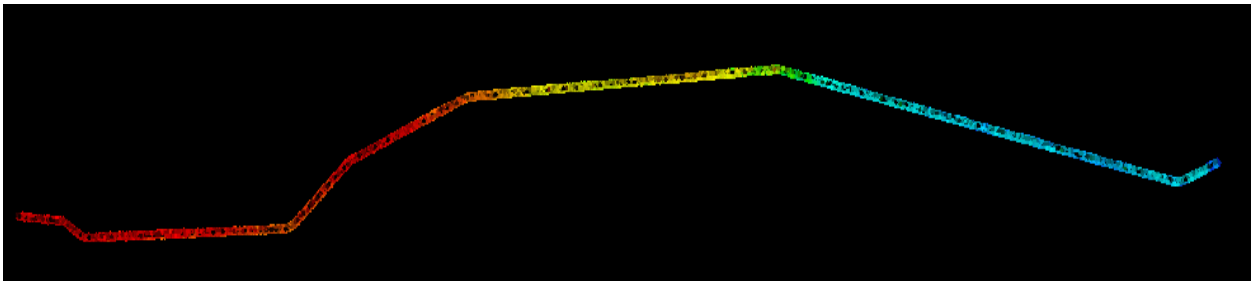

d. Highway 58 (Station 0+000 to Station 68+472)

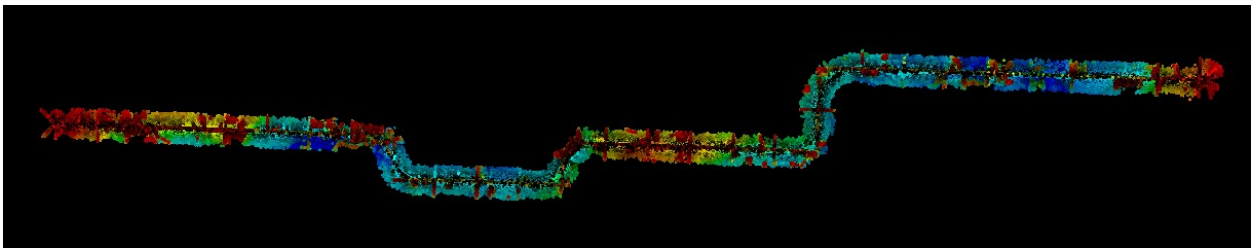

e. Highway 661 (Station 0+000 to Station 23+956)

Figure 9: LiDAR data for 242 km of highways 1, 2, 17, 58, and 661

The algorithm was successful at identifying all the curves along the five highway segments, with a detection rate of 100 % which has been verified using Google maps. As an example, Figure 10 shows the azimuth diagram generated from LiDAR data of Highway 17, the figure demonstrates how effective the algorithm is in distinguishing between tangent elements and curved sections, with curved segments corresponding to changes in the slope of the azimuth diagram and straight segments corresponding to the flat linear portions of the diagram (five curves can be visually identified along this segment).

Table 4 shows the results of running the code on all road segments. The results show that on Highway 2, two false-positive curves were detected (i.e., although the test data contains seven

curves, the algorithm detected nine). A closer examination of this anomaly revealed that two of the detected nine curves had a deflection angle of 0.5°, which is not reasonable for a horizontal curve. An in-depth examination revealed that these two curves were temporary changes in the horizontal alignment resulting from traffic detours during roadwork construction when the data was collected, as seen in Figure 11.

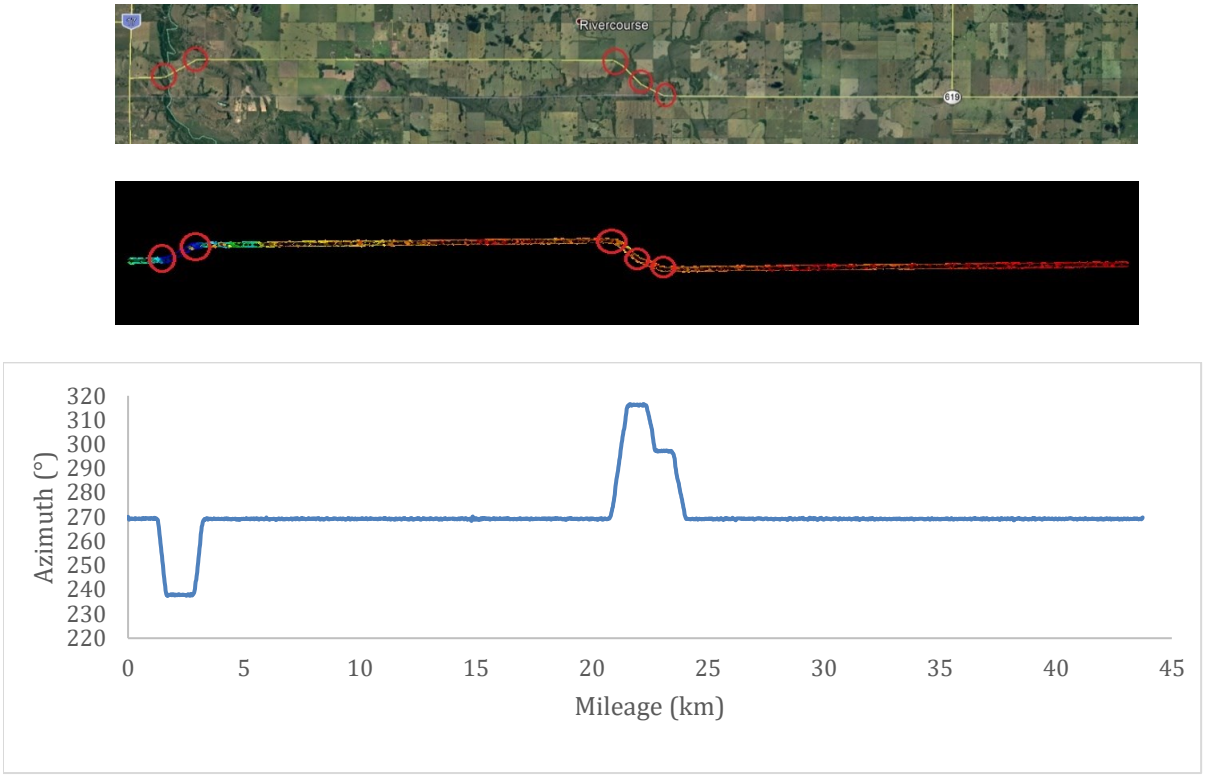

Figure 10*:* Azimuth change along LiDAR data of Highway 17 segment

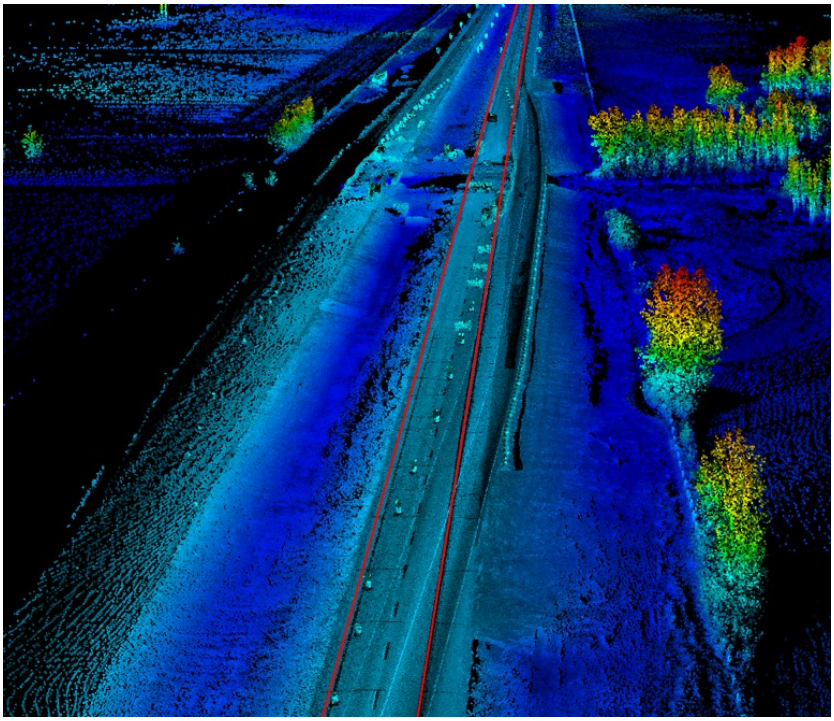

Figure 11*:* Traffic detours detected by the algorithm

Table 4: Results of algorithm application on a network-level using LiDAR data

Highway Class		**Freeway**		**Arterial**		**Collector**
Element	**Attribute**	**HWY 1**	**HWY 2**	**HWY 17**	**HWY 58**	**HYW 661**
Tangent 1	Length (m)	12645.8	623.7	1327.6	2207.2	6068.7
Curve 1	Direction	Right	Right	Left	Right	Right
	Delta (°)	89.8	26.0	-31.5	27.8	63.9
	Radius (m)	616.8	1152.8	663.0	1081.1	501.2
	Superelevation (m/m)	0.073	0.039	0.053	0.045	0.609
	Curve length (m)	844.5	543.4	381.7	542.1	562.7
	Chord Length (m)	768.8	518.6	357.0	517.2	516.8
Tangent 2	Length (m)	13308.1	6032.9	1246.6	682.9	321.3

Highway Class		Freeway		Arterial		Collector
Element	**Attribute**	**HWY 1**	**HWY 2**	**HWY 17**	**HWY 58**	**HYW 661**
Curve 2	Direction	Left	Left	Right	Left	Left
	Delta (°)	-35.6	-26.1	31.4	-34.9	-64.0
	Radius (m)	834.1	845.6	588.3	1128.2	503.9
	Superelevation (m/m)	0.051	0.037	0.055	0.026	0.069
	Curve length (m)	768.8	379.3	318.4	674.0	517.6
	Chord Length (m)	522.9	402.4	341.6	703.6	563.2
Tangent 3	Length (m)	5508.6	5249.6	17837.1	10375.1	2270.4
Curve 3	Direction	Left	Right	Right	Left	Left
	Delta (°)	-54.5	31.7	47.0	-39.6	-58.2
	Radius (m)	1011.5	1062.0	757.6	1087.4	505.6
	Superelevation (m/m)	0.056	0.050	0.059	0.031	0.075
	Curve length (m)	964.9	602.6	623.2	763.4	522.6
	Chord Length (m)	910.1	576.5	591.3	730.9	481.9
Tangent 4	Length (m)	10917.4	7562.1	884.3	3801.7	442.6
Curve 4	Direction	Right	Right	Left	Right	Right
	Delta (°)	48.0	34.0	-19.0	18.5	58.2
	Radius (m)	897.6	952.6	1033.1	1007.6	489.2
	Superelevation (m/m)	0.072	0.057	0.039	0.045	0.054
	Curve length (m)	764.4	584.3	362.2	341.5	502.3
	Chord Length (m)	723.6	558.3	341.0	320.7	463.9
Tangent 5	Length (m)	3638.5	4768.9	884.9	6353.7	3838.3
Curve 5	Direction	Left	Left	Left	Right	Left
	Delta (°)	-48.0	-50.0	-28.0	19.1	-89.9
	Radius (m)	901.0	815.9	916.8	1629.0	504.5
	Superelevation (m/m)	0.071	0.064	0.038	0.045	0.064

Highway Class		Freeway		Arterial		Collector
Element	**Attribute**	**HWY 1**	**HWY 2**	**HWY 17**	**HWY 58**	**HYW 661**
	Curve length (m)	763.8	724.8	462.4	562.8	783.4
	Chord Length (m)	723.8	686.2	439.6	539.9	691.9
Tangent 6	Length (m)	10302.8	4828.2	19828.6	16207.7	422.0
Curve 6	Direction	N/A	Left	N/A	Right	Right
	Delta (°)		-16.3		16.4	89.6
	Radius (m)		571.2		1614.6	539.7
	Superelevation (m/m)		N/A		0.043	0.054
	Curve length (m)		181.1		482.5	944.4
	Chord Length (m)		160.8		461.1	866.8
Tangent 7	Length (m)	N/A	N/A	N/A	21515.7	6953.6
Curve 7	Direction	N/A	N/A	N/A	Left	N/A
	Delta (°)		0.5		-34.7	
	Radius (m)		N/A		1066.0	
	Superelevation (m/m)				0.038	
	Curve length (m)				663.8	
	Chord Length (m)				635.7	
Tangent 8	Length (m)	N/A	N/A	N/A	1942.3	N/A
Curve 8	Direction	N/A	N/A	N/A	N/A	N/A
	Delta (°)		-0.5			
	Radius (m)		NA			
	Superelevation (m/m)					
	Curve length (m)					
	Chord Length (m)					
Tangent 9	Length (m)	N/A	10013.8	N/A	N/A	N/A
Curve 9	Direction	N/A	Right	N/A	N/A	N/A

Highway Class		Freeway		Arterial		Collector
Element	**Attribute**	**HWY 1**	**HWY 2**	**HWY 17**	**HWY 58**	**HYW 661**
	Delta (°)		18.4			
	Radius (m)		1631.9			
	Superelevation (m/m)		0.039			
	Curve length (m)		542.4			
	Chord Length (m)		520.5			
Tangent 10	Length (m)	N/A	2474.2	N/A	N/A	N/A

3.3.4.2 Computer Power and Processing Time

One important element when discussing network-level assessments is the processing time required to achieve such results. The horizontal curve detection and feature extraction was performed using a computer with a 12-core Intel E5-1650V4 CPU at 3.6 GHz with 32 GB RAM. The processing time ranged from 1.82 sec/km for Highway 501 to 4.42 sec/km for Highway 661. For Highway 58, the highway with the longest test segment, the processing time was 3.08 sec/km. For Highways 1 and 2, the processing time was 2.68 sec/km and 2.46 sec/km, respectively. The total processing time was 2.92 sec/km or 13 min and 32 sec to both detect and extract all horizontal alignment characteristics on the entire 242 km of highway segments.

3.3.5 Algorithm Performance and Significance

As demonstrated by the results, the algorithm is effective in efficiently and accurately detecting and extracting attributes of horizontal alignments on a network level. The feasibility of applying the algorithm on a large scale demonstrates the value of the developed procedure not only for establishing the data set required for reliability analysis but also for assisting departments of

transportation manage their road networks. Establishing an accurate inventory of curve information in such a robust manner could transform the way road networks are managed and help alleviate the burden associated with using conventional surveying methods.

Several transportation agencies rely on information about roadway horizontal alignment in planning, design, and safety assessment of roadway facilities. Maintaining an up-to-date inventory of curve data is also useful to both these entities as well as researchers investigating the influence of horizontal alignment attributes on safety. Studies investigating such effects in the past have used a variety of conventional techniques to collect curve data [111-114]. The size of road networks used in these studies ranged from 46.6 km to 543 km highway segments. Curve attribute information was obtained from several different sources including departments of transport, aerial photographs, satellite images, or commercial design software (i.e., AutoCAD) combined with conventional surveying methods. One study by Manan, Jonsson [113] used data measured from Google Earth and local street maps as a result of the lack of available information on road geometry. The authors indicated a lack of accurate information on road geometry including the inability to obtain information about vital variables, such as road vertical profiles, which, could be extracted using LiDAR data [76].

A large scale inventory of horizontal curve attributes is also essential for developing operating speed models [115]. Such models are important for evaluating the roadway design consistency. The literature is full of research studies focusing on the development of speed prediction models using horizontal alignment attributes [116-124]. The number of sites used in these studies varied from 10 to 116 horizontal curves. Similar to safety studies, information on

horizontal alignment attributes were obtained from different sources, which are, in some cases, inaccurate or inefficient. Some studies extracted road geometry data from as-built drawings provided by the ministry of transportation or highway officials, while others used design and GIS software such as AutoCAD and ArcGIS to manually extract the information from design drawings or from survey points collected using conventional methods. The above discussion shows the importance of maintaining an up-to-date repository of roadway alignment information from both an operational and research standpoint. Therefore, adopting a robust and automated data extraction framework such as the developed algorithm is an appealing alternative to departments of transportation.

When discussing the deployment of a technology-driven method such as the developed methodology, potential time and money savings should be discussed. The developed algorithm demonstrated the value of automation in detecting highway horizontal curves and extracting their attributes on a large scale. For example, the code was tested on LiDAR data of 242 km of highway segments, and it detected all 35 horizontal curves and estimated their geometric characteristics in 13 min and 32 s using LiDAR data sets. To conduct a conventional survey for the same highway segments, a crew of at least two people would be needed and they could easily spend a day (i.e., eight working hours) to collect information on a single horizontal curve. Knowing that the average rate of a surveyor in Alberta is around $120 /hr, the total cost to survey all 35 curves would be approximately $ 67,200. Considering the safety risks associated with the surveyors being on or close to adjacent traffic, the time needed to perform manual surveys especially for long highway segments, and the fact that LiDAR data represent 3D models for highways that can be accessed

anytime, the adoption of LiDAR data in asset management could save transportation agencies significant amounts of time and money.

3.4 Available Sight Distance Assessment in a 3D Environment

This section is dedicated to the developed algorithm for sight distance assessment. It describes the developed procedure for 3D ASD computation and includes details about algorithm testing, validation, and application on a large scale.

3.4.1 Background

It is evident from the literature review presented in the previous chapter that there have been several studies dedicated to assessing *ASD* on highways. However, there is also a large need for expansion. Most of the previous work focuses on evaluating *ASD* using GIS data or aerial LiDAR images (i.e., collected by aeroplane) and utilizing commercially available software, such as ArcGIS. This involved manual interventions that hinder the large-scale *ASD* assessment and, more importantly, a recent study by Castro, Lopez-Cuervo [91] showed that using mobile LiDAR data outperforms aerial LiDAR and allows for highly accurate *DSM*, leading to a very accurate representation of the road environment. In addition, many of these previous studies have not provided a reliable validation procedure for the outputs of the proposed methods. This could be due to the absence of as-built information on the *ASD* since it is very hard to compute during site visits. Previous work considered these as limitations and recommended further research to automatically evaluate the *ASD* using 3D roadway models. Developing a method that utilizes a

reliable source of data to determine the *ASD* in an efficient and automated manner is of great value to road design and safety fields.

Therefore, a part of the data acquisition phase in this thesis is developing a procedure by which mobile LiDAR data is used to evaluate the available sight distance on entire highways in a robust and fully automated approach. Mobile LiDAR data provides access to a 3D model of the roadway that can be used to automatically compute the available sight distance and accurately and investigate sight distance obstructions. Thus, this research adds to the existing body of literature in this area by introducing a fully automated ASD assessment framework. The method takes into account the 3D nature of the road environment considering the combined effects of both horizontal and vertical alignments and accounts for the presence of 3D obstacles such as vegetation, buildings, and road furniture that can obstruct the driver's sight lines.

Prior to utilizing the developed method in establishing the curve data needed in reliability calculations, the algorithm was first tested by computing the *ASD* from LiDAR data of 20-km segments of highway in Alberta, Canada. A 3D based validation procedure was conducted following the AASHTO's recommendations to ensure the accuracy of the obtained results [17]. The influence of the interaction between horizontal and vertical alignment has on sight distance limitations was also discussed. The developed algorithm increases the efficiency and robustness of the sight distance evaluation process using mobile LiDAR data and helps alleviate hurdles associated with conventional assessment methods.

3.4.2 Methodology

The sight distance assessment process involves three main stages. It first includes defining observer and target points to represent the driver's eye and objects along the highway. The second step involves LiDAR data voxelization in which LiDAR point cloud is converted into voxels (i.e., 3D representation of road segments) followed by mapping observers and targets onto the voxel grid. The last step includes assessing the visibility between observers and targets and computing the *ASD* along the analyzed segment. The method can be explained in more detail as follows:

3.4.2.1 Defining Observer and Target Points

The first step is to define observer and target points. Observers are points that represent the driver's location along a driving lane centerline. Targets are points that represent objects (i.e., potential obstructions) being observed by the driver. Since the *ASD* is to be assessed along the vehicles' path on a driving lane, observer and target points are the set of points representing the trajectory of the data collection truck travelling along the highway. These points are aligned parallel to the road axis and can be extracted from the collected LiDAR data. This set of points is obtained by filtering the LiDAR point cloud based on the scanning angle of points. Points collected at a zero scanner-angle by the scanning system are the points located right under the scanner on the roadway pavement surface and represent the trajectory of the data collection vehicle. Thus, after the algorithm reads the LAS file of a four km segment, it filters the point cloud data and deletes any points with a non-zero scanner angle. The remainder of the points with a zero scanner is then used to represent observer and target points. To enable an automatic sight distance on an entire highway, the code runs through a number of LAS files for successive road segments (i.e., four km each) and

combines the extracted points to represent the vehicle trajectory (i.e., observers and targets) along the entire roadway. The output is a vector of observes o_i = [i, i+1, i+2, …., n] contains n points and a vector of targets t_j = [j, j+1, j+2, …., m] contains m points.

The number of observer and target points vary based on the interval distance at which the *ASD* is to be assessed. While evaluating *ASD* for every distance up to 50-m is recommended [88], analysis of a large number of segments showed that computing *ASD* at distances from 5 to 20m yields almost the same results. While this distance can be altered by the user (i.e., designer), the sight distance is assessed in this research at 20-m distance intervals. In order to be consistent with the design guidelines' requirements, the height of the observer and target points should be accounted for. The Alberta Highway Design Guide recommends an observer height of 1.05 m (represents the height of the driver's eye) and an object height of 0.38 m (represents the lead vehicle tail's height) be used when evaluating the *ASD* [125]. Thus, after the code extracts the observer and target points, their elevations are modified according to the values suggested by the design guides. Figure 12 shows an example of observer points distributed along the road lane centerline. In order to verify that observer and target points are defined along the trajectory of the data collection truck (i.e., lane centerline) which is the same path of any vehicle would drive inside the lane, observers and targets were mapped onto the 3D LiDAR point cloud using the Quick Terrain Reader Software, visually checked, and found to be accurately defined as shown in Figure 12.

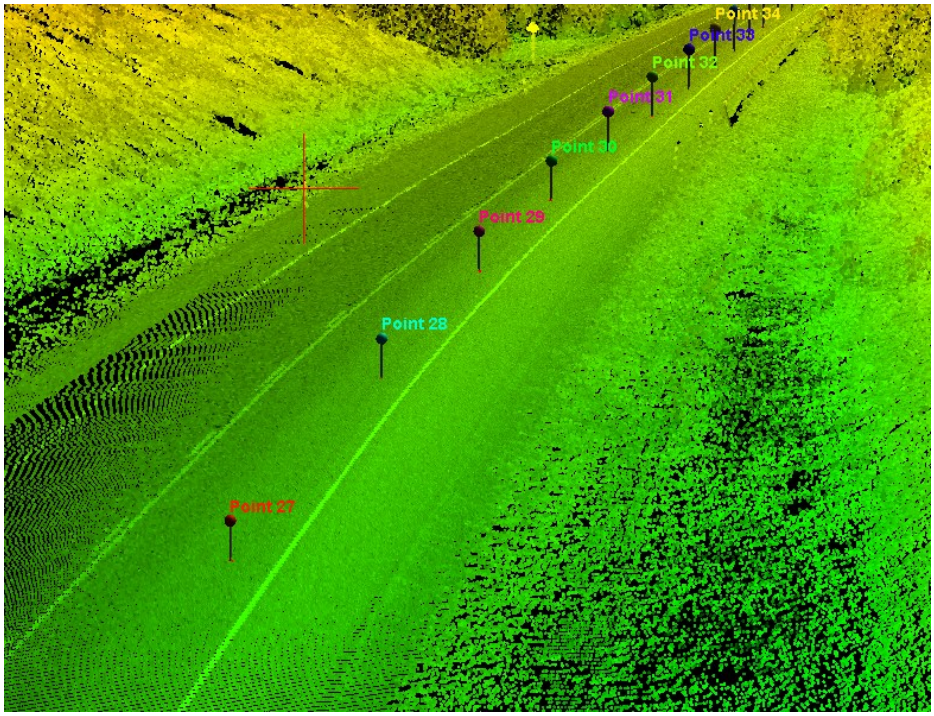

Figure 12: An example of observer points along the road lane centerline

3.4.2.2 LiDAR Point Cloud Voxelization

LiDAR point clouds contain highly dense points that are heterogeneously distributed in the 3D space. Thus, a reduction in the size of the data is required in order to easily identify the features of interest either visually or through a methodology using the reduced data [96]. Reduction of point cloud data size is possible using voxelization without compromising the information on objects in the voxel space [62, 91, 96]. Voxelization is the process of discretizing the LiDAR data by dividing the LiDAR data point cloud into a 3D grid (i.e., voxels) of a certain size (i.e., user-defined). The word voxel is similar to the word pixel, but the voxel is a volumetric pixel in the 3D while a pixel is a 2D representation term used when describing normal images. Voxelization is used to discretize

the LiDAR data point cloud into truly 3D volumes (i.e., voxels) that best represent the continuous road features and are easy to handle compared to dealing with millions of discrete data points. Discretizing LiDAR data into voxels also makes the algorithm faster since the code processes a smaller number of objects "voxels" compared to processing millions of discrete LiDAR data points.

In this step, the point cloud is divided into a 3D grid with millions of volumetric cubes. A unique code is assigned to every cubic voxel to identify them. All points in the point cloud are then assigned the defined voxels. Each group of points is assigned to a voxel in the voxels grid based on their spatial positions. To assign a point into a voxel, let *P (x, y, z)* denote a certain point and *v (i, j, k)* denote a voxel. If the dimensions of a voxel cell in the *x, y,* and *z* directions are Δx, Δy, and Δz; and the origin of the tri-dimensional voxel grid is denoted by x_0, y_0, and z_0, the ID of the voxel *v (i, j, k)* that contains the point *P (x, y, z)* is computed as follows [64]:

$$i = \frac{int\ (x - x_0)}{\Delta_x}$$

$$j = \frac{int\ (y - y_0)}{\Delta_y}$$

$$k = \frac{int\ (z - z_0)}{\Delta_z}$$

The voxelization of a point cloud is based on a 3D histogram counting algorithm [64]. The algorithm considers the size of both the entire 3D grid and the voxel size in order to classify the points contained in the point cloud into bins. The size of the voxel is chosen in a way that retains all information about feature objects. Although the voxel size can be defined by the user, it is

recommended that voxel dimensions be chosen based on the properties of the laser scanning system used to collect the data [63]. The laser scanner collected data that is used in this study has scan lines that are about 20-cm apart. Thus, in this research, using a 20-cm cell size for voxelization is considered. This would ensure that points collected from neighboring scanlines would be assigned into adjacent voxels. It is worth mentioning that the selected voxel size was tested to ensure that sight distance is not obstructed by small objects that would not normally limit the driver's visibility. The outcome of the algorithm was also validated using recommendations of design guidelines as explained in Section 3.4.3. Figure 13 visualizes the voxelization process by showing a sample of LiDAR data before and after conversion into voxels.

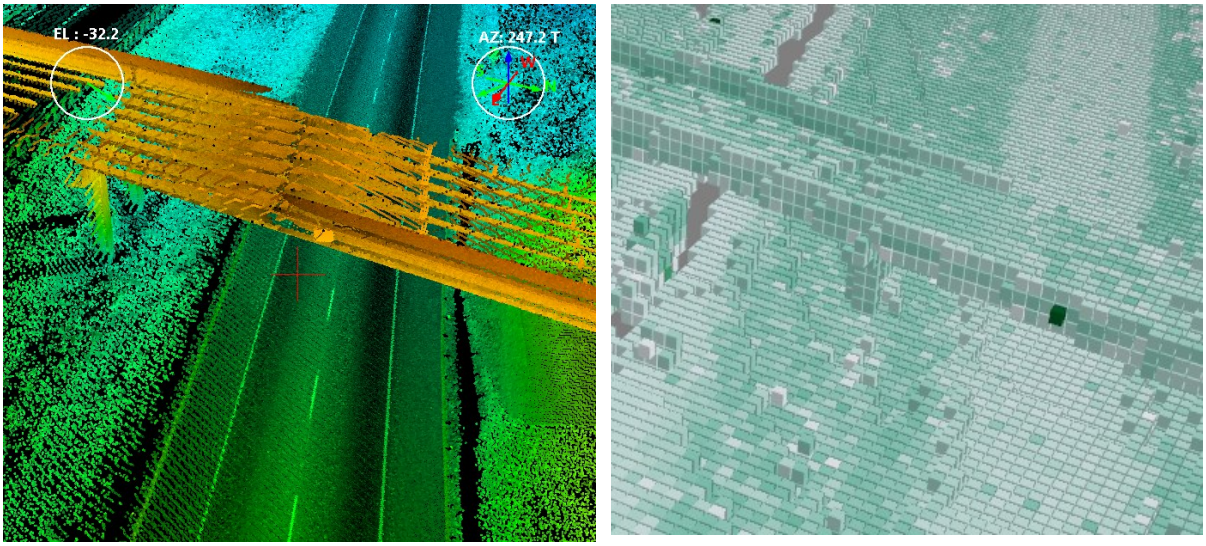

Figure 13: A sample of LiDAR point cloud before and after voxelization

(left side: before, right side: after)

3.4.2.3 Available Sight Distance Computation

Evaluation of the *ASD* involves three steps. The first step is mapping observers and targets onto the grid of voxels created for the LiDAR point cloud. The next step is constructing and assessing sight lines between each observer in the observers' point set; o_i and all targets in the set t_j. For example, the algorithm checks the visibility from the first observer ($i = 1$) to all target points $t_{j=1:m}$. Then, the process is repeated for each observer ($o_{i=1:n}$) in the observers' points set. To check the visibility between an observer and a target, a vector is created between the observer point and the target point. The code then goes along this vector and looks for the obstructing voxel. The algorithm searches for the voxel that touches the vector, which occurs when the vector position is lower than the position of the highest point inside the voxel and higher than the position of the lowest point inside the voxel.

If there is no obstructing voxel found between the observer and the target, the code checks for the next target. The code continues looping through the successive targets (i.e., from the same observer) till the first obstructing voxel has been identified. Once a cubic voxel is found to restrict the visibility from an observer to a target, the distance from the observer to the last visible target (i.e., the previous target) is recorded as the *ASD* at this observer. If the code reaches the end of the array of targets before finding an obstructing voxel, the *ASD* is considered as the distance from the observer to the last target. Figure 14 demonstrates sightlines connected from an observer point to successive target points. The code repeats the same process for the entire observer's array and records the *ASD* at each observer. Once the available sight distance has been computed at all observers' locations, the code compares the *ASD* at each location against the requirements of

design guidelines to determine whether or not the minimum required sight distance is met. The code finally outputs and plots the available sight distance along the highway segment (i.e., or the entire highway).

Finally, to facilitate further investigation about locations identified with sight distance deficiencies, the algorithm also exports KML (Keyhole Markup Language) files containing position (*x,y,z*) information about the obstructing objects (i.e., voxels) at these locations. These KML files can be imported later into the 3D point cloud in case a visual inspection is to be conducted.

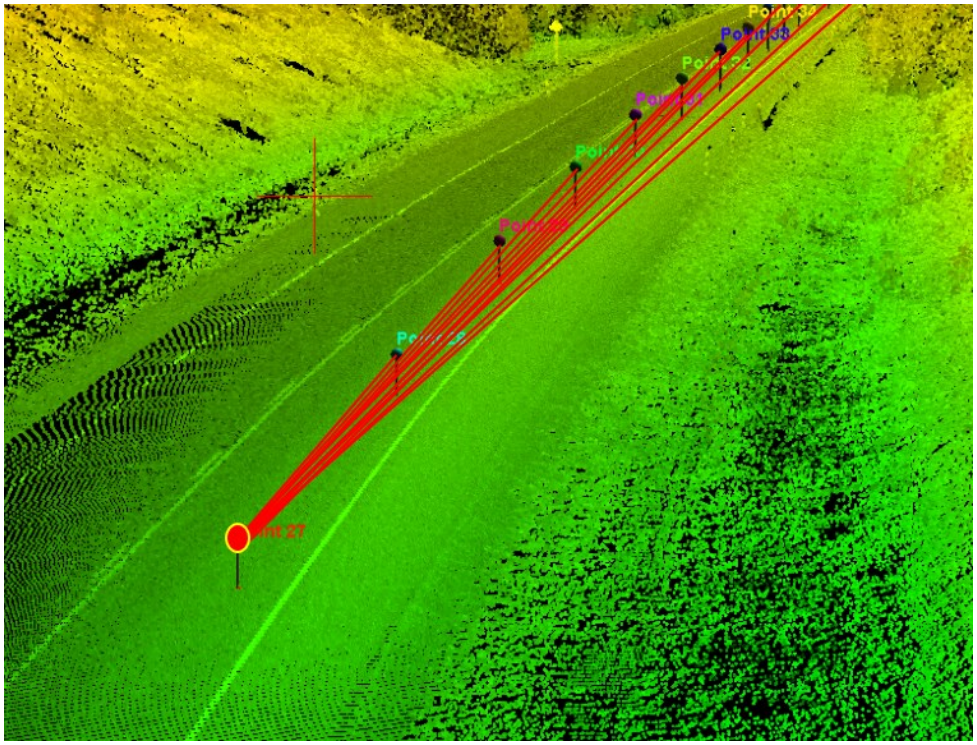

Figure 14: Sightlines connected from an observer to successive targets

3.4.3 Algorithm Testing and Validations

3.4.3.1 Test Segments

The proposed algorithm was coded using MATLAB [110]. In order to apply the introduced procedure to assess *ASD* on highways, the performance of the code should be tested and then validated to verify the applicability and accuracy of the results of the proposed method. For this purpose, the code was tested on LiDAR data for 20-km of highway segments in Alberta, Canada. Two highway segments were used in the testing and validation process as follows:

- *Highway 11*: A 12 km segment on this highway was used. This segment is located in the western part of Alberta. The posted speed limit along this section is 100 km/h. This section contains nine horizontal curves with high variation in the vertical alignment due to its proximity to mountainous areas surrounding Banff National Park. The reason behind the selection of the segment is the fact that its location and the variation in the horizontal and vertical geometry indicate a high potential for having locations with insufficient *ASD*. This would help investigate the influence of horizontal and vertical alignment on sight distance limitations.
- *Highway 63*: An eight km segment that includes two horizontal curves was selected. It is located in the Northeast of the City of Edmonton. The surrounding area is of rolling terrain. This section has a posted speed limit of 100 km/h. It is worth noting that his segment is one of the top ten high collision locations in the province. This indicates the importance of investigating the safety implications of sight distance insufficiencies if found.

3.4.3.2 Results and Discussion

Based on the characteristics of the tested segments, the minimum stopping sight distance required by the Alberta Highway Design Guide is 235 m. The *ASD* was assessed using LiDAR data of the two highways. When the *ASD* and minimum requirements are compared, it was found that the sight distance is satisfied along the two segments except for 19 regions (numbered 1-to-19); 15 were found on Highway 11 (i.e., located in mountainous areas), and four regions located on Highway 63. Figure 15 shows the *ASD* along the first four km of highway 11 segment. It is worth noting that only the *ASD* of the first four km of Highway 11 is shown in the figure and the *ASD* results of the remainder 20-km are summarized in Table 5. As shown in the figure, the *x*-axis represents the distance (i.e., station) at which the observer is located from the start of the segment, and the *y*-axis represents the *ASD*. The horizontal red line shows the minimum stopping sight distance required by the design guide (i.e., 235 m). The figure shows locations of regions one to four; out of 15 zones on Highway 11 were identified to have sight distance restrictions. The stationing of these regions is from (0+350 to 0+600); (1+150 to 1+450); (1+950 to 2+200); and (3+450 to 3+650). More details about these locations are discussed in the next few paragraphs. It is also worth noting that the decreasing trend of the *ASD* towards the end of the segment is because the code is approaching the end of the section (i.e., in LAS point cloud) and there was no additional length to conduct the assessment.

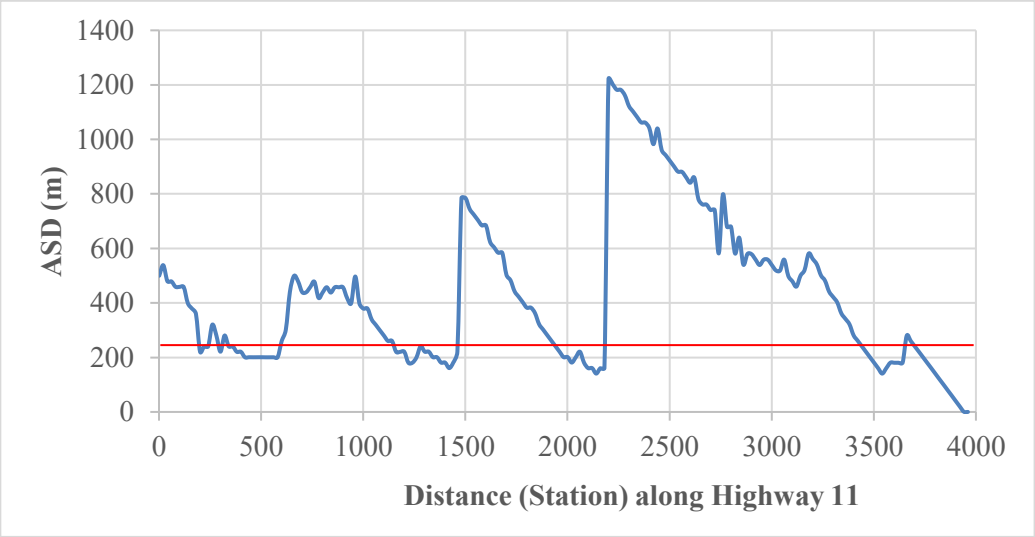

Figure 15: Available sight distance along Highway 11

(Red line: minimum stopping sight distance)

Further investigation was conducted for locations where sight distance was found to be insufficient. The algorithm generated KML files for locations where the code detected obstructions; these were imported to the LAS file of the segment to be visually inspected. Figure 16 reveals that *ASD* at the first four locations was restricted due to the high variation in the vertical alignment of the roadway. It is clearly shown that the limitations on sight distance were caused by vertical crest curves; which is expected considering the location of the segment (i.e., mountainous) and variation in the longitudinal grades.

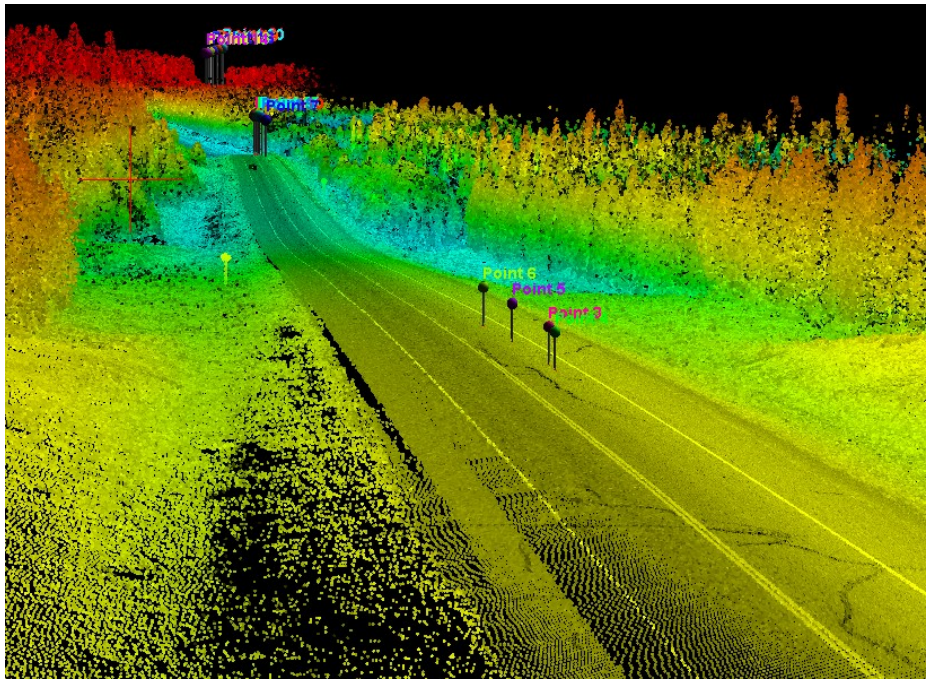

Figure 16*:* A sample of a location where ASD was restricted by vertical curves

Although a number of previous studies proposed sight distance assessment methodologies, the validation of results of the proposed procedure, in most cases, was limited to either visual inspection of GIS files or by conducting site visits to locations identified with visibility problems. Both could be inaccurate and prone to intra- and inter-observer variability due to the reliance on human observers. Inter-observer variation occurs when two or more observers examine the same material with varying results. Conversely, intra-observer variation occurs when a single observer experiences varying results while observing the same material more than once. Obviously, such variations can have profound effects on the overall results of the assessment. This difficulty in the presence of a robust method for validation could be attributed to the fact that sight distance is a

feature that is extremely difficult to be measured in the field and/or documented in as-built drawings.

This research validates the performance of the proposed algorithm considering the effect of both vertical and horizontal geometry along the 20-km of highway segments. Evaluating the *ASD* is usually implemented separately for road vertical and horizontal alignment [126]. For vertical alignment design guidelines also give recommendations about the driver's eye height and the object height that should be used for assessing the vertical profile against meeting the sight distance requirements. For horizontal alignment, AASHTO [17] recommends that "the designer must use graphical methods to check sight distance on horizontal curves". Thus, after applying the code on the tested segments using LiDAR data, the *ASD* was manually assessed against both vertical and horizontal alignment of the 19 locations using graphical methods.

- *For vertical alignment*: The procedure involved generating the road profile along the centerline of the driving lane (i.e., the same lane contains the trajectory points that were used by the algorithm). The road vertical profile was generated using the methodology detailed in the study of Gargoum, El-Basyouny [76]. Vertical lines representing the driver's eye height (1.05m) were drawn to scale on the vertical profile at 20-m apart (the same distance between observers used by the algorithm). A target was then drawn at a distance of 235m (i.e., the minimum sight distance) from each observer. Several lines were drawn between observers and targets connecting the highest point of each. These lines represent the sight lines that need to be checked for continuous visibility. A visual check was then conducted to see whether or not the sight lines are restricted by the pavement surface.

Figure 17 shows the results of the graphical validation that was conducted for locations 1 to 4 on the Highway 11 segment (i.e., the same locations that were discussed when referring to Figure 15). The other locations showed similar trends. It can be clearly seen from the figure that sight lines are not visible since they are overlaid by the pavement surface on crest curves. It can also be observed that, at the four locations, the *ASD* is limited over the same station ranges detected by the code and presented in Figure 15. The inspection of the remaining locations revealed that *ASD* was found to be restricted at the 19 locations, which is in line with the algorithm's output. The summary of results at other locations is contained in Table 5.

- *For horizontal alignment*: Every line of sight connecting observer and target points along the centerline of the driving lane on a horizontal curve should not be restricted by any lateral objects. To ensure this, the horizontal alignment of the vehicle trajectory lane was extracted from LiDAR data and imported into AutoCAD Civil 3D software as detailed in the study of Gargoum, El-Basyouny [47]. LAS files of each road segment were also imported into the software. This was followed by overlaying the trajectory points that represent observer and target points onto the road surface along the extracted alignment of the driving lane centerline. The "check sight distance" tool was used to connect sight lines (235 m each) between each observer and all targets. These sight lines were then visually inspected to look for any lateral restrictions. The investigation revealed that the sight distance was not restricted due to lateral obstructions at any of the identified locations.

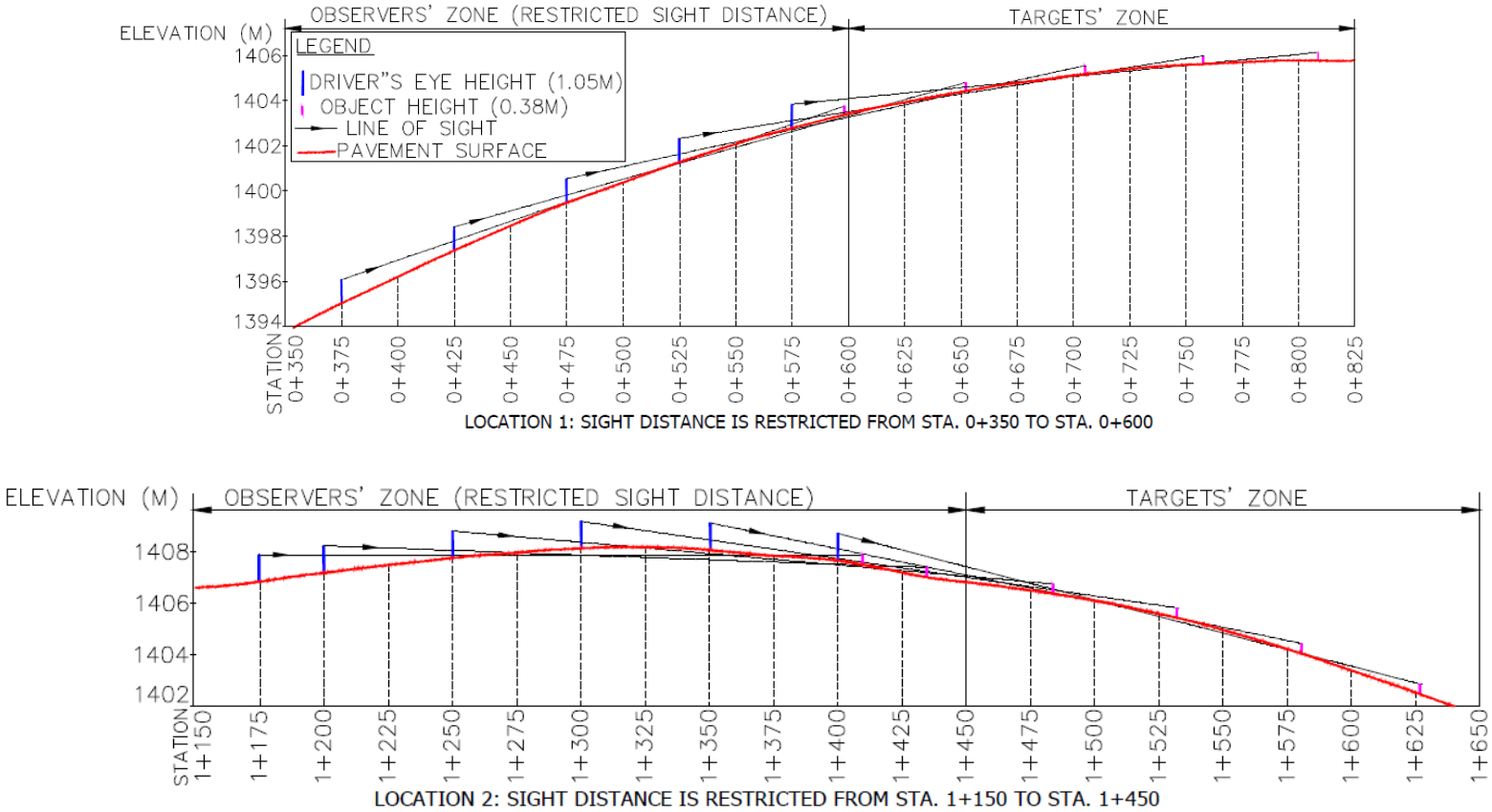

Figure 17: Sight distance restrictions along the vertical alignment of Highway 11

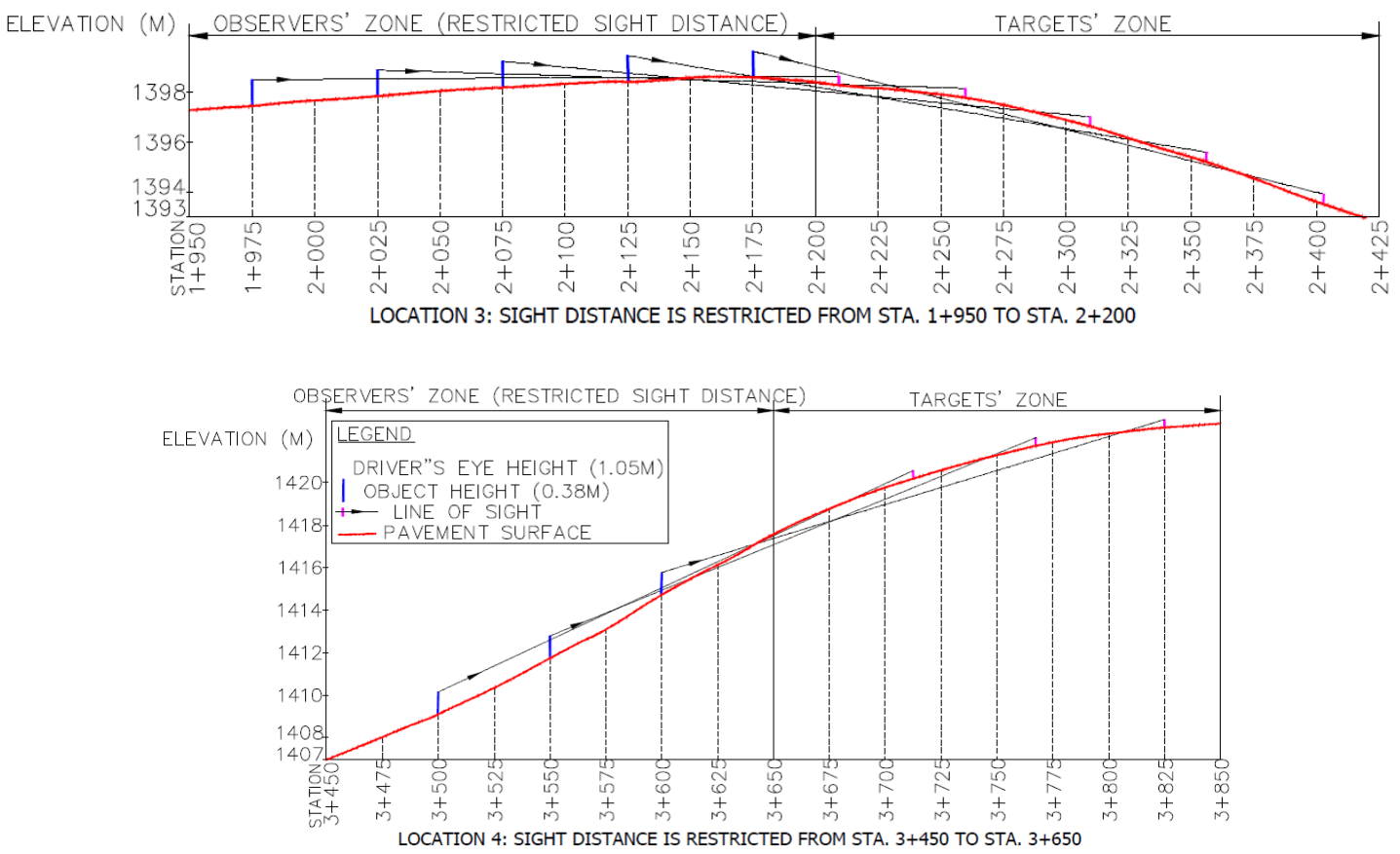

Figure 17: (Continued) Sight distance restrictions along the vertical alignment of Highway 11

Table 5: Results of automated assessment and graphical validation

Location	Sections with Limited ASD		3D Graphical Validation Outcome				
			Is ASD Limited?	Location of ASD limitation *(1: true; 0: false)*			Obstructing object
	From	To		HZ curve	VL curve	Combined HZ and VL curves	
1	0+350	0+600	Yes	1	1	1	a$^{(i)}$ (shown in Fig. 17)
2	1+150	1+450	Yes	1	1	1	a$^{(i)}$ (shown in Fig. 17)
3	1+950	2+200	Yes	0	0	0	a$^{(i)}$ (shown in Fig. 17)
4	3+450	3+650	Yes	0	1	0	a$^{(i)}$ (shown in Fig. 17)
5	4+060	4+320	Yes	1	1	1	a$^{(ii)}$
6	4+880	5+180	Yes	1	1	1	a$^{(i)}$
7	5+420	5+520	Yes	0	0	0	a$^{(i)}$
8	6+180	6+240	Yes	0	1	0	a$^{(i)}$
9	6+520	6+660	Yes	0	1	0	a$^{(i)}$
10	7+060	7+220	Yes	0	0	0	a$^{(i)}$
11	7+340	7+740	Yes	1	1	1	a$^{(ii)}$
12	8+440	8+640	Yes	1	1	1	a$^{(ii)}$
13	9+260	9+580	Yes	0	1	0	a$^{(i)}$
14	10+600	10+780	Yes	0	1	0	a$^{(i)}$
15	11+020	11+320	Yes	1	1	1	a$^{(i)}$
16	2+820	3+100	Yes	0	1	0	a$^{(i)}$
17	4+100	4+200	Yes	0	1	0	a$^{(i)}$
18	4+680	4+920	Yes	0	1	0	a$^{(i)}$
19	5+520	5+800	Yes	0	1	0	a$^{(i)}$

a$^{(i)}$ *Pavement surface of a crest curve*
a$^{(ii)}$ *Roadside cut slope plus pavement surface of a crest curve*
Locations from 1 to 15 are located on highway 11
Locations from 16 to 19 are located on highway 63

Table 5 summarizes the results of both applying the code on LiDAR data of the test segments and the outcome of the graphical validation procedure. Columns 2 and 3 contain

information on the regions where the algorithm found sight lines to be restricted. Regions with insufficient *ASD* on Highway 11 are locations from 1 to 15 while the zones on Highway 63 are from 16 to 19. Columns 4 to 8 provide information about the results of the validation procedure. Column 4 indicates whether or not the *ASD* was found to be limited during the graphical assessment. Columns 5 to 7 describe whether the regions with restricted *ASD* fall on a horizontal curve, a vertical curve, or a combination of both.

Since the interaction between horizontal and vertical alignment is critical when addressing the *ASD* [125], further inspection of the regions defined to have *ASD* deficiencies was done using the 3D point cloud model of each location. Each location was checked closely to confirm and/or identify any other obstructing objects. The last column in the table shows the noted obstructions at each location. It was found that at all locations the visibility was limited by the pavement surface on vertical crest curves. More so, at locations 5, 11, 12; the presence of roadside cut slope was found to be an additional limiting factor. It can also be seen that at all locations where a horizontal and a vertical curve are combined, the *ASD* was limited by the vertical crest curve suggesting that they might be contributing factors in sight distance limitations when there is a combination of vertical and horizontal alignment. In addition, vertical sag curves were found to have no influence on *ASD* restrictions. Finally, while there are no horizontal or vertical curves at locations 3, 7, and 10 (i.e., located on a longitudinal grade); it was found that the sight lines are restricted by vertical crest curves downstream of the observer's location.

3.4.3.3 High-level Road Safety Assessment

As the Highway 63 test segment is one of the top ten high collision locations in the province of Alberta, a high-level safety assessment was done to investigate whether historical collisions might be related to sight distance limitations. Historical collision data from 2009 to 2014 were checked to investigate whether or not the sight distance deficiencies might have contributed to the occurrence of collisions. Road collisions and regions with limited *ASD* were mapped using their coordinate information as shown in Figure 18.

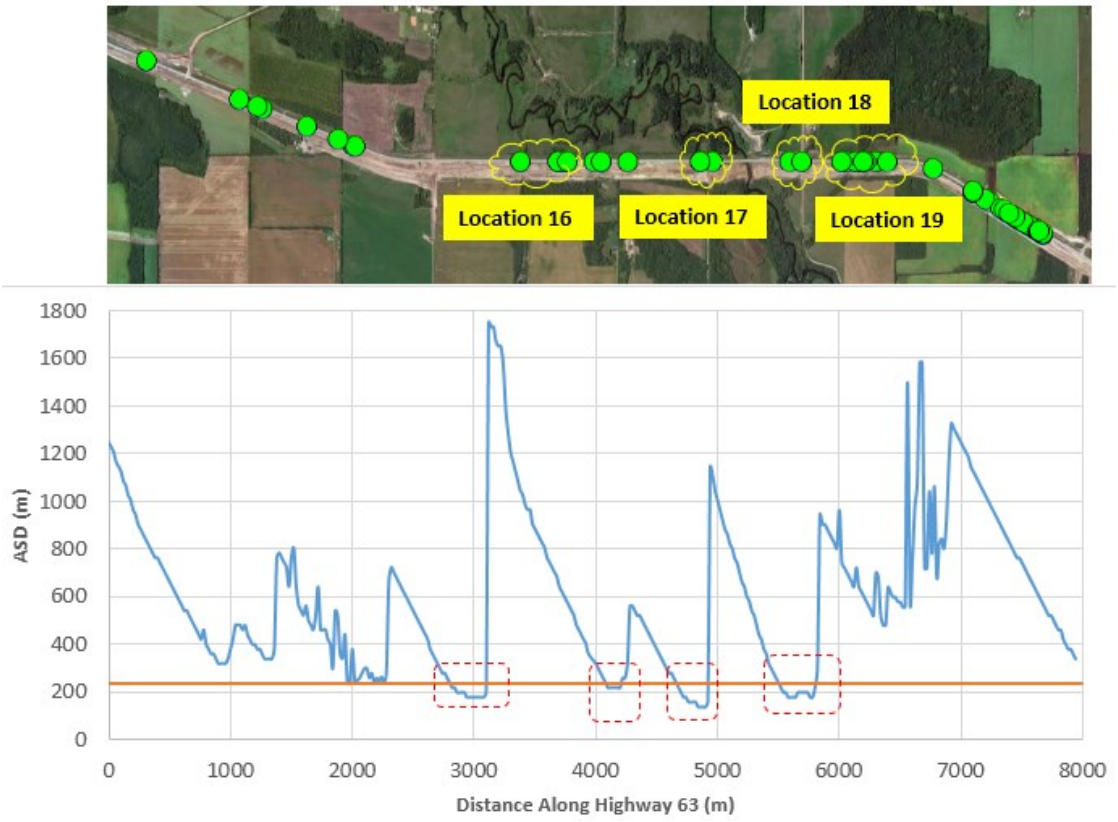

Figure 18: Road collisions on locations with limited ASD on Highway 63

The figure shows that collisions are clustered along regions with insufficient *ASD.* Region 16 had four struck animal-vehicle collisions; region 17 had two animal-vehicle collisions; region 18 had two animal-vehicle collisions; and region 19 has four rear-end, three animal-vehicle, and one run-off-road collisions. The presence of multiple collisions at the same coordinates where *ASD* is found to be limited indicates that sight distance limitations might have been a contributing factor for collision occurrence. In addition, the nature of collisions, such as rear-end and animal-vehicle collisions, especially along a straight segment, indicate that there is a high chance these collisions might have been caused by the driver's inability to see the obstructions (i.e., other slowed or stopped vehicles or animals crossing). In fact, this is in agreement with the results presented in Table 5. At these locations, *ASD* was found to be limited due to the presence of vertical crest curves restricting the ability to see target points from the observer locations. This explains that at one point between the driver and the object, the sight lines intersect with the pavement surface of the vertical crest curves. Thus, sight distance limitations could have been a factor in the occurrence of these collisions.

3.5 Estimation of Longitudinal Grades

As discussed when presenting the literature review on reliability-based highway design, the majority of previous studies ignored the longitudinal grade and assumed level terrain in reliability calculations due to data unavailability [6, 27, 30, 78]. Therefore, this research considers the effect of longitudinal grades on curved segments. The longitudinal grade (*g)* is a deterministic value and is estimated along horizontal curves from LiDAR data using the methodology explained in the study of Gargoum, El-Basyouny [76].

The procedure of computing the longitudinal grade involved centerline identification, road surface creation, overlaying the centerline onto the roadway surface, and road vertical profile generation and fitting. The feature that is used in reliability calculations is the vertical longitudinal grade along highway curved segments. The performance of the algorithm was tested on LiDAR data of Highway 1 and Highway 2 in Alberta, Canada. The values of longitudinal grades extracted by the code were compared to values of longitudinal grades of the same segments documented in as-built drawings and collected in GPS surveys. The comparison showed that the algorithm was very accurate in estimating the vertical grades with an average percent difference of 0.06% compared to as-built drawings and 0.023 to 0.061 compared to GPS data. This high degree of accuracy demonstrates the value of using LiDAR for road profile extraction. The detailed procedure of longitudinal grade estimation is explained in the study of Gargoum, El-Basyouny [76].

3.6 Geometric and Collision Data for Reliability Analysis

As discussed, a set of novel algorithms were used to detect the presence of horizontal curves, extract their geometric attributes, and assess the 3D *ASD* on each curve. The developed algorithms were applied on multiple highways in Alberta, identifying locations of horizontal curves, extracting their attributes, and assessing the *ASD*. This resulted in data set of 244 horizontal curves on two-lane two-way highways which are used in reliability calculations.

Previous studies on reliability-based horizontal curve design investigated sight distance restrictions within the most inside lane and/or the lane closest to the median in the other direction of travel [6, 27, 30, 31, 38]. Thus, this thesis assesses the risk associated with sight distance

deficiencies and vehicle skidding along the innermost travel lane (i.e., the closest to the roadside), which is the lane defined as the most critical lane by Highway Design Guidelines to calculate the lateral clearance on horizontal curves for stopping sight distance [17, 125]. Even though the analysis is performed on the most critical lane, the proposed framework can be repeated at any lane of interest.

Using the 3D-based sight distance estimation algorithm, the *ASD* was assessed along the most inside lane on all studied horizontal curves. The minimum *ASD* along each curve was considered as the sight distance supply and is used in the reliability calculations, which is the standard practice in previous studies [6, 7, 27, 30, 31]. Longitudinal grades were also extracted along the innermost travel lane in the same direction of travel at driver locations where sight distance is limited.

Traffic volumes and data of sight distance-related collisions that occurred on these curves from 2009 to 2014 were also added to the dataset. Only collision types that are likely occurred due to insufficient sight distance or vehicle skidding were considered, which is consistent with previous research [5, 127]. This includes rear-end collisions, same-direction sideswipe collisions, run-off-road crashes, and struck-animal collisions. Collision causes of the collision data set were also reviewed to include only relevant collisions (e.g., run-off-road collisions on curves). Table 6 provides descriptive statistics of the dataset used in this dissertation.

Table 6: A Descriptive statistics of horizontal curve data

Description	Min	Max	Mean	STDEV
Injury and Fatal collisions/5-yrs	0.00	9.00	0.73	1.27
Property-Damage-Only collisions/5-yrs	0.00	43.00	2.93	4.93
Total collisions/5-yrs	0.00	47.00	3.66	5.71
AADT (veh/day)	242	45220	3959	6670
Curve Length (m)	181	1547	586	263
Superelevation (m/m)	0.01	0.08	0.05	0.01
Deflection angle (Degrees)	7.57	89.97	40.69	18.89
Radius (m)	267	2048	867	365
Chord Length (m)	160.29	1465.67	549.43	248.36
Degree of Curvature	0.84	6.44	2.38	1.00
***ASD* (m)**	80.1	185.2	152.4	27.0
Longitudinal grade (%)	-7.41	6.30	0.12	1.95

4 RELIABILITY ANALYSIS & RISK ASSESSMENT

This chapter is dedicated to quantifying the risk associated with inadequate sight distance and vehicle skidding on curved segments. The first part of the chapter provides examples where using a 2D-based approach to assess *ASD* could be misleading. The consequent section provides details on applying a multi-mode reliability analysis to estimate the risk levels at studied horizontal curves. It describes the limit state functions of the non-compliance modes and provides details on the random and deterministic variables included in the LSFs, followed by applying Monte Carlo Simulation to estimate the P_{nc} levels. The closing section of the chapter includes a discussion of the results and their implications.

4.1 Using a 3D-based Sight Distance Assessment

This thesis assesses the risk associated with non-compliance on horizontal curves resulting from insufficient sight distance combined with vehicle skidding. As discussed, the majority of previous studies used 2D *ASD* calculations which does not account for the 3D nature of the driving environment and potential sight obstructions [6, 7, 27, 30, 31, 34, 35, 38, 39, 42]. It is therefore of utmost importance to highlight how using 2D projection could lead to misleading conclusions about sight distance limitations and consequently the associated safety levels. In the 2D-based approach, *ASD* is considered to be controlled only by the available lateral clearance and curve radius. In this case, the *ASD* can be calculated using the following equation [17] :

$$ASD = \frac{R}{28.65} * COS^{-1}(1 - \frac{M}{R}) \quad (15)$$

where R = curve radius (m); M = middle ordinate (m), which is the distance between the centerline of the inside lane to the sight obstruction (e.g., roadside barrier).

Although these studies have been beneficial in establishing the ground for developing probabilistic highway design guides, the use of 2D sight distance assessment could be inaccurate and misleading. Considering only the horizontal alignment in assessing the *ASD* without accounting for the vertical alignment and other 3D features (e.g., roadside barriers, embankments, etc.) could result in misleading conclusions that do not represent the real driving environment which in turn would affect the non-compliance and safety levels resulting in deceptive conclusions. For example, by examining the road plan (i.e., 2D approach) shown in Figure 19, the sightline appears to be obstructed by the presence of a hill causing the Object to be invisible. In this case, the *ASD* can be estimated using Equation 15 (i.e., limited by M and R). However, when using a 3D-based approach, the sightline profile reveals that the elevation of the hilltop is lower than that of the sightline connecting the driver's eye to the Object. This indicates the opposite conclusions in which the Object is visible. This affirms the need to evaluate sight lines in a 3D world considering the effect of both horizontal and vertical alignments along with other potential obstructions of roadside features.

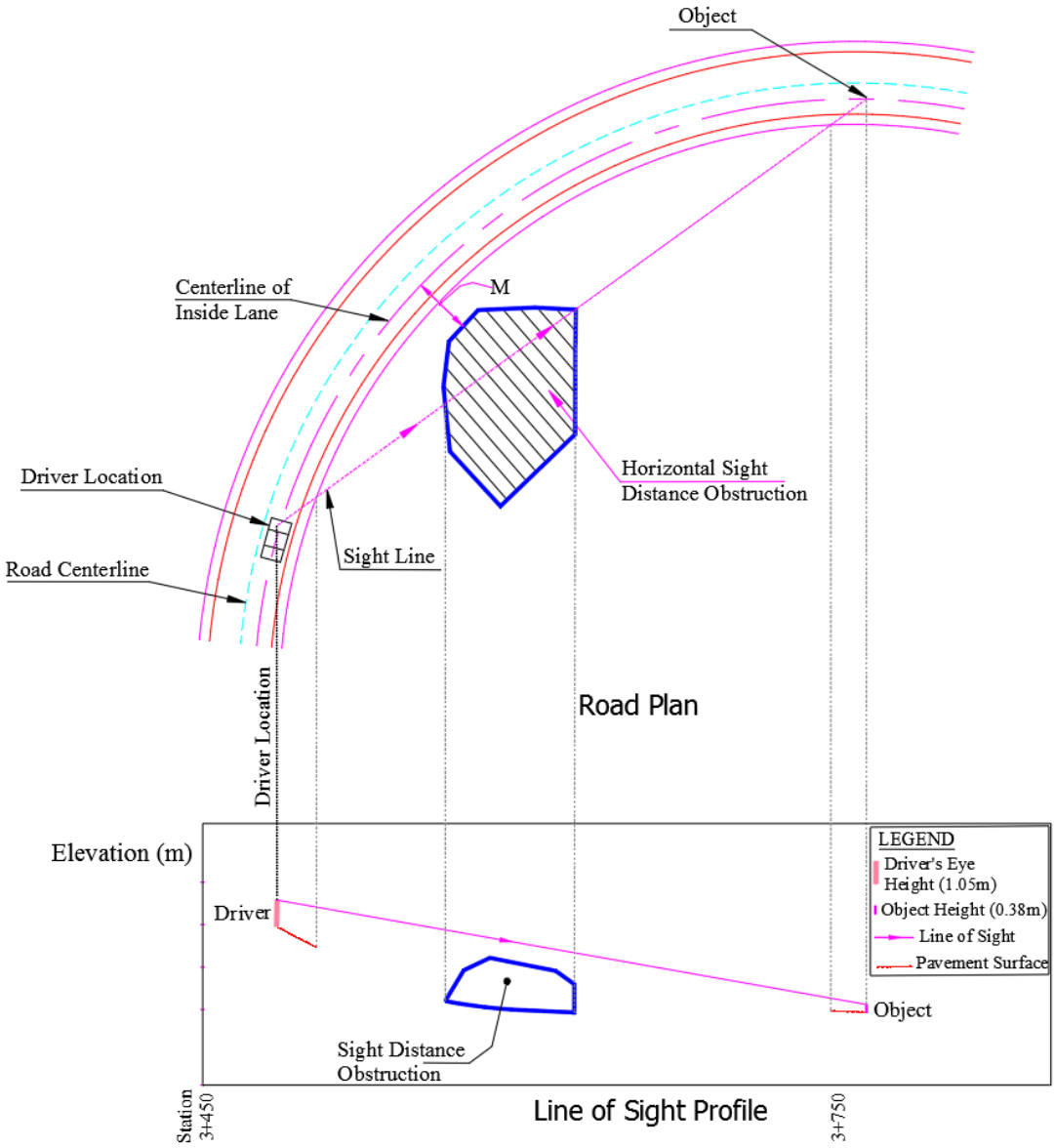

Figure 19: Misleading 2D sight distance assessment

The sight distance computation approach in this dissertation overcomes the limitations associated with the traditional method of sight distance calculations and considers the use of LiDAR data to compute the 3D *ASD* using the algorithm discussed in the previous chapter. This

accounts for the 3D nature of combing both highway horizontal and vertical alignments along with all 3D features that could obstruct the driver's vision resulting in a more realistic and representative *ASD*. To demonstrate the value of utilizing LiDAR data in 3D *ASD* assessment and that it is superior to using the traditional approach, Figure 20 shows LiDAR data, Road Plan, and Profile of a segment for which the *ASD* was assessed using LiDAR data. Examination of the horizontal alignment revealed that there are no lateral sight distance obstructions (i.e., the 2D approach would conclude that there are no sight distance restrictions). However, using LiDAR data to compute the *ASD* along the segment revealed that the sight is obstructed along the horizontal curve due to the presence of a substandard vertical curve combined with the horizontal alignment, as seen in Figures 20 and 21. Also, plotting the driver's eye height and object height on the road profile onto a scale (Figure 20) demonstrates that sightlines are obstructed by the pavement surface of a sharp vertical curve which also can be seen in the virtual image of LiDAR data of this highway segment (Figure 21).

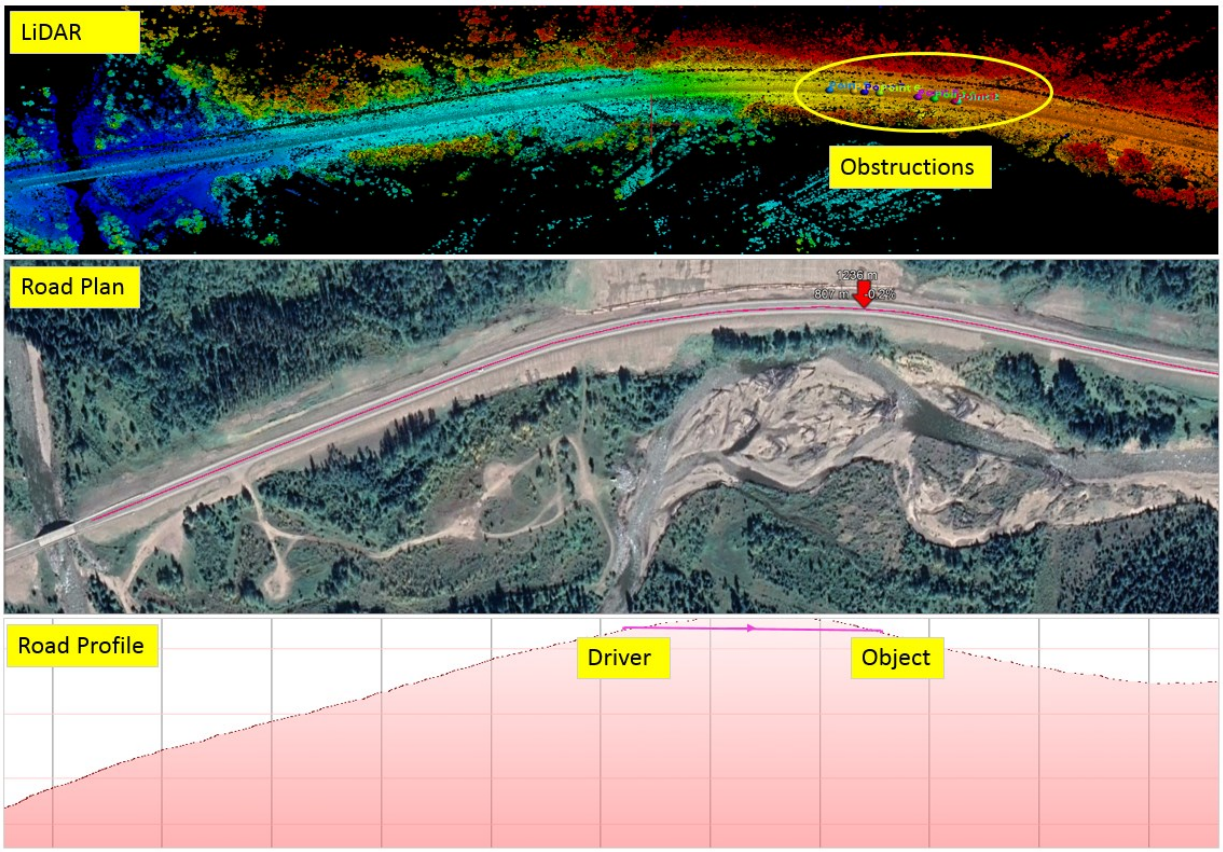

Figure 20: Sight distance assessment for a highway segment using LiDAR data

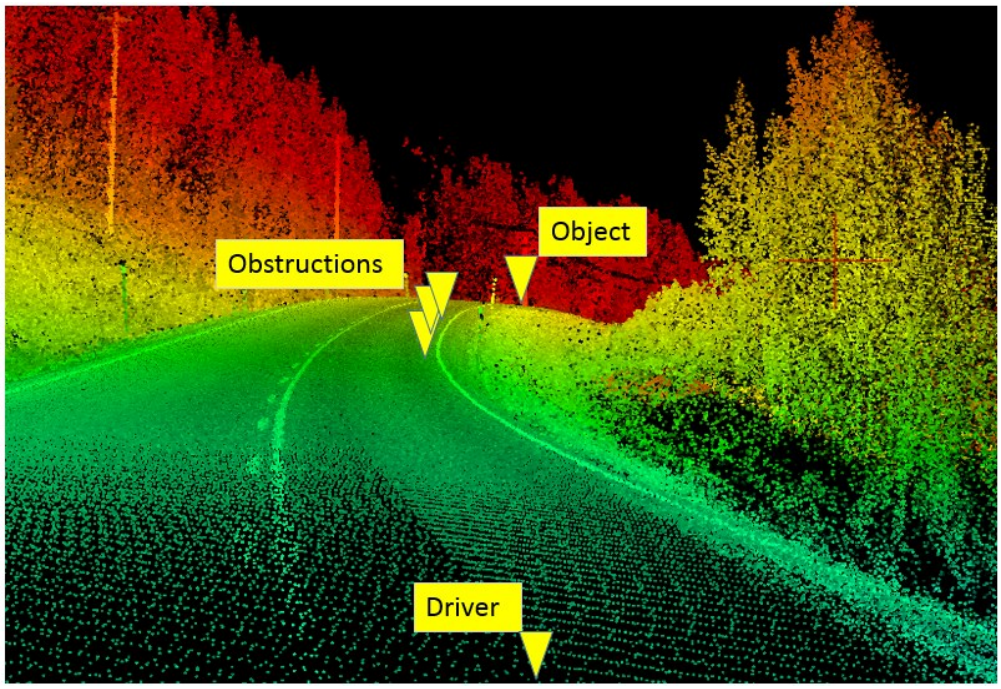

Figure 21: Virtual image of LiDAR data of a horizontal curve with sight obstructions

4.2 System Reliability Analysis

The theory and structure of system reliability analysis are discussed in Section 2.1.2. This section discusses the limit state functions and their random and deterministic variables, provides details on using Monte Carlo Simulation to estimate the risk levels, and present the risk assessment results.

4.2.1 Limit State Functions

The first mode of non-compliance is insufficient sight distance and the second one is vehicle skidding. When designing horizontal and vertical curves, the design guidelines aim to provide a

sufficient length of a roadway ahead, so a driver can see any obstruction in their field of view and react accordingly. Hazardous locations where sight distance is restricted usually have countermeasures to alleviate the risk associated with the existing limitations. As discussed earlier, the current design guides do not provide a framework to quantify the non-compliance associated with limited sight distance or any other mode of noncompliance on existing curves. For insufficient sight distance, the limit state function of the reliability problem can be written as shown in Equation 16 below. The failure in this LSF occurs when the supply (i.e., *ASD*) is less than the demand (i.e., required Stopping Sight Distance: *SSD)*, noting that estimating the demand is based on considering the stochastic nature of the design inputs incorporated in the *SSD* calculation model The demand (i.e., *SSD*) is usually calculated using the AASHTO's model shown in Equation 17 [17] which has been a standard practice when using a reliability-based approach for the design of horizontal curves. Thus, the first limit state function can be expressed as shown by Equation 18.

$$G = ASD - SSD \tag{16}$$

where *ASD* = the available sight distance on the road (Supply, *S*); *SSD* = the required stopping sight distance (Demand, *D*), and the noncompliance occurs when the *ASD* is less than the *SSD* (i.e., $G < 0$).

$$SSD = 0.278\, v * PRT + \frac{v^2}{254(\frac{a}{9.81}+g)} \tag{17}$$

where v is the operating speed (km/h) and is a random variable; *PRT* is the Perception and Reaction Time (seconds) and is a random variable; a is the deceleration rate (m/s^2) and is a random variable; g is the vertical longitudinal grade (%/100) and is a deterministic value.

$$LSF_1 = ASD - (0.278\, v * PRT + \frac{v^2}{254\left(\frac{a}{9.81}+g\right)}) \quad (18)$$

The second mode of non-compliance is vehicle skidding in which the failure occurs when the vehicle skids out of a curved segment. The balance of a vehicle against skidding is governed by design guidelines [17] as shown in Equation 19. The non-compliance occurs when the required side friction (Demand) exceeds the available side friction (Supply). The limit state function of this mode of non-compliance can be written as shown in Equation 20.

$$e + f_s = \frac{v^2}{127\, R} \quad (19)$$

$$LSF_2 = f_s - (\frac{v^2}{127\, R} - e\,) \quad (20)$$

where e = superelevation rate (m/m) and is a deterministic value; f_s = side friction factor (i.e., Supply) and is a random variable, and R = curve radius (m) and is a deterministic value.

The two limit state functions (Equations 18 and 20) contain eight variables (*ASD*, *v*, *PRT*, *a, g, fs, R,* and *e).* According to the current deterministic design approach, all these design inputs are represented by deterministic values, leading the LSF to yield a single value. In other words, in current design guidelines, there is a single value for each of these variables (including the random variables) that is assumed to represent all drivers. As highlighted, this is a drawback in the deterministic design approach as the stochastic nature of random variables is ignored. Using the reliability-based design approach, design inputs are treated as random variables with specific

probability distributions, and so are the LSFs. In this research, four of these variables are random variables and therefore they are treated as stochastic variables (*v*, *PRT*, *a,* and *fs).* In contrast, the remainder of the variables (*ASD*, *g, R, and e)* are considered deterministic. The consideration of random variables and the estimation of deterministic variables are explained below.

4.2.2 Random Variables

The probability distributions of the random variables (*v*, *PRT*, *a,* and *fs*) and the corresponding mean and standard deviation values are shown in Table 7 and summarized below. These distributions are used in the majority of previous work focused on the reliability-based design of horizontal curves [6, 7, 13, 25, 27, 30, 31, 35, 38-40, 42].

- Vehicle operating speeds (*v*): as per the Natural Research Council (NRC), operating speeds are usually assumed to follow a normal distribution and are estimated using speed prediction models [128]. The operating speed in this research is assumed to be normally distributed with mean and standard deviation obtained from the speed prediction models of Richl and Sayed [129]; the models that have been used in the majority of studies focused on reliability-based horizontal curve design [25, 27, 30, 31, 39]. These speed prediction models are shown in Table 8. To compute the operating speed on a horizontal curve, geometric attributes such as curve radius (*R*), superelevation rate (*e*), curve length (*LC*), and deflection angle (I) were estimated using LiDAR data, as discussed in Section 3.2. These attributes were then used to predict the corresponding operating speed using the speed prediction models. The mean value of the operating speed was considered as the

average of the operating speed values obtained using these models, and the standard deviation explains the variation between the speed values predicted by the models [6, 30, 31, 38].

- *Perception and reaction time (PRT):* In the majority of the previous work cited above, the *PRT* is assumed to be lognormally distributed with a mean of 1.5 seconds and a standard deviation of 0.40 seconds based on a study conducted by [130]. Thus, this has been adopted in this study.
- *Deceleration rate (a):* The [17] assumes that the deceleration rate follows a normal distribution with a mean of 4.2 m/s^2 and a standard deviation valued at 0.60 m/s2 as found by Fambro, Fitzpatrick [131] and commonly used in previous work [6, 27, 30, 31, 35, 38].. Therefore, the analysis here assumes *a* is normally distributed with the same mean and standard deviation values.
- For the side friction factor, *fs,* previous work considered the wet surface condition as the case in reliability calculations, since it is more critical [25, 30, 31]. The side friction factor is taken as a portion (0.925) of the longitudinal friction as given by Equation 21 [25, 132]. The friction factor in the tangential direction is assumed to follow a normal distribution with mean and standard deviation values depend on the operating speed as shown in Table 9 [132].

$$f_s = 0.925\, f_T \tag{21}$$

where f_s = side friction factor; f_T = the friction factor in the tangential direction.

Table 7: Probability distributions of design inputs

Variable	Distribution	Mean	Standard Deviation	Reference
PRT	Lognormal	1.5 seconds	0.4 seconds	[6, 30, 31, 38, 130]
a	Normal	4.2 m/s^2	0.6 m/s^2	[6, 17, 27, 30, 31, 35, 38, 131]
v	Normal	Prediction models	Prediction models	[25, 27, 30, 31, 39, 129]
fs	Normal	Model	0.0845	[25, 30, 31, 132]

Table 8: Speed prediction models used to estimate operating speeds on curves*

Speed Prediction Model (V_{85} = operating speed)	R^2
$V_{85} = 94.398 – 3188.656/R$	0.79
$V_{85} = 95.594 – 1.597DC$, where $DC = 1746.38/R$	0.79
$V_{85} = \exp(4.561 – 0.0058D$, where $D = 5729.58/R$	0.63
$V_{85} = 102.45 + 0.0037LC-(8995+5.73LC)/R$	N/A
$V_{85} = 103.66 – 1.95DC$	0.80
$V_{85} = 102.44 – 1.57DC + 0.012LC – 0.01DC \times LC$	0.81
$V_{85} = 99.61 – 2951.37/R + 0.014LC – 0.131I + 71.82e$	0.84
$V_{85} = 129.88 – 623.10/R1/2$	0.78
$V_{85} = 95.41 – 1.48DC – 0.012DC2$	0.99
$V_{85} = 103.03 – 2.41DC – 0.029DC2$	0.98
$V_{85} = 96.11 – 1.07DC$	0.90

**From: [5, 25, 129]*

Table 9: Coefficient of friction distributions

Pavement condition	**Mean speed (km/h)**	**Mean**	**Standard deviation**
Wet distribution	80.4	0.4192	0.0913
Wet distribution	85.0	0.4013	0.0913
Wet distribution	90.0	0.3826	0.0913
Wet distribution	95.0	0.3571	0.0913
Wet distribution	99.8	0.3498	0.0913
Dry distribution	All speeds	0.8852	0.0949

** From: [25, 129, 132]*

4.2.3 Deterministic Variables

The four deterministic variables used in the two LSFs are *ASD*, *R, e, and* g. These variables are calculated for each of the 244 horizontal curves using the set of novel algorithms and methodology explained in Chapter 3. This 3D *ASD* is a deterministic value and is estimated along the most inside lane of each horizontal curve using the procedure discussed in Section 3.3. The horizontal curve radius (R) and superelevation rate (e) are also deterministic values for each curve and are estimated following the procedure detailed in Section 3.2. The longitudinal grade (g) is another deterministic value that is calculated from using the methodology explained in Section 3.4. Once the values of these variables were obtained from LiDAR data of the studied curves, they were used in the LSFs along with the distributions of the random variables to quantify the system P_{nc} associated with each curve as explained in the next section.

4.2.4 Monte Carlo Simulation

Direct or exact methods are not available to estimate the P_{nc} when the LSF contains more than two variables, non-linear, and when the random variables are not normally distributed [133]. Under these circumstances, simulation and various approximate methods can be used to estimate the P_{nc} [25]. Simulation methods include Monte Carlo Simulation (MCS) while approximate methods include the Mean Value First-Order Second Moment (MVFOSM), the First Order Reliability Method (FORM), and the Second Order Reliability Method (SORM). The theoretical background of these methods can be found in various structural and transportation engineering studies, such as Melchers and Beck [134], Ellingwood, Galambos [133], and Dhahir [4].

MCS is a numerical sampling method that can be used to estimate the P_{nc} through sampling the LSF around the mean of the design inputs. In this approach, MCS is used in drawing samples of random variables included in the LSF following their probabilistic characteristics (i.e., random samples around the mean of design inputs). While this technique requires computer capabilities to generate a series of values for random variables included in LSFs, it is regarded as a robust numerical sampling method for estimating the P_{nc} [35, 38]. Considering the availability of computer abilities to perform the simulation and the use of MCS in previous work to solve system reliability problems [31, 58], this thesis utilizes MCS to quantify the risk levels associated with studied modes of non-compliance.

To run the sampling using MCS, a MATLAB script was developed to perform the MCS and calculate the $P_{nc\ system}$ incorporating the two LSFs. Using a large number of samples, every LSF is evaluated to determine whether or not the supply of a certain design element (i.e., non-

compliance mode) would meet the demand requirements. For each LSF, the failure probability is calculated by dividing the number of failures by the total number of samples. To calculate the $P_{nc\ system}$, the joint probability of failure needs to be calculated. The code calculates the number of failures of the first non-compliance mode, given that the second mode has already failed. By multiplying this probability by the probability that the first mode fails, the joint probability can be calculated, as shown by Equation 10. The $P_{nc\ system}$ is then calculated following Equation 8.

The $P_{nc\ system}$ can also be calculated directly by applying the definition of a series system reliability problem. Since the system is considered failed if there is either insufficient sight distance or potential for vehicle skidding, the code counts the number of samples in which the first and/or the second LSF yields a negative value, which represents the number of failures of the system. The $P_{nc\ system}$ equals this number divided by the total number of samples used in the simulation. When using the MCS technique, a target coefficient of variation is typically selected to measure the error of the estimated P_{nc} value. A target coefficient of variation of 2-5% is commonly assumed [31]. In this research, a target coefficient of variation of 2.5% is used. An example of using MCS to estimate the P_{nc} is discussed in the next section.

4.2.5 Reliability Outcome and Risk Measures

As discussed, each of the studied 244 curves has its own attributes such as *ASD, R*, *v*, *G*, *e*, etc. Using the data set summarized in Table 6, the MCS technique was used to compute the P_{nc1} and $P_{nc\ system}$ associated with each curve. To illustrate the estimation process of P_{nc1} and $P_{nc\ system}$ for a given horizontal curve, the process involves: (i) computing the operating speed (*v*) on the horizontal curve using the speed prediction models shown in Table 8 and curve geometric

attributes such *R, e, and DC* that were extracted from LiDAR data; (ii) determining curve-specific values of deterministic variables (*ASD*, *R*, e, and *G*) that exist in the two LSFs (Equations 18 and 20); (iii) using Monte Carlo Sampling to compute P_{nc1} and $P_{nc\ system}$ considering the values of deterministic variables from the previous step and the probability distributions of random variables shown in Table 7 (i.e., v, PRT, a, f_s).

Using MCS, a series of values (e.g., 100,000) for each random variable in the two LSFs are generated following their probability distributions. For each of the 100,000 samples, the two LSFs are evaluated to determine whether or not the supply (e.g., *ASD*) fails to meet the demand requirements (e.g., required sight distance) which occurs when the LSF yields a negative value. To illustrate, let's assume that LSF_1 failed (i.e., yielded a negative outcome) for 10,000 out of 100,000 instances; LSF_2 failed 7,000 times, and both LSF_1 and LSF_2 shared 4,000 failures. In this case, P_{nc1} is calculated by dividing the number of failures in LSF_1 by the total number of samples (P_{nc1} =10,000/100,000 = 0.10). Similarly, P_{nc2} =7,000/100,000 = 0.07. The probability $P_{nc1,nc2}$ can be calculated in two ways: (i) directly by definition (i.e., $P_{nc1,nc2} = P\ (A \cap B)$ =4,000/100,000 = 0.04); or (ii) using Equation 10: $P_{\mathrm{nc1,nc2}} = P\ (\mathrm{A} \cap \mathrm{B}) = P(\mathrm{A}|\mathrm{B}) * P(\mathrm{B})$ = (4,000/7,000) * (7,000/100,000) = 0.04. The $P_{nc\ system}$ can then be calculated using Equation 8 where $P_{nc\ system} = P_{nc1} + P_{nc2} - P_{nc1,nc2}$ = 0.10 + 0.07 – 0.04 = 0.13. It is worth noting that using MCS, the $P_{nc\ system}$ can be calculated directly by applying the definition of a series system reliability problem. Since the system is considered to fail if there is either insufficient sight distance or potential for vehicle skidding, therefore $P_{nc\ system}$ can be calculated through counting

the number of instances in which the first or the second mode has failed (i.e., Pnc $_{system}$ = 13,000/10,000 = 0.13.

For the studied 244 curves, the $P_{nc\ system}$ ranged from 0.01 to 0.94, with a mean of 0.22 and a standard deviation of 0.26. More details on the effect of curve attributes on both P_{nc1} and $P_{nc\ system}$ and the differences between the P_{nc} of a single non-compliance mode and $P_{nc\ system}$ are discussed in the next chapter (Section 5.3). It should be noted that the $P_{nc\ system}$ corresponding to 30% of curves is greater than 0.24, indicating a high risk associated with the studied curves. Since the safety consequences of this non-compliance are unknown, SPFs were developed to relate the $P_{nc\ system}$ to historical collisions on curved segments as discussed in the next chapter.

5 SAFETY-BASED DESIGN APPROACH

This chapter is divided into three main sections. The first section gives a brief introduction to the safety-based design approach. The consequent section provides details on developing safety performance functions that relate curve attributes to the system reliability outcome and collision frequency. The last section of the chapter calibrates performance-based design charts where curve attributes are linked to risk levels and safety.

5.1 Background

Adopting a performance-based design approach leads to forgiving highway design that accounts for human fallibility. In a safety-based design framework, design elements from existing highways are linked to collision frequency while accounting for road users and the variation in their capabilities. The relationships established can then be used and integrated into the initial stages of the design process

Ghobarah [135] defines Performance-Based Design (PBD) as a framework where design criteria can be referred to as achieving a number of performance objectives. The ultimate goal of PBD of highways is to minimize the failure of a designed highway to perform as intended by minimizing the expected collision frequency. This is accomplished through understanding road users' capabilities and accounting for the random nature of driver behaviour, in lieu of assuming that all drivers will drive the same way. Instead of designing highways based on the current deterministic design approach, the PBD approach is based on establishing a link between design requirements and performance metrics from highways currently in operation. Design guidelines

can then be updated or calibrated based on the ability of highways to serve the existing driver population. Predetermined levels of performance (i.e., safety) can also be used as target levels allowing designs to be proposed accordingly.

For the design of horizontal curves, adopting such a safety-based approach requires information on the geometric attributes of curved segments, accounting for the variation in driver abilities, and historical collisions which are used as performance metrics. As discussed throughout the thesis, curve attributes were extracted along with safety performance records on the studied segments. The reliability theory was then utilized to translate the non-compliance on existing roads into risk levels that explain how far a design element is not complied with to meet the driver demand. The next step is to: (i) establish a link between these risk levels (P_{nc}) and historical collisions and (ii) utilize the relationship developed between P_{nc} and safety to calibrate performance-based design charts where curve attributes can be linked to both associated levels of non-compliance and safety performance. More details on these two steps are discussed in the next two sections

5.2 Safety Performance Functions Incorporating P_{nc}

This section is divided into three subsections. The first subsection provides background information on SPFs including model form, regression models, and parameter estimation methods. The following subsection discusses the methodology of developing the SPFs developed in this thesis. The last subsection presents the SPFs developed and discusses the results.

5.2.1 Background

After using the reliability theory to quantify the risk associated with the noncompliance as a result of insufficient sight distance and vehicle skidding, the next step is to develop SPFs incorporating non-compliance levels to investigate the relationship between the $P_{nc\ system}$ and collision frequency. SPFs are statistical models that are mathematically developed to relate road geometric features and traffic characteristics to the frequency and severity of collisions. SPFs are important for both existing and planned facilities. For existing roads, these models are used to quantify the collisions frequency due to any implemented treatments, while for planned facilities, they are used as a tool to estimate the predicted collision frequency [136]. Reliability analysis is not intended to replace the use of SPFs but rather, it complements SPFs by incorporating the risk associated with design non-compliance (P_{nc}) into the model [25]. The next few subsections provide background information on model form, regression models, and parameter estimation methods when developing SPFs.

5.2.1.1 Model Form

SPFs usually provide estimates of expected collision frequency as a function of roadway geometric and traffic characteristics. Hadayeghi [137] presented a generic form for SPFs as follows:

$$\mu = f\{\beta, X\}. \tag{22}$$

where μ is the expected number of collisions for the unit under the analysis; β is a vector of regression parameters to be estimated from the data; X is a vector of site-specific attributes

The functional form for curved horizontal road segments can be expressed as follows [6]:

$$\mu = L^{\beta 1}\,(F_{1i} + F_{2i})^{\beta 2}.\exp\,(\beta_0 + \beta_3 x_{3i} + \cdots + \beta_k x_{ki}) \quad (23)$$

where L is the segment length; $F_{1,2}$ is traffic volumes for the two directions of travel of the road segment; x_k are a set of site-specific traffic or geometrical attributes; $\beta_{0,1,2,3,x}$ are a set of regression parameters.

5.2.1.2 Regression Models

There are various types of regression models with different probability distributions for road collisions used when developing SPFs. This includes Poisson, Poisson-Gamma (also known as Negative-Binomial), Poisson-Lognormal (PLN), and other enhanced regression models. The literature indicates that most SPFs that relate road geometric attributes to collision frequency were developed using either PLN or NB regression model [138-142]. This thesis uses PLN as it accounts for outliers in crash data.

More specifically, this research uses Multivariate Poisson Log-normal (MVPLN) regression to develop SPFs. Multivariate Regression is the method of modelling multiple dependent variables with a single set of predictor variables. The MVPLN approach presents an opportunity to account for the correlations across various collision severity levels and their effect on safety analyses [48]. It is worth mentioning that while MVPLN can handle more than two collision severity levels, the collision data analyzed in this thesis involves only two severity levels namely Property Damage Only (PDO) and Injuries plus Fatalities (I + F), leading to a bivariate PLN. It is also important to note that MVPLN regression is preferred to the Multivariate Poisson model when analyzing multivariate collision data (i.e., multiple collision severity) because: (i) it accounts for over-

dispersion which is frequently observed in crash data; and (ii) it allows for a full general correlation structure [48]. As the classical parameter estimation of the MVPLN regression models is not straightforward, the Markov chain Monte Carlo (MCMC) simulation method is typically used to estimate the model parameters [143].

5.2.1.3 Parameter Estimation Methods

Calibrating the parameters of SPFs can be performed using two common methods namely; Empirical Bayes (EB) and the full Bayes (FB). The two methods are different in the way the prior parameters are determined. In the EB approach, parameters are estimated using the Maximum Likelihood Technique or any other technique involving the use of collision data. In the FB approach, the parameters are assigned a distribution to reflect some prior idea about the behaviour of the data.

This research considers estimating SPFs parameters using the FB approach and MVPLN regression. The FB approach has been suggested as a useful, though a more complex alternative to the EP approach. Modelling using FB offers a number of potential advantages: (i) the application of an integrated procedure to obtain outcomes, (ii) the ability to better accounts for uncertainty in crash data used; (iii) the small sample properties of FB approach may allow estimating crash models with smaller sample sizes; (iv) the ability to reflect some prior knowledge on the values of the coefficients in the modelling along with the behaviour of the data; (v) the ability to specify more complex model forms; (vi) the ability to provide the posterior distributions of outcomes; and (vii) the ability to provide more flexibility in selecting crash count distributions [144, 145].

5.2.2 Methodology

Considering MVPLN regression, for a dataset of collision data at *n* locations with *k* severity levels, let $y_i = (y_{i1} \quad y_{i2} \quad \cdots \quad y_{iK})'$ where y_{ik} is the collision frequency at the i^{th} location in the severity category k. The collisions at *n* locations are assumed to be independent. Given λ_{ik}, the Poisson distribution of y_{ik} can be expressed as follows:

$$f(y_{ik}|\lambda_{ik}) = \lambda_{ik}^{y_{ik}} e^{-\lambda_{ik}} / y_{ik}!, \quad i = 1,2,...,n, \quad k = 1,2,...,K. \tag{24}$$

To account for extra variations, let $ln(\lambda_{ik}) = ln(\mu_{ik}) + \varepsilon_{ik}$ where

$$ln(\mu_{ik}) = \beta_{k0} + \beta_{k1} X_{i1} + ... + \beta_{kJ} X_{iJ}, \tag{25}$$

where X_{ij} represents geometric and traffic characteristics, $\beta_k = \{\beta_1, \beta_2, ..., \beta_K\}$ refers to the vector containing the regression coefficients and ε_{ik} represent multivariate normal errors distributed as $\varepsilon_i \sim N_K(0, \Sigma)$, where

$$\varepsilon_i = \begin{pmatrix} \varepsilon_{i1} \\ \varepsilon_{i2} \\ \cdots \\ \varepsilon_{iK} \end{pmatrix} \text{ and } \Sigma = \begin{pmatrix} \sigma_{11} & \sigma_{12} & \cdots & \sigma_{1K} \\ \sigma_{21} & \sigma_{22} & \cdots & \sigma_{2K} \\ \cdots & \cdots & \cdots & \cdots \\ \sigma_{K1} & \sigma_{K2} & \cdots & \sigma_{KK} \end{pmatrix}$$

Where:

Σ is an unrestricted covariance matrix;

N_K denotes K-dimensional multivariate normal distribution; and

The variance of y_{ik} is greater than the mean (allowing for over-dispersion) as long as the diagonal elements of Σ are greater than 0

Let λ denote the set { $\lambda_1, \lambda_2, \ldots, \lambda_n$}. To obtain the estimates of the full Bayes (λ, ∑, β) prior distributions for the hyper parameters (β, Σ) need to be specified. Prior distributions are meant to reflect to some extent prior knowledge about the parameters of interest. If such prior information is available, it should be used to formulate the so-called informative priors (hyper parameter specification). In the absence of sufficient prior knowledge of the distributions for individual parameters, uninformative (vague) proper prior distributions are usually specified. The most commonly used priors are diffused normal distributions (with zero mean and large variance) for the regression parameters.

Thus, the diffused normal distributions (with zero mean and large variance) are regularly used as priors for the regression parameters. A Wishart (P, r) is used as prior for Σ^{-1}, where both P and $r \geq K$. P represents the prior guess at the order of magnitude of the precision matrix Σ^{-1}, and r denotes the degrees of freedom.

The MCMC sampling techniques in the open-source WinBUGS 2.2.0 statistical software were used to obtain the posterior distributions needed in the full Bayes approach [146]. The values of Brooks-Gelman-Rubin (BGR) statistics [147] (A value under 1.2 of BGR statistics indicates convergence), visual inspection of MCMC trace plots of model parameters, and ratios of the Monte Carlo errors relative to the particular standard deviations of the estimates (as a rule of thumb these ratios should be less than 0.05) were all monitored to watch for the convergence.

The goodness-of-fit of the model was assessed using a posterior predictive approach [148] in which replicates under the postulated model are generated and the distribution of a discrepancy measure, such as the chi-square statistic, are compared to the chi-square value obtained through using observed data. A model is considered not a good fit for the data if the observed chi-square value is far from the predictive distribution; the discrepancy cannot reasonably be explained by chance if the *p*-values are close to 0 or 1 [148].

5.2.3 Results and Discussion

Using the data set summarized in Table 6 and the resulting P_{nc} values of $n = 244$ curved segments, SPFs were developed to relate the collision frequency on these curves to their traffic, geometric characteristics, and their corresponding risk measures. SPFs for injury plus fatal ($I+F$) and Property Damage Only (PDO) were developed for collision data covering the period from 2009 to 2014. Independent variables included in the final model are traffic volume, curve length, and P_{nc}. It is worth noting that including other curve attributes such as curve radius and superelevation rate would be redundant as these attributes were used in calculating the operating speed which is a major contributing factor in the P_{nc} calculations.

Table 10 summarizes posterior estimates of MVPLN models and their standard errors for the developed SPFs. The resulting SPF models are shown in Equations 26 and 27. The analysis was performed in WinBUGS using two chains with 90,000 iterations each, 10,000 of which were excluded as a burn-in sample [48]. The BGR statistics, trace plots for model parameters, and ratios of the Monte Carlo errors relative to the specific standard deviations of the estimates were all monitored till convergence is indicated [149-152]. To assess goodness-of-fit, the distribution

of the chi-square discrepancy measure in replicated datasets was generated. The chi-square observed value was located near the center of the replicated distribution, with an associated *p*-value of 0.438 and 0.629 for the *PDO* and *I*+*F* models, respectively. This indicates that the PLN models were found to perform well in terms of accommodating the variation in collision frequency across the curved segments.

Table 10: Parameter Estimates and Standard Errors of MVPLN models

Model	Injuries and Fatalities (*I+F*) [(i)]				Property Damage Only (*PDO*) [(i)]			
	Estimate	**Standard Error**	**95% credible intervals**		**Estimate**	**Standard Error**	**95% credible intervals**	
			Lower limit	**Upper limit**			**Lower limit**	**Upper limit**
Intercept	-10.670	1.645	-13.970	-7.474	-10.290	1.120	-12.530	-8.113
Ln(V)(AADT)	0.571	0.085	0.404	0.741	0.635	0.063	0.511	0.760
Ln(L)	0.829	0.232	0.377	1.287	0.914	0.157	0.610	1.222
$P_{nc\ system}$	0.784	0.341	0.097	1.440	0.801	0.238	0.331	1.264
σ_{11}	NA	NA	NA	NA	0.444	0.084	0.299	0.629
σ_{22}	0.299	0.122	0.122	0.587	NA	NA	NA	NA
Covariance								
σ_{12}	Estimate = 0.16; Standard Error = 0.08						0.013	0.328
Correlation								
$\rho=\sigma_{12}/\sqrt{\sigma_{11}\sigma_{22}}$	Estimate = 0.45; Standard Error = 0.18						0.045	0.743
DIC	1326.0							

[(i)]PDO and I+F models were significant at 95% credible interval

$$\mu_{1(PDO)} = e^{-10.290}\ L^{0.914}\ V^{0.635}\ e^{0.801\ Pnc\ system} \quad (26)$$

$$\mu_{1(I+F)} = e^{-10.670}\ L^{0.829}\ V^{0.571}\ e^{0.784\ Pnc\ system} \quad (27)$$

where $\mu_{PDO}$is the expected number of *PDO* collisions; μ_{I+F} is the expected number of injuries plus fatal collisions; *L* is the curve length (m); *V* is the AADT (veh/day); P_{nc} is the probability of non-compliance.

As shown in the table, the regression coefficients of the traffic volume (*AADT*), curve length (*L*), and the system probability of non-compliance ($P_{nc\ system}$) are all significant at 95% confidence level. The results presented in the table show that: (i) there is a significant and positive relationship between the $P_{nc\ system}$ and predicted collisions, indicated by the positive sign of the $P_{nc\ system}$. This indicates that the expected number of collisions increases with the increase of non-compliance resulting from sight distance limitation and the potential of vehicle skidding. More details on the individual influence of each non-compliance criteria on the predicted collision frequency will be discussed in the following section (Section 5.3.2); (ii) the coefficients of both *AADT* and *L* are positive, indicating a positive relationship between the traffic volume, curve length, and both *PDO* and *I+F* collisions. Traffic volume also has a higher impact on *PDO* collisions than on *I+F* collisions. This is demonstrated by the higher value of the traffic volume regression parameter in the *PDO* models compared to those of the *I+F* models (e.g., 0.635 for *PDO* vs. 0.571 for *I+F*); (iii) the P_{nc} estimates have a higher impact on *PDO* collisions than on *I+F* collisions. The regression coefficient of $P_{nc\ system}$ is 0.801 for *PDO* and 0.718 for *I+F* collisions. The values of these regression parameters indicate that there is a sharper increase in the expected *PDO* crashes than *I+F* crashes. This may suggest that road collisions resulting from

the studied non-compliance modes are more likely to be less severe (i.e., *PDO* collisions) compared to, for example, overturning collisions, which are usually of high severity. This can be attributed to the fact that when a collision occurs due to sight distance limitations, the driver still has an available distance that gives them a chance to apply the brakes thereby mitigating the severity of the collision.

It can also be seen that there is a statistically significant moderate correlation of 0.45 between the two collision severity levels (i.e., *PDO* and *I*+*F*), indicating that horizontal curves with higher *PDO* crashes are likely to have higher *I*+*F* rates. This correlation suggests that sight distance deficiency and vehicle skidding could result in collisions with different severities (i.e., *PDO* and *I*+*F*) and that crash occurrences could be due to deficiencies in other design aspects.

5.3 Calibration of Safety-based Design Charts

This section is divided into two subsections. The first subsection summarizes the method used in the calibration of design charts. The second subsection presents and discusses the design charts developed. It also provides information about the key differences between the developed charts and current design guidelines. Finally, it provides guidance to road design practitioners on the use and significance of the developed design charts.

5.3.1 Calibration of Design Charts

The next step is to develop safety-based design charts that directly link horizontal curve geometric and traffic attributes to collision frequency. The calibration process uses the limit state functions of the two non-compliance modes (Equations 18 and 20). The design inputs *v*, *PRT*, *a,* and *fs* are considered random variables with the distributions outlined in Table 7. The variables *ASD*, *G, R,* and *e* are considered deterministic values. Operating speed (*v)* values range from 70 km/h to 100 km/h were considered. As the operating speed is calculated using speed prediction models in which the curve radius (*R*) in the main independent variable, these speed prediction models are the link between operating speeds and curve radius. This corresponds to *R* values ranging from 150 m to 900 m using the speed prediction models shown in Table 8 [6, 25, 31, 129]. Highway design guides provide design charts for horizontal curves based on superelevation rates (*e*) of 0.06 and 0.08, with $e = 0.06$ being more common. The calibration charts in this thesis are based on a superelevation rate of 0.06. Values of longitudinal grade (g) range from 0 to 3% were considered ($g = 3\%$, $g = 0$, $g = +3\%$).

The calibration process aims to develop design charts that incorporate P_{nc} values for different R, v, and ASD values. These charts can then be linked to another set of charts that relate P_{nc}values to collision frequency. Design charts for ASD range from 50 m to 100 m were developed. As previously indicated, MCS was used to calculate the probability of non-compliance associated with both sight distance limitation (P_{nc1}) and vehicle skidding (P_{nc2}) modes and the system probability of non-compliance ($P_{nc\ system}$). Using the two LSFs and design parameters discussed above, charts were calibrated for different geometric and traffic characteristics. The calibrated design charts are presented and discussed in the next subsection

5.3.2 Results and Discussion

First, considering the case of level terrain ($g = 0$), Figure 22 shows the calibrated charts at different ASD and v values considering one mode of non-compliance (sight distance: P_{nc1}); and the system (sight distance combined with vehicle skidding: $P_{nc\ system}$). The figure shows that the P_{nc} increases with increasing the operating speed. The results indicate that there are significant differences between the non-compliance rates calculated using the system reliability ($P_{nc\ system}$) and those estimated using only one mode of non-compliance (P_{nc1}), especially at lower operating speeds. It can also be seen that the differences between the $P_{nc\ system}$ and P_{nc1} decrease as the value of operating speed (or R) increase. For example, at a speed of 75 km/h and an ASD of 80 m, the $P_{nc\ system} = 0.53$ and $Pnc_1 = 0.46$ (difference = 0.07). While at a speed of 80 km/h, ASD of 80 m, the $P_{nc\ system} = 0.65$ and $Pnc_1 = 0.63$ (difference = 0.02). These differences decrease as the value of operating speed increases until reaching a point (almost at 90 km/h) after which there is no difference between the $P_{nc\ system}$ and P_{nc1} (of limited sight distance). The reason behind this is that

at higher speeds, the sight distance demand is high resulting in increasing the influence of the P_{nc1} compared to the effect of P_{nc2} within the system (Equation 8), making the P_{nc1} prevailing (since P_{nc1} is the major contributor to the value of $P_{nc\ system}$). In other words, at higher operating speeds, the limited sight distance controls the failure of a system of two modes. This shows the importance of applying system reliability on horizontal curves, especially on curves with sharp radii and low operating speeds where is a significant difference between P_{nc1} and $P_{nc\ system}$ as shown.

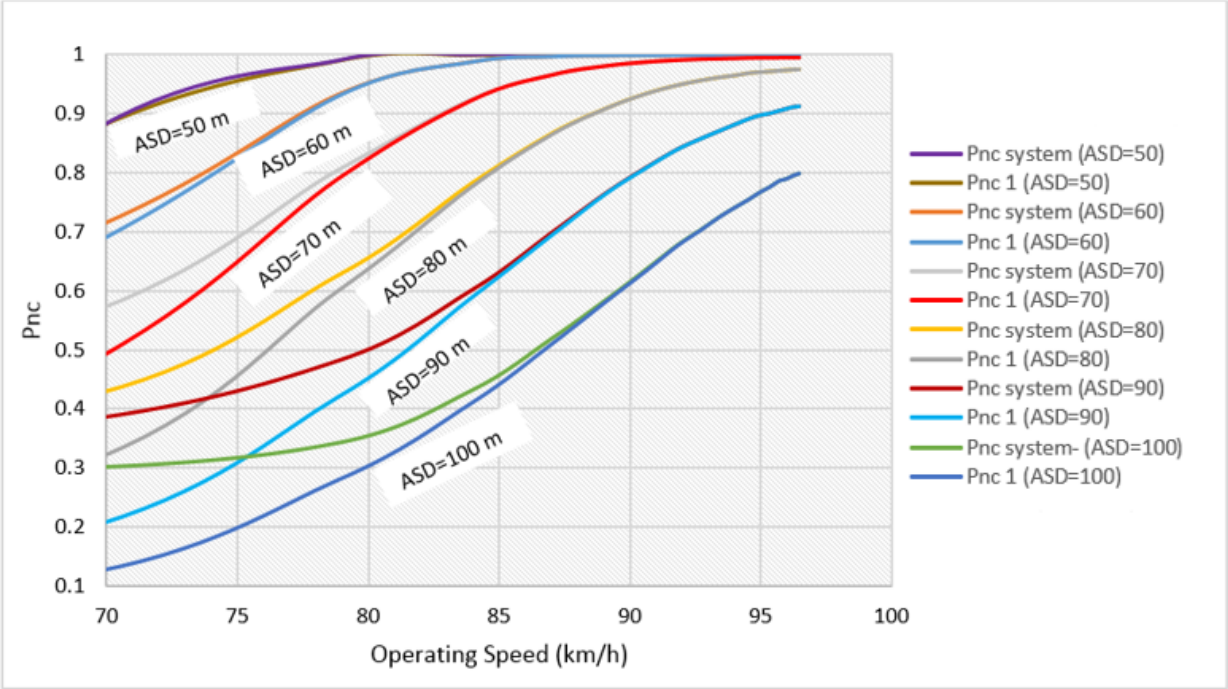

Figure 22: Calibrated design charts at different geometric and traffic characteristics ($G = 0$ & e = 0.06)

It can also be seen that the differences between the $P_{nc\ system}$ and P_{nc1} decrease as the *ASD* decreases. For example, at a speed of 75 km/h and an *ASD* of 100 m, the $P_{nc\ system} = 0.32$ and P_{nc1}=

0.20 (difference = 0.12) compared to $P_{nc\ system} = 0.53$ and $P_{nc1} = 0.46$ (difference = 0.07) at an *ASD* of 80 m. The reason behind this is that at the same operating speed, as the value of *ASD* decreases, the P_{nc1} of sight distance mode increases while the P_{nc2} of vehicle skidding does not change (i.e., as demonstrated by Equation 20). Also, at lower *ASD* values, the P_{nc1} is much higher than $P_{nc2,}$ which is the reason that the effect of P_{nc2} on the $P_{nc\ system}$ is becoming lower with the decrease of *ASD*. In other words, at the same operating speed, when *ASD* decreases, P_{nc1} increases, P_{nc2} does not change, $P_{nc\ system}$ increases as a result of increasing P_{nc1}, but the P_{nc1} becomes the major contributor to the $P_{nc\ system}$ compared to P_{nc2}, therefore, the influence of P_{nc2} on the $P_{nc\ system}$ is smaller.

Figure 23 shows design charts that translate the information in the SPFs summarized in Table 10 into a visual guide to easily predict the collision frequency for different AADT and P_{nc} levels. Figure 23 can be used in conjunction with Figure 22 where P_{nc} levels (i.e., system or one mode) for a specific design are obtained using Figure 22 while Figure 23 can then be used to estimate the corresponding predicted number of crashes. For example, a curve that has an *AADT* of 25,000 and $P_{nc\ system}$ of 0.8 is expected to have 27 collisions/5 years for every km of curve length as a result of the non-compliance resulting from sight distance limitation and vehicle skidding.

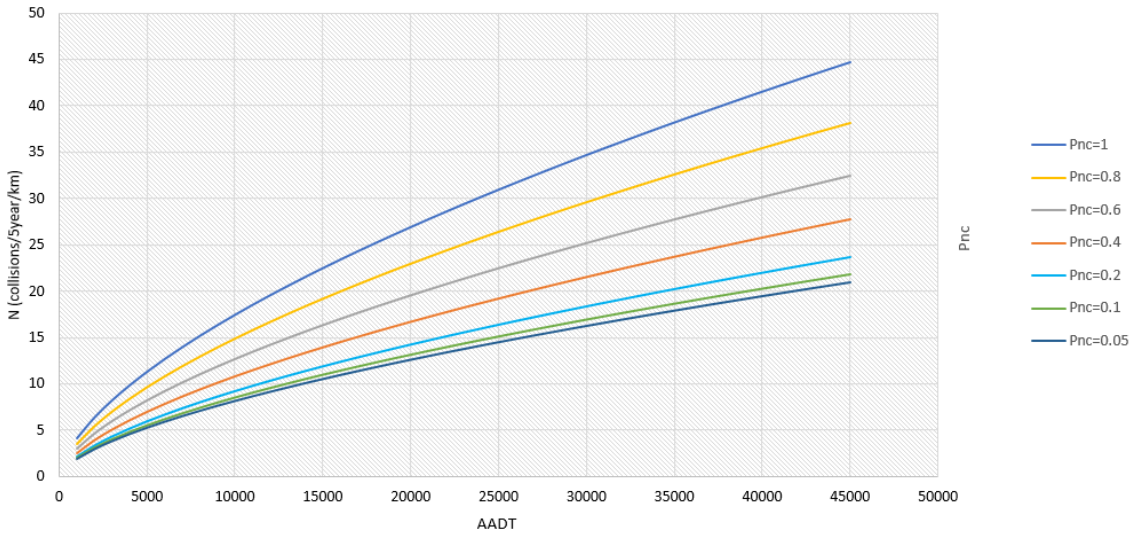

Figure 23: Design charts showing the relationship between Pnc, AADT, and total collisions

Second, considering longitudinal grades of g = -3% and g = +3%, Figure 24 shows the calibrated charts at different *ASD* and v values for both grade levels. The figure contains charts for G = 0 (which was previously discussed when referring to Figure 22) with newly overlaid charts for G = -3% and G = +3%. As shown, similar conclusions can be drawn for each of grade levels (i.e., G = -3% and G = +3%). However, at G = -3%, the $P_{nc\ system}$ and P_{nc1} are higher than those corresponding to G = 0. This is because, at downgrades, a vehicle would need a longer stopping distance resulting in higher *SSD* demand and subsequently higher P_{nc} values.

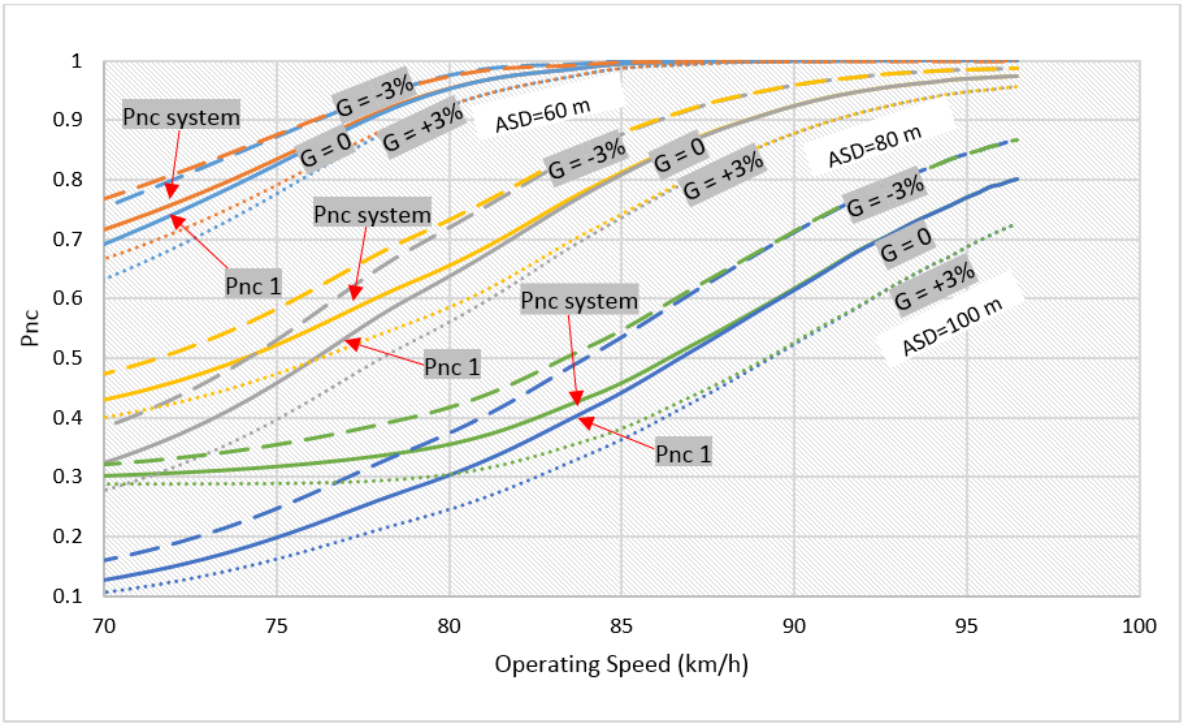

Figure 24: Calibrated design charts at different geometric and traffic characteristics (G = 0, G = -3 %, G = +3 % & e = 0.06).

It is worth noting that the value of G does not influence the second non-compliance mode (P_{nc2}), and the increase in the $P_{nc\ system}$ results from the increase in P_{nc1}. In upgrades (e.g., G = +3 %), vehicles need shorter distances to come to a complete stop resulting in lower *SSD* demand and non-compliance rates. Thus, the values of the $P_{nc\ system}$ and P_{nc1} for G = +3 % are lower than those corresponding to G = 0. This figure can be used to determine non-compliance levels for specific design scenarios when information on profile grades is available (i.e., G). Figure 23 can then be used to estimate the expected collision frequency.

The proposed design charts differ from existing design guidelines in different ways. Compared to the calibrated charts, the design proposed by the current guidelines is associated

with high P_{nc} levels at relatively low operating speeds. For example, as per Alberta Highway Geometric Design Guide, a design speed of 70 km/h on a +3% upgrade segment require an *ASD* of 100 m. Using Figure 24, it can be obtained that the design proposed by current guidelines corresponds to $P_{nc\ system}$ of 0.29 and P_{nc1} = 0.11 (Difference = 0.18). At higher design speeds, current design guidelines have shown to be conservative resulting in uneconomic designs. For example, at a design speed of 100km/h, on a +3% upgrade segment require an *ASD* of 174 m. The developed charts show that the non-compliance associated with the studied modes would reach Zero at a sight distance supply that is less the provided by current guidelines. Therefore, these findings indicate that (i) design guidelines are conservative at higher design speeds and associated with high risk levels at lower design speeds; (ii) when associated with high risk levels (i.e., at low design speeds), there is a significant difference between P_{nc} of one mode and that of two modes demonstrating the importance of considering multi-modes of non-compliance as discussed; and (iii) there is inconsistency in risk levels associated with design guidelines across various design speeds.

Moreover, the design proposed by current guidelines is deterministic with unknown risks or safety consequences of deviation from the proposed values. Since current design guides provide minimum requirements, a designer could decide to provide a design value that exceeds the minimum requirements. This could lead to more conservative designs resulting in higher costs of highway construction projects. However, the safety level of these conservative designs remains unknown. The proposed charts however represent a scientific-based tool that can be used by highway design engineers to assess the risks associated with proposed design values and the

influence of proposed designs on safety. For example, by knowing the AADT, the expected collision frequency corresponding to the design values discussed above can be estimated. Also, using Figures 22-23, different proposed measures (e.g., reducing speed or providing more ASD) can be evaluated and their safety consequences can be determined, which cannot be achieved using current design guidelines. These charts are not only a useful tool for designers but also represent a tool that can provide beneficial insights to departments of transportations about the safety consequences of rehabilitation projects and hence their economic feasibility. In summary, the calibrated charts could have significant practical implications for both design engineers and transportation agencies.

The results of this research demonstrate that practitioners are advised to use $P_{nc\ system}$ in the design process, especially when designing curves with sharp radii. As discussed, previous research showed that non-compliance on horizontal curves could result from limited sight distance combined with vehicle skidding. The results demonstrate that there is a significant difference between P_{nc} of one mode and that of two modes especially at lower operating speeds, which is in line with the recommendations of previous work. Therefore, it is important to consider $P_{nc\ system}$ in the design stage especially on curves with sharp radii and low operating speeds. More so, practitioners could use the proposed design charts as a tool to assess the risk levels associated with various design options or estimate the safety benefits of different design improvements. This can help study the economic feasibility of rehabilitation projects of horizontal curves through employing a benefit-cost analysis framework to decide whether it is feasible to construct a specific design modification.

The following example demonstrates to a road designer how to estimate the expected collision reductions that could result from a potential geometric improvement. For a curved segment with a curve radius of 152 m, a longitudinal grade of +2.8%, a minimum *ASD* of 62 m, and an *AADT* of 4410, using Figures 23 and 24 (operating speed = 78 km/h), the $P_{nc\ system}$ is 0.87, and the expected collision frequency is 8 collisions/5 year/km. A designer could use the proposed figures to conclude that improving the *ASD* from 62 m to 100 m would reduce the $P_{nc\ system}$ to 0.29 and the expected crashes to 5 collisions/5 year/km. A designer would also notice that implementing speed reduction measures that reduce the operating speed from 78 km/h to 70 km/h would drop the $P_{nc\ system}$ to 0.67 and the expected crashes to 7 collisions/5 year/km. Therefore, it can be concluded that improving the *ASD* provides more safety benefits compared to speed reduction measures. However, a benefit-cost analysis would still be recommended to decide which improvement option is more feasible.

Thus, the proposed charts are ready to use by designers in the province of Alberta, Canada, based on data was collected on Alberta highways. However, other jurisdictions could use the proposed framework to develop similar charts. This would be through utilizing geometric and collision data collected on highways of that province or jurisdiction. The same framework could then be followed to develop safety models and design charts similar to those presented in this thesis. Although the developed methodology focuses on horizontal curves, it could be applied to other highway features.

6 THE ASSOCIATION BETWEEN CURVE FEATURES, RELIABILITY MEASURES, AND SAFETY

This chapter explores the interaction between P_{nc}, curve features, and safety. It provides details on using SEM to study the impacts of curve attributes on the P_{nc} as well as the direct and indirect (through the impacts on P_{nc}) impacts of those attributes on safety. The chapter is divided into four sections. The first section provides background information on the objectives and significance of studying the interaction between P_{nc}, curve attributes, and collision frequency. The subsequent section gives some details on SEM and mediation analysis. The third section is dedicated to model development while the last section discusses the results and the interaction between curve geometric characteristics, associated non-compliance levels, and safety. It also highlights the importance of using SEM in understanding these relationships and concludes by giving some guidance to road designers.

6.1 Background

With the majority of previous studies focusing on the mere quantification of risk levels, some recent studies developed relationships between reliability outcomes and safety, focusing on horizontal curves with limited sight distance [6, 7, 34]. However, these studies were fully dedicated to establishing a statistical relationship between the P_{nc} and collisions without addressing the effects of curve attributes on P_{nc}, the potential direct influence of curve geometric features on collisions or the indirect effect of geometric attributes on safety, that could be mediated through P_{nc}. Therefore, it is unknown whether or not the relationship between P_{nc} and

safety is confounded by having curve attributes directly affect collision frequency or have indirect effects on safety that is transferred through P_{nc}. The lack of information on these interactions has led P_{nc} to stand merely as a statistical measure that does not give enough to roadway designers. Therefore, understanding these relationships is crucial for practitioners and it could help understand the influence of different curve geometric attributes on design non-compliance corresponding and safety levels.

As the insufficient sight distance is the prevailing non-compliance mode across the studied curves, the SEM in this chapter is dedicated to studying the association between curve features, P_{nc} (i.e., due to inadequate sight distance), and collision frequency. A path analysis approach is used to model the P_{nc}-safety relationship and identify different curve attributes that confound this relationship by directly or indirectly affecting collisions. As previously mentioned, to the best of the author's knowledge, no previous studies investigated the interaction between geometric features, risk levels, and safety. The model presented in this chapter provides valuable insights on both the direct and indirect impacts of horizontal curve features on sight distance limitations and safety. It demonstrates that the influence of some curve attributes on safety can be indirect and transmitted through the impact on the probability of non-compliance to meeting SSD requirements. This highlight the importance of giving considerable attention to these features with indirect influence on collisions, which would be ignored in case these interactions are unexplored. This information provides more understanding to designers on the impacts different attributes have on non-compliance and safety levels. Indeed, this practical objective along with others

discussed throughout the thesis represents a step further towards developing performance-based design frameworks in which the interaction between proposed design and safety can be expected.

6.2 Structural Equation Modelling

As previously discussed, this analysis aims to study the P_{nc}-safety relationship while accounting for other geometric and traffic attributes that can mediate and confound this relationship. In this framework, the dependent variable (DV) is the outcome variable to be predicted. Therefore, the DV is considered the expected number of collisions due to non-compliance to meeting sight distance requirements. The mediator variable, as defined by Elvik, Christensen [153], is a risk factor that influences the DV if modified. It is also a variable through which other variables could impact the DV. In this analysis, the mediator was assumed to be the P_{nc1} while confounding factors include traffic and geometric characteristics of horizontal curves. The hypothesized relationships are illustrated by the path diagram shown in Figure 25. Based on the findings of previous studies, it was assumed that some variables have direct effects on crashes only, P_{nc} only, or both P_{nc} and collisions. Variables with effects on P_{nc} are also tested for indirect effects on safety.

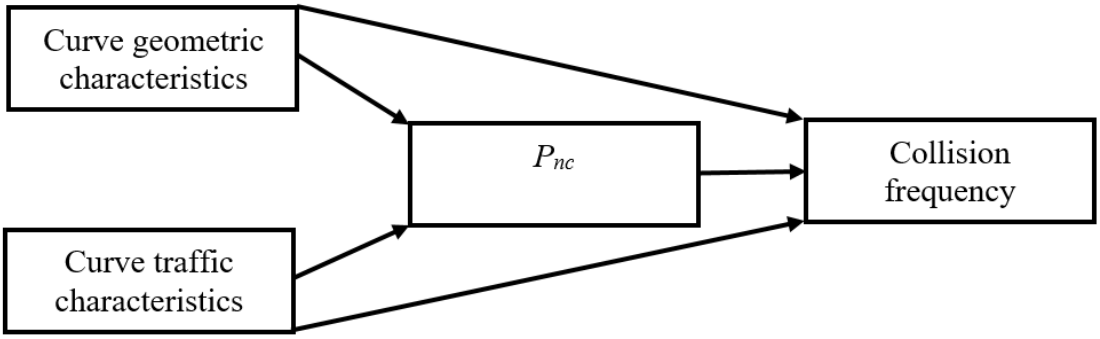

Figure 25: The proposed path model

Path analysis is a form of SEM which has two significant advantages. Using SEM, multiple relationships can be tested simultaneously while considering potential mediation or moderation effects between relationships. As previously discussed, the relationship between P_{nc} and safety can be mediated or confounded by other features, especially curve attributes. To properly study this relationship, this mediation needs to be accounted for. The ability to test for the presence of mediated effects is the second advantage of using SEM with the main aim of testing the validity of certain relationships. As indicated by Kline (2015), it is typically required that SEM can be performed only on large sample sizes (n > 200). This requirement is met in the analysis performed in this research (n = 244).

Mediation analysis is a statistical approach used to test whether a variable *x* transmits its effects to another variable *y* and determine if the influence of *x* on *y* is (i) direct only; (ii) indirect only through a mediator variable (known as full mediation); or (iii) both direct and indirect (known as partial mediation). Mediation analysis is used to test a proposed relationship that is assumed based on theoretical backgrounds, logical assumptions, or research design [154]. In a

simple mediation model, a variable x is assumed to have a direct effect on another variable y and also affect y indirectly through a mediator variable m. The regression equations that represent these mediation models are as follows:

$$y_i = \beta_0 + \beta_1 m_i + \beta_2 x_i + \varepsilon_{1i} \quad (28)$$

$$m_i = \gamma_0 + \gamma_1 x_i + \varepsilon_{2i} \quad (29)$$

where y_i represents the dependent variable (e.g., collision frequency); m_i is the mediator variable; x_i represents all independent variables; β_0 and γ_0 represent the intercepts of the models; β_1, β_2, and γ_1 are regression coefficients; and ε_{1i} and ε_{2i} are error factors.

Equation 28 combines the paths from x to y and m to y, while Equation 29 shows the path from x to m. The coefficient γ_1 represents the magnitude of change in m corresponding with a unit change in x, representing the effect of x on m. Similarly, the coefficient β_2 denotes the magnitude of change in y associated with a unit change in x, representing the direct effect of x on y. The coefficient β_1 represents the magnitude of change in y when m changes by one unit. Thus, the indirect effect of x on y can be quantified using the product-of-coefficient estimator $\gamma_1 \beta_1$ [155].

6.3 Model Development

Collisions are random and discrete events that cannot be modelled using linear regression, as presented by Equation 28. Road crashes are typically modelled using Negative Binomial regression [138, 139, 141]. Y denotes the collision frequency at a site. It is assumed that Y follows a Poisson distribution with a parameter λ. To account for the over-dispersion that usually exists in collisions datasets, it is regularly assumed that λ follows a gamma distribution with shape

parameter k and scale parameter k/μ. Thus, Y follows a negative binomial (Poisson-Gamma) distribution [138] with an expected value (i.e., mean) and variance expressed as follows:

$$E(Y_i) = \mu_i, Var(Y_i) = \mu_i + \mu_i^2/k \quad (30)$$

where μ is the predicted number of collisions which can be given by the following relationship:

$$ln(\mu_i) = ln(\gamma_0) + \gamma_1 ln(\theta_i) \quad (31)$$

where γ_0 and γ_1 represent the parameters of the model, and θ_1 represents the model covariates.

SEM software Mplus version 6 was used to simultaneously model: (i) the relationship between the exogenous variables and crash frequency; and (ii) the relationship between those variables and the mediator (P_{nc}), which was modelled using Ordinary Least Squares (OLS) regression as shown in Equation (29). Model parameters were computed using maximum likelihood estimation [154].

6.4 Results and Discussion

Following the hypothesized relationships illustrated by the path diagram shown in Figure 25, the modelling was completed using SEM software Mplus. The final path diagram is shown in Figure 26, and the final modelling results are summarized in Table 11. The table shows a summary of the final model with all the statistically significant variables that have direct effects on P_{nc}, direct effects on collisions, and indirect impacts on collision frequency. Variable selection was conducted through a backward elimination procedure, whereby variables that did not have significant effects on the mediator or the response variable were removed one step at a time from the model. The process is repeated for the remaining variables until the significance level of all

of the variables included in the model is below the significance threshold. Before discussing the implications of the results, it is worth noting that the *ASD* was not included as an independent variable in the models as this variable was already used to compute the mediator (P_{nc}) and, hence, including it in the model again would be redundant. Also, the model fit was assessed by comparing multiple models based on the Akaike Information Criterion (AIC) minimization criteria, where the model with the lowest AIC was assumed to have the best fit. To further verify the model fit, the AIC of the fitted model was compared to the baseline model (i.e., without predictor variables). Both the AIC (Baseline = 4903.4, Fitted = 3098.7) and Bayesian Information Criterion (BIC) (Baseline = 4983.8, Fitted = 3182.6) were lower for the model used, indicating that the full model fits the data better.

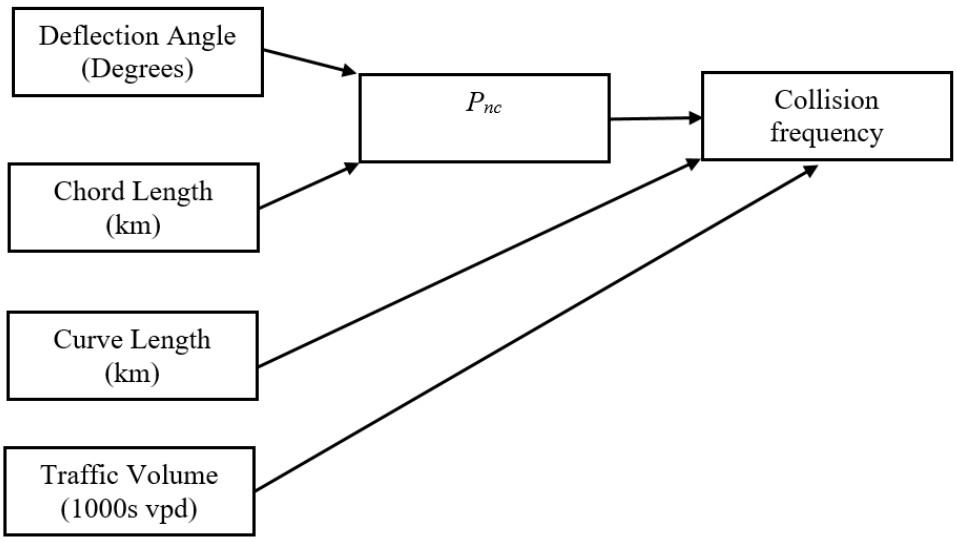

Figure 26: The final path model

Table 11: Path analysis modelling results

	Variable	**Estimate (Est)**	**SE**	**Est/SE**	**P-Value**
Effects on P_{nc}	Deflection Angle (Degrees)	0.005	0.001	4.239	0.000**
	Chord Length (km)	-0.362	0.074	-4.923	0.000**
Effects on Collision Frequency	P_{NC}	0.634	0.256	2.48	0.013**
	Curve Length (km)	1.39	0.23	6.03	0.000**
	Traffic Volume (1000s vpd)	0.074	0.009	8.631	0.000**
Indirect Effects on Collision Frequency	Deflection Angle (Degrees)	0.003	0.002	2.035	0.042**
	Chord Length (km)	-0.229	0.106	-2.165	0.030**

*** Significant at 5% level*
S.E.: Standard Error

The model shows that curve geometry has statistically significant effects on both the mediator (i.e., the probability of non-compliance) and the response variable (i.e., the total number of collisions). For some independent variables, the effects on the total number of collisions were direct, while for other variables, the effects were mediated through the probability of non-compliance.

First, as for the variables that influence the P_{nc}, it is important to note here that the impacts of curve radius were already integrated into the P_{nc} estimate. Curve radius was the main parameter

in the speed prediction models that were used to predict the operating speed (v) which is a major contributor to P_{nc} calculations as shown in Equation 18. The speed prediction models used in predicting the operating speed include the curve radius or the degree of curvature (= 5729/R) as a predictor. Since curve radius was used to estimate operating speed (which was then used to calculate the P_{nc}), including the curve radius again in the model along with P_{nc} would be redundant. Thus, the curve radius should not be expected to have a significant relationship with the P_{nc}.

In contrast, other additional curve attributes were found to have a statistically significant influence within the model. Curve features such as chord length and deflection angle were found to have statistically significant effects on the probability of non-compliance (P_{nc}). It should be noted here that none of the speed prediction models included the chord length and only one model included the deflection angle. Chord length was negatively proportional to the probability of non-compliance, whereby increases in the chord length decreased the probability that the curve would not satisfy the SSD requirements of drivers. In contrast, the curve deflection angle was positively correlated with P_{nc}. In this case, increases in the curve deflection angle increased the probability that the curve would fail to satisfy driver demand for SSD. These findings are highly intuitive considering that increasing the chord length while keeping all other variables in the estimated model (including the deflection) constant reduces the sharpness of the curve (i.e., by increasing the radius) as demonstrated by Figure 27. As shown, when the curve deflection angle is fixed, increasing the chord length is possible only by increasing the curve radius.

Similarly, increasing the curve's deflection angle while fixing the chord length increases the sharpness of the curve. The reason is that sharper curves often limit a driver's ability to see a hazard in time to safely come to a complete stop.

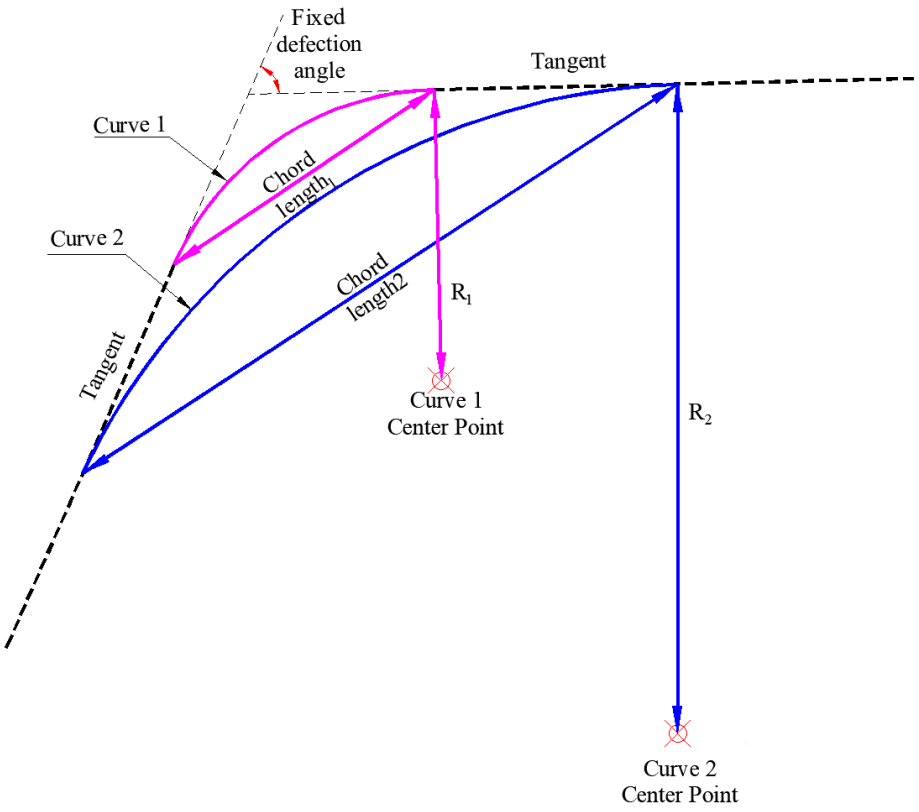

Figure 27: The relationship between chord length and curve length

In addition to their impacts on the P_{nc}, both the deflection angle and the chord length also had indirect statistically significant effects on the number of collisions with p-values of 0.042 and 0.030, respectively. The model shows that, despite not having direct effects on safety (i.e., not

directly impacting collision frequency), both the curves deflection angle and the chord length impact collision frequency indirectly. This indirect effect is transmitted through the effects of those variables on the probability of non-compliance to stopping sight distance requirements. This can be explained by the fact that changes in these variables influence the P_{nc} to sight distance requirements and consequently affect safety. In other words, as chord length and deflection angle increase/decrease they decrease/increase the likelihood of limitations to sight distance on a curve. This limited sight distance then contributes to an increase/decrease in collisions. This finding shows the importance of considering these attributes when designing horizontal curves instead of focusing entirely on the curve radius, which is consistent with previous literature.

Unlike the deflection angle and the chord length, the curve length (i.e., the length of the curve's arc) had direct impacts on collision frequency. The relationship was positive and statistically significant, indicating increases in the length of a curve increased the possibility of collisions occurring on that curve. Similarly, curves with higher traffic volumes were also more likely to experience a higher collision frequency, an effect that was also observed to be statistically significant in the model at a 5 % significance level. These findings are consistent with safety literature that shows that both segment length and traffic volume increase driver exposure to risk and, as a result, increase the likelihood of collision occurrence [6, 34, 60].

Besides curve length and traffic volume, the probability of non-compliance also had statistically significant effects on collision frequency with a *p*-value of 0.013. The model shows that the relationship was a directly proportional relationship whereby increases in the probability of non-compliance were associated with increases in collision frequency on segments, as

expected. In other words, a higher collision frequency is expected on segments that are less likely to comply with stopping sight distance requirements of the driving population. It should be noted that the *ASD* is not included directly as an independent variable in the model. However, its effect is accounted for by the mediator (P_{nc}). In other words, since the ASD was used to estimate the P_{nc} of each curve, adding it as an independent variable to the model would be redundant.

As demonstrated, this chapter proposed an approach through which direct and indirect effects between safety, sight distance limitations, and geometric attributes could be assessed. Such an approach had not been proposed in previous work. This approach helps engineers understand more about the underlying reasons that might result in a poor safety record. Instead of attributing a poor safety record to limited sight distance, designers now could understand that specific changes to some curve attributes might help improve safety through their effect on reducing the associated non-compliance rates. Ultimately, this approach helps designers have a better understanding of these relationships and make well-informed decisions on design improvements of curved segments based on the knowledge of which curve attributes have the highest influence on risk levels and safety. This information is essential to roadway design experts attempting to account for uncertainty in design while understanding how different geometric design attributes impact this uncertainty. Besides helping experts create safer roads, such an understanding also assists engineers design roads that are inclusive for all road users by accounting for the stochastic nature of design inputs and the variation in driver capabilities.

7 CONCLUSIONS

This chapter presents a summary of the research conducted in this thesis and summarizes the main contributions. It also discusses research limitations and potential areas for future research.

7.1 Research Summary

Road design guidelines provide a framework for designers to exercise their critical engineering judgment when designing roadways including horizontal curves. However, there is a need to address the limitations associated with the current deterministic design approach including the uncertainties in design inputs, commonly providing conservative designs, and the unknown safety levels of the proposed design. This was made possible by utilizing the reliability theory to evaluate the risk levels corresponding to highway curved sections, followed by establishing a relationship between the noncompliance in design and collision frequency. The thesis then demonstrated a considerable application of utilizing the reliability theory in highway design where safety-based design charts were calibrated for horizontal curves using 3D models of highway corridors. A path analysis approach was then utilized to study the interaction between curve attributes, non-compliance, and safety to provide designers and engineers with more information on the influence of various design elements on P_{nc} and safety. The work presented in this thesis can be summarized as follows:

This first phase of this thesis developed a set of novel algorithms that utilize LiDAR data to automatically detect and extract information on horizontal alignment on a large scale. The developed algorithms aimed to detect horizontal curves and extract their geometric attributes and

perform an assessment of the *ASD* along highway corridors in a 3D world. The performance of the proposed algorithms was validated using ground truth data. The validation of proposed algorithms showed their robustness to detect curved sections and extract their features in a highly accurate and efficient manner. A comprehensive database of information on 244 horizontal curves including curve attributes, *ASD*, and longitudinal grades was established and prepared for reliability analysis.

Unfortunately, performing such a large-scale reliability assessment was not possible in previous research due to the lack of an efficient methodology that can be used to establish an inventory of road geometric elements (e.g., supply of *ASD*). This led to previous work in this area to focus on 2D sight distance assessment utilizing traditional sources of curve data such as as-built documents or aerial maps. When extracting curve attributes or evaluating *ASD* in a 2D space using as-built drawings, this source of information could be outdated due to the regular maintenance and pavement operations that affect the accuracy of original as-built documents.

As opposed to previous studies, this thesis adopted the use of Mobile LiDAR data to detect highway curved segments, extract their geometric characteristics, and evaluate sight lines using a 3D approach. In many situations, the sight distance could be limited by the road's vertical profile or by combined horizontal and vertical curves, emphasizing the importance of using 3D sight distance calculations in reliability analysis. The high density of LiDAR point cloud creates a 3D model of the road environment, which enables an accurate assessment of the *ASD* and helps identify potential obstacles and safety problems robustly and efficiently. The automated approach of data extraction minimizes human errors associated with current practices, such as subjective

evaluation. The reliance on mobile LiDAR is also of great benefit as it is collected without causing any disruptions to traffic movement.

The automated and efficient data extraction approach makes information on horizontal alignment readily available to transportation agencies on an unprecedented scale providing them with access to an abundant amount of information about highway infrastructure. In fact, the data acquisition framework in this thesis, on its own, demonstrates that adopting a LiDAR-based method, to maintain an updated inventory of information on horizontal alignments could transform the way DOTs manage and assess geometric features their road networks, which is essential to DOTs looking to develop an effective Transportation Asset Management Plan.

The second phase of the thesis focused on performing a multimode reliability analysis to quantify the risk associated with inadequate sight distance and vehicle skidding on curved sections. This is to assess the ability of horizontal curves to handle stochastic road user demands followed by quantifying the safety impacts of the failure to do so through developing SPFs incorporating P_{nc}. The results showed that the studied curves are associated with high risk levels. Since the safety consequences of this non-compliance were unknown, SPFs were developed using MVPLN regression to relate the noncompliance rates to historical collisions on curved segments. This was followed by calibrating safety-based design charts that relate curve geometric and traffic attributes to P_{nc} and crashes.

The results showed that there is a statistically significant relationship between the P_{nc} and the collision frequency, indicating that higher non-compliance rates are associated with higher expected crashes. The findings also demonstrated that there are significant differences between

non-compliance levels when considering system reliability analysis compared to using only one non-compliance mode, especially on curves with sharp radii and low operating speeds. This emphasises the crucial importance of considering multimode reliability assessment instead of single mode, especially when analyzing sharp curves with low operating speeds. More so, the results also showed that the P_{nc} resulting from insufficient sight distance is dominant at high operating speeds and very limited *ASD*. This demonstrates that at higher speeds, the sight distance demand is high and when it exceeds the *ASD* supply, this results in higher non-compliance levels due to limited sight distance compared to non-compliance associated with the potential of vehicle skidding. The findings also suggest that there is a moderate correlation between the *PDO* and *I+F* severity levels, suggesting the presence of a latent relationship between both *PDO* and *I+F* collisions. This correlation can be interpreted as curves with higher *PDO* crashes that are likely to experience higher *I+F collisions*.

The proposed charts are ready to use by practitioners in Alberta, Canada, based on data was collected on Alberta highways. A designer could use the developed charts to compare different design alternatives from a safety perspective. The feasibility of using the calibrated design charts to estimate the expected benefits of potential geometric improvements was also demonstrated. The charts can also be used. Such a safety-based design approach facilitates the adoption of a PBD approach whereby highways are designed based on the demands of the driving population while the safety levels of proposed designs can be expected.

Finally, the thesis utilized structural equation modeling to model the relationship between P_{nc} associated with inadequate sight distance and collision frequency while accounting for curve

geometric and traffic attributes that confound this relationship. Path analysis was used to (i) model the relationship between P_{nc} and safety while accounting for other variables that confound this relationship; (ii) model the relationship between curve features and P_{nc} to identify curve attributes that could increase the likelihood of non-compliance to sight distance requirements; and (iii) assess the indirect effects of curve features on collisions that could be mediated through P_{nc}. Modelling these relationships is a critical step to help design engineers understand the influence of curve attributes on P_{nc} and safety. This helps translate non-compliance levels into acceptable and unacceptable geometric attributes that designers are more familiar with compared to P_{nc} statistical measures. The results of this analysis showed that the influence of curve deflection angle and chord length incorporate the impacts of curve radius on both P_{nc} and safety. The findings of this approach demonstrate the importance of studying and accounting for other curve attributes such as deflection angle and chord length instead of focusing only on the curve radius.

7.2 Research Contributions

Paving the way for the adoption of a safety-based design approach, this thesis presented multiple contributions to the state-of-the-art in the field of highway design from both theory and practice standpoints. The major contributions of this dissertation can be summarized as follows:

- It contributes to the literature by assessing the risk of design non-compliance (P_{nc}) associated with multi-modes of non-compliance and establishing a link between this risk and collision frequency utilizing 3D sight distance calculations, which have not been investigated in previous work. Understanding this relationship will provide significant insights into the reliability of a proposed road design and its influence on road safety in

terms of collision impacts. Quantifying the safety influence of randomness in design parameters and deficiencies in design, such as limited sight distance, allows decision-makers to study the safety benefits of implementing improvements on existing roads. Since the relationship between design and safety is now established, a designer can estimate the expected number of road collisions for a proposed design.

- It calibrates safety-based design charts demonstrating the feasibility of adopting performance-based probabilistic design guides. Departments of Transportation can use the findings of this research as a predictive tool to estimate the safety benefits of different design improvements or estimate the safety consequences of deviation from a specific design. More so, the findings can also be used in a benefit-cost analysis framework to assess the economical feasibility of various design alternatives or safety countermeasures for highway rehabilitation projects. A road designer can use the findings as a predictive tool to compare different design alternatives and investigate the cost-effectiveness of various dimensioning scenarios.
- It provides a framework through which a risk measure (P_{nc}) can be calculated to incorporate the inherent safety impact of random design inputs, such as operating speed, perception and reaction time, and deceleration rate on safety. This risk measure can be then used as a target safety level in future designs based on the desired level of safety.
- The results of studying the interaction between curve attributes, risk levels, and safety could help design engineers understand the influence of curve attributes on P_{nc} and safety and provide invaluable insights into the interaction between various geometric features

and expected collisions. The findings also help designers translate non-compliance levels into acceptable and unacceptable geometric attributes that they are more familiar with compared to P_{nc} measures.

- The novel algorithms developed in this research can be utilized to help transportation agencies establish a reliable inventory of highways curve data, which can facilitate the management of highway networks including safety audits and assessment of the compliance of existing roads to standard requirements. The efficiency of the proposed algorithms means that inventory of geometric features can be made readily available in a timely manner and can be applied on a large scale. Using the developed algorithms to collect information on highways from LiDAR data help avoid the hurdles associated with traditional methods that are time-consuming, labour-intensive, and traffic disruptive. More so, the automation of data extraction makes large scale data collection on highways feasible.

In summary, this thesis presented a probabilistic design approach in which uncertainties in design inputs are considered and safety levels of the proposed design can be expected. Opposed to the current design approach set by existing highway design guides and supplemented by the Highway Safety Manual, the developed design framework can be used to assess the risk directly connected to the suggested design by highway guidelines without the reliance on data about sites similar to the road facility being designed. Indeed, the ultimate goal of a more reliable approach is to have similar sites constructed based on a reliability-based approach. Performance metrics about these sites can be later collected and then used to assess the safety risk associated with another proposed

design that is also designed following a probabilistic approach. This would be a new generation of safety assessments of proposed designs.

The research presented in this dissertation is a step forward towards adopting a performance-based design of highways. The developed design framework is a safety-based approach that accounts for uncertainty in design inputs and the variation in road user capabilities which could help design more inclusive roadways that accommodate a large proportion of the driving population. Even though the thesis focuses on analyzing horizontal curves, the proposed framework can be applied to other roadway features.

7.3 Limitations and Future Research

Although this research has covered multiple aspects of the reliability-based design of horizontal curves, some areas still need further improvement and investigation. As with any research study, several limitations and assumptions were made. For example, probability distributions for design inputs used in the analysis were obtained from numerous previous studies. However, a more rigorous analysis would entail the development and testing of these distributions based on field data. Therefore, obtaining field data to validate the assumed distributions is a future area of research. Also, the analysis used speed prediction models that are commonly cited in previous reliability studies, however, using real operating speed data (when available) and studying the influence of using various speed prediction models on the resulting risk levels is another area of improvement. The analysis also assumed that there is no correlation between the design inputs, which requires more investigation in future work. When weather data is available, considering

additional factors such as various weather conditions and driving at nighttime is also recommended.

Although the thesis studied the risk associated with locations where design supply is the most critical (e.g., minimum *ASD*), studying the risk levels at different locations on horizontal curves and beyond the curve limits (i.e., approach and departure tangents) is encouraged. The thesis used a 3D-based approach in calculating the *ASD*, however, the available and required coefficient of side friction were based on probability distributions obtained from previous work which was based on 2D analysis. Thus, when filed data is available, a 3D-based analysis of side friction supply and demand is recommended. Future research is suggested to extend this work by applying the proposed design methodology to evaluate other aspects of sight distance, such as passing sight distance along with studying other highway elements. As the work in this thesis focused on analyzing two-lane two-way highways with similar characteristics and considered a passenger car in the analysis, applying the proposed framework on various highway classifications and considering heavy vehicles while accounting for its potential of rollover is highly encouraged. Another possible extension of this work is establishing a benefit-cost analysis framework in which various proposed design alternatives can be evaluated while highlighting the safety benefits and economic feasibility of each option.

This path analysis focused on studying the effect of curve attributes in the P_{nc} – safety relationship. Future work is also recommended to consider other factors such as climate conditions. In this study, all studied curves are located on two-lane two-way highways with the same class, and therefore, there was very minor (negligible) variation in some curve attributes

such as lane width and shoulder width among the studied segments. Therefore, the lane width and shoulder width do not influence the developed model. Thus, future research is recommended to study different highway classes and develop models that include other curve attributes such as lane width and shoulder width. More work is also encouraged to advance the proposed model by introducing a moderated mediation analysis to understand how design attributes impact P_{nc} and Safety differently in high and low-speed regimes.

REFERENCES

1. Said, D. (2008). *Development of the interrelationship between driver behaviour and highway design and safety* (Doctoral dissertation, Carleton University).
2. Felipe, E., & Navin, F. (1998). Automobiles on horizontal curves: experiments and observations. *Transportation Research Record*, *1628*(1), 50-56.
3. Glennon, J. C., Neuman, T. R., & Leisch, J. E. (1983). *Safety and operational considerations for design of rural highway curves. Final report* (No. FHWA-RD-83-035).
4. Dhahir, B. (2018). *Reliability-Based, Safety-Explicit Horizontal Curve Design Using Naturalistic Driving Study* (Doctoral dissertation, Carleton University).
5. Ibrahim, S. E. B. (2011). *Risk-based design of horizontal curves with restricted sight distance* (Masters dissertation, University of British Columbia).
6. Ibrahim, S. E. B., & Sayed, T. (2011). Developing safety performance functions incorporating reliability-based risk measures. *Accident Analysis & Prevention*, *43*(6), 2153-2159.
7. Dhahir, B., & Hassan, Y. (2019). Probabilistic, safety-explicit design of horizontal curves on two-lane rural highways based on reliability analysis of naturalistic driving data. *Accident Analysis & Prevention*, *123*, 200-210.
8. Charlton, S. G. (2007). The role of attention in horizontal curves: A comparison of advance warning, delineation, and road marking treatments. *Accident Analysis & Prevention*, *39*(5), 873-885.
9. Xu, H., & Wei, D. (2016). Improved identification and calculation of horizontal curves

with geographic information system road layers. *Transportation Research Record*, *2595*(1), 50-58.

10. Li, Z., Chitturi, M. V., Bill, A. R., & Noyce, D. A. (2012). Automated identification and extraction of horizontal curve information from geographic information system roadway maps. *Transportation research record*, *2291*(1), 80-92.

11. Darren, J., Ronald, P., Neuman, T (2004). *A guide for reducing collisions on horizontal curves.* National Cooperative Highway Research Program (NCHRP, Report No. 500), Washington, DC.

12. de Leur, P., & Sayed, T. (2003). A framework to proactively consider road safety within the road planning process. *Canadian Journal of Civil Engineering*, *30*(4), 711-719.

13. Ismail, K. A. S. (2006). *Probabilistic calibration of highway geometric design: theoretical issues and applications* (Masters dissertation, University of British Columbia).

14. Russo, F., Busiello, M., & Dell, G. (2016). Safety performance functions for crash severity on undivided rural roads. *Accident Analysis & Prevention*, *93*, 75-91.

15. Mehta, G., & Lou, Y. (2013). Calibration and development of safety performance functions for Alabama: Two-lane, two-way rural roads and four-lane divided highways. *Transportation research record*, *2398*(1), 75-82.

16. Sarhan, M., & Hassan, Y. (2008). Three-dimensional, probabilistic highway design: sight distance application. *Transportation Research Record*, *2060*(1), 10-18.

17. AASHTO (2018). A policy on geometric design of highways and streets. *American Association of State Highway and Transportation Officials: Washington, DC, USA*.

18. Chiu, M., C. Clayton, and G. Millen (2017). *Geometric Design Guide for Canadian Roads: Chapter 1: Design Philosophy.* 2017.

19. Gargoum, S. (2019). *Performance-Based Assessment of Road Design Elements using LiDAR Technology: Towards Adopting a Safe System Approach* (Doctoral dissertation, University of Alberta).

20. Felipe, E. L. (1996). *Reliability-based design for highway horizontal curves* (Doctoral dissertation, University of British Columbia).

21. Highway Safety Manual (2010). *American Association of State Highway and Transportation Officials: Washington, DC, USA.*

22. Hauer, E. (1988). A case for science-based road safety design and management. In *Highway Safety: at the crossroads: proceedings of a conference* (241-267).

23. Hauer, E. (2000). *Safety in geometric design standards I: Three anecdotes*. In *2nd International Symposium on Highway Geometric DesignTransportation Research Board; Road and Transportation Research Association, Germany; American Association of State Highway and Transportation Officials; American Society of Civil Engineers; Federal Highway Administration; International Road Federation*; (No. FGSV 002/67).

24. Navin, F. P. (1992). Reliability indices for road geometric design. *Canadian Journal of Civil Engineering*, *19*(5), 760-766.

25. Richl, L., & Sayed, T. (2006). Evaluating the safety risk of narrow medians using reliability analysis. *Journal of transportation engineering*, *132*(5), 366-375.

26. Sarhan, M., & Hassan, Y. (2011). Reliability-based three-dimensional design of horizontal

lateral clearance. *Canadian Journal of Civil Engineering*, *38*(8), 900-908.

27. Hussein, M., Sayed, T., Ismail, K., & Van Espen, A. (2014). Calibrating road design guides using risk-based reliability analysis. *Journal of Transportation Engineering*, *140*(9), 04014041.

28. Dhahir, B., & Hassan, Y. (2016). Reliability-based design of horizontal curves on two-lane rural highways. *Transportation Research Record*, *2588*(1), 22-31.

29. Crowell, B. N. (1979). Highway design standards—their formulation, interpretation, and application. In *Proceedings of Seminar N, PTRC*.

30. Essa, M., Sayed, T., & Hussein, M. (2016). Multi-mode reliability-based design of horizontal curves. *Accident Analysis & Prevention*, *93*, 124-134.

31. Alsaleh, R., Sayed, T., Ismail, K., & AlRukaibi, F. (2020). System reliability as a surrogate measure of safety for horizontal curves: methodology and case studies. *Transportmetrica A: transport science*, *16*(3), 957-986.

32. You, K., & Sun, L. (2013). Reliability analysis of vehicle stability on combined horizontal and vertical alignments: Driving safety perspective. *Journal of Transportation Engineering*, *139*(8), 804-813.

33. Navin, F. P. (1990). Safety factors for road design: Can they be estimated?. *Transportation Research Record*, 1280.

34. Jesna, N. M., & Anjaneyulu, M. V. L. R. (2016). Reliability analysis of horizontal curves on two lane highways. *Transportation research procedia*, *17*, 107-115.

35. Ismail, K., & Sayed, T. (2009). Risk-based framework for accommodating uncertainty in

highway geometric design. *Canadian Journal of Civil Engineering*, *36*(5), 743-753.

36. Haukaas, T. (2007). *Engineering Decision Making with Numerical Simulation Models. Vancouver, BC, Canada*.

37. Hassan, Y., Sarhan, M., & Salehi, M. (2012). Probabilistic model for design of freeway acceleration speed-change lanes. *Transportation research record*, *2309*(1), 3-11.

38. Ismail, K., & Sayed, T. (2012). Risk-optimal highway design: Methodology and case studies. *Safety science*, *50*(7), 1513-1521.

39. Ismail, K., & Sayed, T. (2010). Risk-based highway design: Case studies from British Columbia, Canada. *Transportation Research Record*, *2195*(1), 3-13.

40. Wood, J. S., & Donnell, E. T. (2017). Stopping sight distance and available sight distance: new model and reliability analysis comparison. *Transportation research record*, *2638*(1), 1-9.

41. Wood, J. S., & Donnell, E. T. (2014). Stopping sight distance and horizontal sight line offsets at horizontal curves. *Transportation Research Record*, *2436*(1), 43-50.

42. Ibrahim, S. E., Sayed, T., & Ismail, K. (2012). Methodology for safety optimization of highway cross-sections for horizontal curves with restricted sight distance. *Accident Analysis & Prevention*, *49*, 476-485.

43. Bassani, M., Grasso, N., Piras, M., & Catani, L. (2019). Estimating the Available Sight Distance in the Urban Environment by GIS and Numerical Computing Codes. *ISPRS International Journal of Geo-Information*, *8*(2), 69. doi: 10.3390/ijgi8020069.

44. Khattak, A. J., Hallmark, S., & Souleyrette, R. (2003). Application of light detection and

ranging technology to highway safety. *Transportation research record*, *1836*(1), 7-15.

45. de Santos-Berbel, C., Essa, M., Sayed, T., & Castro, M. (2017). Reliability-based analysis of sight distance modelling for traffic safety. *Journal of advanced transportation, 2017*. doi: 10.1155/2017/5612849.

46. de Santos-Berbel, C., & Castro, M. (2015). Stopping-sight-distance simulation using a new probabilistic approach. In *Proceedings of the 5th International Symposium on Highway Geometric Design* (22-24).

47. Gargoum, S., El-Basyouny, K., & Sabbagh, J. (2018). Automated extraction of horizontal curve attributes using LiDAR data. *Transportation Research Record*, *2672*(39), 98-106.

48. El-Basyouny, K., & Sayed, T. (2009). Collision prediction models using multivariate Poisson-lognormal regression. *Accident Analysis & Prevention*, *41*(4), 820-828.

49. Himes, S. C., & Donnell, E. T. (2014). Reliability approach to horizontal curve design. *Transportation Research Record*, *2436*(1), 51-59.

50. Haukaas, T. (2012). *System Reliability.* University of British Columbia, Vancouver, BC, Canada.

51. Navin, F.P. (1991). *Safe road design as limit state*. VTI Rapport 372A, Part 2 (No. VTI Rapport 372A, Part 2).

52. Faghri, A., & Demetsky, M. J. (1988). Reliability and risk assessment in the prediction of hazards at rail-highway grade crossings. *Transportation Research Record*, *1160*, 45-51.

53. Easa, S. M. (1993). Reliability-based design of intergreen interval at traffic signals. *Journal of Transportation Engineering*, *119*(2), 255-271.

54. Easa, S. M. (1994). Reliability-based design of sight distance at railroad grade crossings. *Transportation research part A: policy and practice*, *28*(1), 1-15.

55. Echaveguren, T., Bustos, M., & De Solminihac, H. (2005). Assessment of horizontal curves of an existing road using reliability concepts. *Canadian Journal of Civil Engineering*, *32*(6), 1030-1038.

56. Dhahir, B., & Hassan, Y. (2015, March). Design of Horizontal Curves Using Reliability Analysis. In *The 5 th International Symposium on Highway Geometric Design, Vancouver, BC, Canada*.

57. De Solminihac, H. E., Echaveguren, T., & Vargas, S. (2007). Friction reliability criteria applied to horizontal curve design of low-volume roads. *Transportation research record*, *1989*(1), 138-147.

58. You, K., Sun, L., & Gu, W. (2012). Reliability-based risk analysis of roadway horizontal curves. *Journal of Transportation Engineering*, *138*(8), 1071-1081.

59. Khoury, J. E., & Hobeika, A. (2007). Incorporating uncertainty into the estimation of the passing sight distance requirements. *Computer-Aided Civil and Infrastructure Engineering*, *22*(5), 347-357.

60. Dhahir, B., & Hassan, Y. (2019). Probabilistic, safety-explicit design of horizontal curves on two-lane rural highways based on reliability analysis of naturalistic driving data. *Accident Analysis & Prevention*, *123*, 200-210.

61. Hassan, Y., Easa, S. M., & Halim, A. A. E. (1997). Design considerations for combined highway alignments. *Journal of Transportation Engineering*, *123*(1), 60-68.

62. Williams, K., Olsen, M. J., Roe, G. V., & Glennie, C. (2013). Synthesis of transportation applications of mobile LiDAR. *Remote Sensing*, *5*(9), 4652-4692.

63. Gargoum, S., & El-Basyouny, K. (2019). Effects of LiDAR point density on extraction of traffic signs: a sensitivity study. *Transportation research record*, *2673*(1), 41-51.

64. Duffell, C. G., & Rudrum, D. M. (2005). Remote sensing techniques for highway earthworks assessment. In *Site Characterization and Modeling* (1-13).

65. Charlton, S. G. (2007). The role of attention in horizontal curves: A comparison of advance warning, delineation, and road marking treatments. *Accident Analysis & Prevention*, *39*(5), 873-885.

66. Xu, H., & Wei, D. (2016). Improved identification and calculation of horizontal curves with geographic information system road layers. *Transportation Research Record*, *2595*(1), 50-58.

67. *Fatality Analysis Reporting System (FARS)*. (2015). National Highway Traffic Safety Administration (NHTSA).

68. Li, Z., Chitturi, M. V., Bill, A. R., & Noyce, D. A. (2012). Automated identification and extraction of horizontal curve information from geographic information system roadway maps. *Transportation research record*, *2291*(1), 80-92.

69. Khan, G., Bill, A. R., Chitturi, M., & Noyce, D. A. (2012). Horizontal curves, signs, and safety. *Transportation research record*, *2279*(1), 124-131.

70. Schneider IV, W. H., Savolainen, P. T., & Moore, D. N. (2010). Effects of horizontal curvature on single-vehicle motorcycle crashes along rural two-lane

highways. *Transportation Research Record*, *2194*(1), 91-98.

71. Hallmark, S., & McDonald, T. (2007). Low-Cost Strategies to Reduce Speed and Crashes on Curves. *Center for Transportation Research and Education (CTRE), Iowa State University (ISU), Iowa, United States*.

72. Coelho, A. H., Borges Jr, N. P., Borges, N. P., Gallo, M. D., & Valente, A. M. (2015). Automatic horizontal road design information extraction from georeferenced polygonals: A brazilian federal highway network study. *Journal of Civil Engineering and Architecture*, *9*, 1513-1522.

73. Drakopoulos, A., & Örnek, E. (2000). Use of vehicle-collected data to calculate existing roadway geometry. *Journal of transportation engineering*, *126*(2), 154-160.

74. Hans, Z., Souleyrette, R., & Bogenreif, C. (2012). *Horizontal curve identification and evaluation* (No. InTrans Project 10-369).

75. Gargoum, S. A., El-Basyouny, K., Froese, K., & Gadowski, A. (2018). A fully automated approach to extract and assess road cross sections from mobile lidar data. *IEEE Transactions on Intelligent Transportation Systems*, *19*(11), 3507-3516.

76. Gargoum, S. A., El-Basyouny, K., Shalkamy, A., & Gouda, M. (2018). Feasibility of extracting highway vertical profiles from LiDAR data. *Canadian Journal of Civil Engineering*, *45*(5), 418-421.

77. Tsai, Y., Ai, C., Wang, Z., & Pitts, E. (2013). Mobile cross-slope measurement method using lidar technology. *Transportation research record*, *2367*(1), 53-59.

78. Gargoum, S. A., & El Basyouny, K. (2019). A literature synthesis of LiDAR applications

in transportation: feature extraction and geometric assessments of highways. *GIScience & Remote Sensing*, *56*(6), 864-893.

79. Holgado-Barco, A., González-Aguilera, D., Arias-Sanchez, P., & Martinez-Sanchez, J. (2015). Semiautomatic extraction of road horizontal alignment from a mobile LiDAR system. *Computer-Aided Civil and Infrastructure Engineering*, *30*(3), 217-228.

80. Carlson, P. J., Burris, M., Black, K., & Rose, E. R. (2005). Comparison of radius-estimating techniques for horizontal curves. *Transportation research record*, *1918*(1), 76-83.

81. Milstead, R., Qin, X., Katz, B., Bonneson, J. A., Pratt, M., Miles, J., & Carlson, P. J. (2011). *Procedures for setting advisory speeds on curves* (No. FHWA-SA-11-22). United States. Federal Highway Administration. Office of Safety.

82. Pratt, M. P., Miles, J. D., & Bonneson, J. A. (2009). *Workshops on using the GPS method to determine curve advisory speeds* (No. FHWA/TX-10/5-5439-01-1). Texas Transportation Institute.

83. Imran, M., Hassan, Y., & Patterson, D. (2006). GPS–GIS-Based procedure for tracking vehicle path on horizontal alignments. *Computer-Aided Civil and Infrastructure Engineering*, *21*(5), 383-394.

84. Ai, C., & Tsai, Y. (2015). Automatic horizontal curve identification and measurement method using GPS data. *Journal of Transportation Engineering*, *141*(2), 04014078.

85. Findley, D. J., Zegeer, C. V., Sundstrom, C. A., Hummer, J. E., Rasdorf, W., & Fowler, T. J. (2012). Finding and measuring horizontal curves in a large highway network: a GIS

approach. *Public Works Management & Policy*, *17*(2), 189-211.

86. Rasdorf, W., Findley, D. J., Zegeer, C. V., Sundstrom, C. A., & Hummer, J. E. (2012). Evaluation of GIS applications for horizontal curve data collection. *Journal of Computing in Civil Engineering*, *26*(2), 191-203.

87. Hassan, Y., Easa, S. M., & Abd El Halim, A. O. (1995). Sight distance on horizontal alignments with continuous lateral obstructions. *Transportation research record*, *1500*, 31-42.

88. Gargoum, S. A., El-Basyouny, K., & Sabbagh, J. (2018). Assessing stopping and passing sight distance on highways using mobile LiDAR data. *Journal of Computing in Civil Engineering*, *32*(4), 04018025.

89. Nehate, G., & Rys, M. (2006). 3D calculation of stopping-sight distance from GPS data. *Journal of transportation engineering*, *132*(9), 691-698.

90. Bassani, M., Grasso, N., & Piras, M. (2015). 3D GIS based evaluation of the available sight distance to assess safety of urban roads. *International Archives of the Photogrammetry, Remote Sensing & Spatial Information Sciences*, *40*.

91. Castro, M., Lopez-Cuervo, S., Paréns-González, M., & de Santos-Berbel, C. (2016). LIDAR-based roadway and roadside modelling for sight distance studies. *Survey Review*, *48*(350), 309-315.

92. Castro, M., Iglesias, L., Sánchez, J. A., & Ambrosio, L. (2011). Sight distance analysis of highways using GIS tools. *Transportation research part C: emerging technologies*, *19*(6), 997-1005.

93. ESRI, R. (2011). *ArcGIS desktop: release 10. Environmental Systems Research Institute, CA*.

94. Lovell, D. J. (1999). Automated calculation of sight distance from horizontal geometry. *Journal of Transportation Engineering*, *125*(4), 297-304.

95. Khattak, A. J., & Shamayleh, H. (2005). Highway safety assessment through geographic information system-based data visualization. *Journal of computing in civil engineering*, *19*(4), 407-411.

96. Castro, M., Anta, J. A., Iglesias, L., & Sánchez, J. A. (2014). GIS-based system for sight distance analysis of highways. *Journal of computing in civil engineering*, *28*(3), 04014005.

97. Yen, K. S., Ravani, B., & Lasky, T. A. (2011). *LiDAR for data efficiency* (No. WA-RD 778.1). Washington (State). Dept. of Transportation. Office of Research and Library Services.

98. Schwarz, B. (2010). Mapping the world in 3D. *Nature Photonics*, *4*(7), 429-430.

99. Jalayer, M., Gong, J., Zhou, H., & Grinter, M. (2015). Evaluation of remote sensing technologies for collecting roadside feature data to support highway safety manual implementation. *Journal of Transportation Safety & Security*, *7*(4), 345-357.

100. Riveiro, B., Díaz-Vilariño, L., Conde-Carnero, B., Soilán, M., & Arias, P. (2015). Automatic segmentation and shape-based classification of retro-reflective traffic signs from mobile LiDAR data. *IEEE Journal of Selected Topics in Applied Earth Observations and Remote Sensing*, *9*(1), 295-303.

101. Gargoum, S., El-Basyouny, K., Sabbagh, J., & Froese, K. (2017). Automated highway sign extraction using lidar data. *Transportation research record*, *2643*(1), 1-8.

102. Soilán, M., Riveiro, B., Martinez-Sanchez, J., & Arias, P. (2016). Traffic sign detection in MLS acquired point clouds for geometric and image-based semantic inventory. *ISPRS Journal of Photogrammetry and Remote Sensing*, *114*, 92-101.

103. Yan, W. Y., Morsy, S., Shaker, A., & Tulloch, M. (2016). Automatic extraction of highway light poles and towers from mobile LiDAR data. *Optics & Laser Technology*, *77*, 162-168.

104. Kumar, P. (2012). *Road features extraction using terrestrial mobile laser scanning system* (Doctoral dissertation, National University of Ireland Maynooth).

105. Guan, H. (2014). *Automated extraction of road information from mobile laser scanning data* (Doctoral dissertation, University of Waterloo).

106. Ai, C. (2013). *A sensing methodology for an intelligent traffic sign inventory and condition assessment using GPS/GIS, computer vision and mobile LiDAR technologies* (Doctoral dissertation, Georgia Institute of Technology).

107. Olsen, M. J. (2013). *Guidelines for the use of mobile LIDAR in transportation applications* (Vol. 748). Transportation Research Board.

108. Langston, J. W., & Walker, T. L. (2001). Highway study benefits from helicopter laser survey. *Public Works*, *131*(3).

109. Stone, D. (1999). County reaps rewards from airborne laser survey. *Civil Engineering News*, *11*(10).

110. MathWorks (2018). *MATLAB and Statistics Toolbox Release (R2018a)*. *Natick* (*Massachusetts, United States*).

111. Hosseinpour, M., Yahaya, A. S., & Sadullah, A. F. (2014). Exploring the effects of roadway characteristics on the frequency and severity of head-on crashes: Case studies from Malaysian Federal Roads. *Accident Analysis & Prevention*, *62*, 209-222.

112. Park, B. J., Fitzpatrick, K., & Lord, D. (2010). Evaluating the effects of freeway design elements on safety. *Transportation research record*, *2195*(1), 58-69.

113. Manan, M. M. A., Jonsson, T., & Várhelyi, A. (2013). Development of a safety performance function for motorcycle accident fatalities on Malaysian primary roads. *Safety science*, *60*, 13-20.

114. Caliendo, C., Guida, M., & Parisi, A. (2007). A crash-prediction model for multilane roads. *Accident Analysis & Prevention*, *39*(4), 657-670.

115. Jacob, A., & Anjaneyulu, M. V. L. R. (2013). Operating speed of different classes of vehicles at horizontal curves on two-lane rural highways. *Journal of Transportation Engineering*, *139*(3), 287-294.

116. Maji, A., Sil, G., & Tyagi, A. (2018). 85th and 98th percentile speed prediction models of car, light, and heavy commercial vehicles for four-lane divided rural highways. *Journal of Transportation Engineering, Part A: Systems*, *144*(5), 04018009.

117. Shallam, R. D. K., & Ahmed, M. A. (2016). Operating speed models on horizontal curves for two-lane highways. *Transportation Research Procedia*, *17*, 445-451.

118. Semeida, A. M. (2013). Impact of highway geometry and posted speed on operating speed

at multi-lane highways in Egypt. *Journal of Advanced Research*, *4*(6), 515-523.

119. Discetti, P., Dell'Acqua, G., & Lamberti, R. (2011). Models of operating speeds for low-volume roads. *Transportation research record*, *2203*(1), 219-225.

120. Abbas, S. K. S., Adnan, M. A., & Endut, I. R. (2011). Exploration of 85th percentile operating speed model on horizontal curve: a case study for two-lane rural highways. *Procedia-Social and behavioral sciences*, *16*, 352-363.

121. Faezi, S. F., Hamid, H., & Davoodi, S. R. (2011). Predicting speed model of horizontal curves on exclusive motorcycle lane. *Aust J Basic Appl Sci*, *5*(5), 590-598.

122. Memon, R. A., Khaskheli, G. B., & Qureshi, A. S. (2008). Operating speed models for two-lane rural roads in Pakistan. *Canadian Journal of Civil Engineering*, *35*(5), 443-453.

123. Gong, H., & Stamatiadis, N. (2008). Operating speed prediction models for horizontal curves on rural four-lane highways. *Transportation Research Record*, *2075*(1), 1-7.

124. Misaghi, P., & Hassan, Y. (2005). Modeling operating speed and speed differential on two-lane rural roads. *Journal of Transportation Engineering*, *131*(6), 408-418.

125. Alberta Infrastructure (1999). *Highway geometric design guide.*

126. Nehate, G., & Rys, M. (2006). 3D calculation of stopping-sight distance from GPS data. *Journal of transportation engineering*, *132*(9), 691-698.

127. Cook, D. J., Harwood, D. W., Potts, I. B., Donnell, E. T., & Hamadeh, B. (2019). Reliability analysis for roadway curves with horizontal sightline obstructions. *Transportation research record*, *2673*(8), 611-622.

128. National Research Council (US). Transportation Research Board. Committee for

Guidance on Setting, & Enforcing Speed Limits. (1998). Managing Speed: Review of Current Practice for Setting and Enforcing Speed Limits.

129. Richl, L., & Sayed, T. (2005). Effect of speed prediction models and perceived radius on design consistency. *Canadian Journal of Civil Engineering*, *32*(2), 388-399.

130. Lerner, N. (1995, August). Age and driver perception-reaction time for sight distance design requirements. In *1995 Compendium of Technical Papers. Institute of Transportation Engineers 65th Annual Meeting. Institute of Transportation Engineers (ITE)*.

131. Fambro, D. B., Fitzpatrick, K., & Koppa, R. J. (1997). *Determination of stopping sight distances.* National Cooperative Highway Research Program (Report No. 400). Transportation Research Board, Washington, DC.

132. Lamm, R., Psarianos, B., & Mailaender, T. (1999). *Highway design and traffic safety engineering handbook*.

133. Ellingwood, B. (1980). *Development of a probability based load criterion for American National Standard A58: Building code requirements for minimum design loads in buildings and other structures* (Vol. 13). US Department of Commerce, National Bureau of Standards.

134. Melchers, R. E., & Beck, A. T. (2018). *Structural reliability analysis and prediction*. John wiley & sons.

135. Ghobarah, A. (2001). Performance-based design in earthquake engineering: state of development. *Engineering structures*, *23*(8), 878-884.

136. Shen, Q. (2007). *Development of safety performance functions for empirical Bayes estimation of crash reduction factors* (Doctoral dissertation, Florida International University).

137. Hadayeghi, A. (2009). *Use of advanced techniques to estimate zonal level safety planning models and examine their temporal transferability*. Toronto, Ontario, Canada: University of Toronto.

138. Hauer, E. (1997). *Observational before/after studies in road safety. estimating the effect of highway and traffic engineering measures on road safety*. *Pergamon Press.*

139. Kulmala, R. O. (1998). *Safety at rural three-and four-arm junctions: Development and application of accident prediction models.* VTT Technical Research Centre of Finland, 33.

140. Maher, M. J., & Summersgill, I. (1996). A comprehensive methodology for the fitting of predictive accident models. *Accident Analysis & Prevention*, *28*(3), 281-296.

141. Sawalha, Z., & Sayed, T. (2001). Evaluating safety of urban arterial roadways. *Journal of Transportation Engineering*, *127*(2), 151-158.

142. Sawalha, Z., & Sayed, T. (2006). Traffic accident modeling: some statistical issues. *Canadian journal of civil engineering*, *33*(9), 1115-1124.

143. Gilks, W. R., Richardson, S., & Spiegelhalter, D. (Eds.). (1995). *Markov chain Monte Carlo in practice*. CRC press.

144. Lan, B., Persaud, B., Lyon, C., & Bhim, R. (2009). Validation of a full Bayes methodology for observational before–after road safety studies and application to evaluation of rural signal conversions. *Accident Analysis & Prevention*, *41*(3), 574-580.

145. Persaud, B., Lan, B., Lyon, C., & Bhim, R. (2010). Comparison of empirical Bayes and full Bayes approaches for before–after road safety evaluations. *Accident Analysis & Prevention*, *42*(1), 38-43.

146. Lunn, D. J., Thomas, A., Best, N., & Spiegelhalter, D. (2000). WinBUGS-a Bayesian modelling framework: concepts, structure, and extensibility. *Statistics and computing*, *10*(4), 325-337.

147. Brooks, S. P., & Gelman, A. (1998). General methods for monitoring convergence of iterative simulations. *Journal of computational and graphical statistics*, *7*(4), 434-455.

148. Gelman, A., Meng, X. L., & Stern, H. (1996). Posterior predictive assessment of model fitness via realized discrepancies. *Statistica sinica*, 733-760.

149. El-Basyouny, K., & Sayed, T. (2010). A method to account for outliers in the development of safety performance functions. *Accident Analysis & Prevention*, *42*(4), 1266-1272.

150. El-Basyouny, K., & Sayed, T. (2010). Safety performance functions with measurement errors in traffic volume. *Safety science*, *48*(10), 1339-1344.

151. El-Basyouny, K., & Sayed, T. (2012). Measuring direct and indirect treatment effects using safety performance intervention functions. *Safety science*, *50*(4), 1125-1132.

152. Sacchi, E., Sayed, T., & El-Basyouny, K. (2014). Collision modification functions: Incorporating changes over time. *Accident Analysis & Prevention*, *70*, 46-54.

153. Elvik, R., Christensen, P., & Amundsen, A. H. (2004). *Speed and road accidents: an evaluation of the Power Model*. Transportøkonomisk Institutt.

154. Gargoum, S. A., & El-Basyouny, K. (2016). Exploring the association between speed and

safety: A path analysis approach. *Accident Analysis & Prevention*, *93*, 32-40.

155. Hayes, Andrew F. *Introduction to mediation, moderation, and conditional process analysis: A regression-based approach*. Guilford publications, 2017.